12-2019

# Power V. Threhsold: Near-Channel Morphology Controls Sediment Rating Curve Shape in Coastal Redwood Watersheds

Adam Caspian Nebraska Fisher
*Utah State University*

# POWER V. THREHSOLD: NEAR-CHANNEL MORPHOLOGY CONTROLS SEDIMENT RATING CURVE SHAPE IN COASTAL REDWOOD WATERSHEDS

by

Adam Caspian Nebraska Fisher

A thesis submitted in partial fulfillment
of the requirements for the degree

of

MASTER OF SCIENCE

in

Watershed Science

Approved:

| | |
|---|---|
| _____ | _____ |
| Patrick Belmont, Ph.D.<br>Major Professor | Belize Lane, Ph.D.<br>Committee Member |
| _____ | _____ |
| Steve Voelker, Ph.D.<br>Committee Member | Richard S. Inouye, Ph.D.<br>Vice Provost for Graduate Studies |

UTAH STATE UNIVERSITY
Logan, Utah

2019

# ABSTRACT

Power v. Threshold: Near-channel Morphology Controls Sediment Rating Curve Shape in Coastal Redwood Watersheds

by

Adam Caspian Nebraska Fisher

Utah State University, 2019

Major Professor: Patrick Belmont, Ph.D.
Department: Watershed Science

We explored discharge-suspended sediment relationships in 71 watersheds within nine larger basins in the North Coast of California. These watersheds are highly influenced by their tectonic setting and have a long history of timber harvest activity. We summarized these relationships by generated sediment rating curves (SRC) taking the form of a power function in log-log space: $SSC = aQ^b$. Where SSC represents suspended sediment concentration and Q represents normalized discharge. The rating parameters *a* and *b* define the vertical offset and slope of the relationship, respectively. We investigated how these relationships varied spatially and temporally among our study watersheds.

We quantified watershed and near-channel characteristics and land management metrics to understand controls on SRC relationships using Random Forest modeling. Random Forest models are a class of machine learning methods that can model complex,

nonlinear interactions between response variables and a large number of predictor variables.

We found two distinct SRC shapes within our study watersheds: simple power functions and threshold functions. We found a longitudinal trend in the SRC offset and slope, with the most extreme parameters located in basins closest to the Mendocino Triple Junction, an area of extremely high tectonic activity. Additionally, we found that SRC offsets increase and slopes decrease following timber harvest, with suspended sediment concentrations at low flows increasing faster than concentrations at high flows. Lastly, our Random Forest models explain about 40% of the variance in the SRC parameters. We found that timber harvest activity and near-channel local relief influence SRC offset while uplift rates and precipitation patterns influence SRC slope. Furthermore, our model correctly classified 96% of the SRC shapes using only near-channel morphological metrics, specifically, near-channel precipitation-sensitive deep-seated landslide susceptibility and near-channel soil erodibility.

(103 pages)

# PUBLIC ABSTRACT

Power v. Threshold: Near-channel Morphology Controls Sediment Rating Curve Shape in Coastal Redwood Watersheds

Adam Caspian Nebraska Fisher

River sediment is one of the most pervasive pollutants in the world. Excess amounts of fine sediment can reduce water quality, damage stream ecosystems, and harm aquatic life. Both natural and human-caused processes can add sediment to a river, such as tectonic uplift, landslides, and timber harvesting. Therefore, it is important to understand how fine sediment enters and moves through a rive system to inform policymakers and land-managers on effective ecosystem management.

In this study, we determined how the relationship between river flow and suspended sediment changed among watersheds along the North Coast of California. We found a rise in suspended sediment concentration at median flows following extreme timber harvesting. Additionally, our results indicate that river flow and suspended sediment relationships are influenced by timber harvest activity, tectonic uplift, rainfall patterns, and near-channel environments.

These results support previous findings that extreme land disturbance in a watershed, be it natural or human-caused, can change river flow and suspended sediment relationships. Our results suggest that policymakers and land-managers should take into account tectonic uplift when making regulation and should prioritize protecting near-channel environments.

# DEDICATION

To Camrin,

Thank you for always believing in me.

# ACKNOWLEDGMENTS

I gratefully acknowledge the support from and the extensive amount of data collected by Green Diamond Resource Company, Humboldt Redwood Company, the National Park Service, the U.S. Geological Survey, and the U.S. Forest Service. Without this data, my research would not have been possible. I would also like to thank my funding sources in part by Green Diamond Resource Company, Humboldt Redwood Company, and the National Council on Air and Stream Improvement.

I have had the tremendous advantage of learning from and working with Dr. Patrick Belmont throughout my undergraduate and graduate degrees. He has taught me how to become a systematic scientist, a better critical thinker, and an active community member. I thank him for his leadership and mentorship. I especially thank him for the first month of work that he assigned me, through which I learned to love all the different sizes of sediment. I also thank my committee members, Drs. Belize Lane and Steve Voelker, for their guidance and feedback throughout this project.

I would like to thank Dr. Sara Kelly for her support and friendship. She has been an exceptional friend and outstanding example of a model scientist. She has also shared her grandfather's pickled beet recipe, which I will covet for the rest of my life. I would also like to thank Dr. Brendan Murphy for always being available to grab coffee and talk science. His friendship and guidance have been invaluable in my development as a scientist. I thank all my friends in the Belmont Lab who have come and gone over the last six years. Their support, friendship, and feedback have helped me learn and grow. I would especially like to thank Natalie Gillard and Angie Merritt for teaching me that success is a team effort.

I thank everyone at the College of Natural Resources and Watershed Science Department for creating a welcoming, fun, and safe community. I apologize to Peter Wilcock for hotdogging his house. Finally, I would not have been able to complete this tremendous amount of work without the love and support of my family.

Adam C. N. Fisher

# CONTENTS

Page

# LIST OF TABLES

# LIST OF FIGURES

# INTRODUCTION

Suspended sediment dynamics within a watershed can strongly influence water quality and aquatic ecosystem health. Understanding processes controlling erosion and sediment transport at the watershed scale is therefore essential to inform resource policy and management decisions. Although suspended sediment occurs naturally in rivers, excess amounts can degrade water quality and impair stream ecosystems. Chronically high suspended sediment concentrations can alter water chemistry and temperature (Bilotta and Brazier, 2008), inhibit growth in primary producers (Schwartz et al., 2011), damage aquatic invertebrates (Henley et al., 2010), and raze salmonid redds (Wood and Armitage, 1997). Thus, identifying mechanisms and sources that influence suspended sediment concentrations can lead to better management and restoration of these ecosystems. However, diagnosing these sources and mechanisms has proven exceptionally challenging due to immense variability in erosional processes over space and time, heterogeneity in sediment transport and deposition, and a paucity of sediment monitoring data.

A variety of natural and anthropogenic factors influence erosion and sediment yield in watersheds. Various watershed characteristics (e.g., geology, climate, slope, vegetation, topographic relief), changes in base level, and land-use practices (e.g., agriculture, timber harvest, and construction) influence processes that contribute sediment to rivers (Langbein and Schumm, 1958; Ahnert, 1970; Merritts et al., 1994; Syvitski et al., 2000, 2014; Riebe et al., 2001; Mueller and Pitlick, 2013, Vaughan et al., 2017, Belmont and Foufoula-Georgiou, 2017). Most previous erosion research has primarily focused on hillslope processes and mass wasting events such as landslides and

debris flows (Cashman et al., 1995; Roering et al., 1999; Graham and O'Green, 2016). However, recent research has also highlighted the importance of sediment sources within the stream network corridor across a wide range of landscape settings (Walter and Merritts, 2008; Belmont et al., 2011; Donovan et al., 2015; Vaughan et al., 2017). A considerable body of research has demonstrated close coupling between tectonic activity and sediment production (Merritts and Bull, 1989; Merritts et al., 1994; Riebe et al., 2001; Tolorza et al., 2019).

Here we investigate watershed-scale sediment dynamics in the Coast Range of California, which is characterized by an unusually broad range of tectonic uplift and subsidence. This range of tectonic rates is reflected in the spatial patterns of long-term erosion (Ferrier et al., 2005; Balco et al., 2013, Moon et al., 2018). Superimposed on this naturally dynamic landscape, redwood forests have been harvested by a variety of practices since the mid-1800s. By the 1950s, 90% of all old-growth redwood forests had been harvested, with varying degrees of disturbance in each watershed as harvesting practices changed over space and time (Mooney and Dawson, 2016; Stewart et al., 2016). The coupling of these two high-order controls (regional tectonics and timber harvesting) on sediment production muddles understanding of natural versus management-induced influences on the sediment regimes, which presents considerable challenges for determining how these systems should be managed, monitored and regulated.

Previous attempts to link timber harvest practices practices, road building, and sediment production have consisted of multivariate linear regression models (Keppeler and Ziemer, 1990; Lewis, 1998; Syvitski et al., 2000; Klein et al., 2012) but such models are limited in their ability to capture the myriad nonlinear processes governing erosion

and sediment transport (Montgomery and Brandon, 2002; Ouimet et al., 2009). More importantly, no previous studies have considered both timber harvest practices and tectonic forcing in attempting to explain the observed spatial patterns in sediment production.

In this research, we use a combination of sediment rating curves (i.e., relationships of streamflow versus suspended sediment concentration), analysis of watershed geologic, pedologic, and topographic features, and Random Forest statistical models to examine dominant controls on sediment production within select watersheds draining redwood forests in the California Coast Ranges. Our dataset includes data generated by federal and state agencies as well as private commercial timber harvest companies spanning the coast of northern California over the past 15-30 years, comprising a total of 70,000 measurements of both sediment and discharge from 71 catchments. Three questions guide our research. How do sediment rating curves vary among rivers draining primarily redwood forests in northern California? How have these relationships changed over time? Which watershed or near-channel characteristics or timber harvest practices most influence the shape, steepness, and vertical offset of these relationships?

## BACKGROUND

The north coast of California exhibits an extraordinarily wide range of tectonic activity. The north-west trending California Coast Range was formed through the transform movement of the San Andreas Fault where the Pacific Plate and the North American Plate meet (Harden, 1998; Norris and Webb, 1990). The two plates of the San

Andreas Fault meet the Gorda Plate at the Mendocino Triple Junction (MTJ) (Figure 1). There, the Pacific Plate shares a transform boundary with the Gorda Plate, which is simultaneously subducting under the North American Plate. Rates of rock uplift are highest in the vicinity of the MTJ and decay to the north and south (Merritts and Bull, 1989; Merritts et al., 1994; Harden, 1998; Stallman and Kelsey, 2006). Basin-scale erosion rates mirror this pattern (Balco et al., 2013) with denudation rates falling systematically below uplift rates, implying that these systems are not in topographic steady-state (Ferrier et al., 2005; Stallman and Kelsey 2006).

This active tectonic setting is continuously creating structurally controlled topography from loosely to moderately consolidated sandstone and shale (Norris and Webb, 1990; Cashman et al., 1995; Harden, 1998). Shallow- and deep-seated landslides are frequent in the area with a majority of landslides occurring in the winter months when the region receives the majority of its precipitation (Norris and Webb, 1990; Willett et al., 2014).

The climate of the Coast Range is Mediterranean with warm, dry summers and cool, wet winters. Precipitation occurs almost exclusively as rain during the winter months and averages around 1300 mm annually (Daly et al., 1994; Daly et al., 2008). Precipitation intensities are generally low, ranging between 30-40 mm/hr at the 2 yr-15 min frequency (Bonnin et al., 2006). El Niño/Southern Oscillation cycles influence regional climatic patterns, fluctuating between warm winter storms with heavy precipitation and cool, dry spells (Iacobellis et al., 2016). These patterns drive high seasonality in the regional hydrology, with rainstorm dominated peak flows in the winter

months and base flow controlled low flows in the summer months (Power et al., 2016, Lane et al., 2017).

Coastal redwood forests were first commercially harvested by Euro-American settlers in the mid-1800s. A wide array of harvesting practices, including clear-cutting, were often accompanied by broadcast burning and yarding by oxen and horses or by "steam donkeys" in the late 1800s and early 1900s. Thereafter, logs were transported by narrow gauge railroads and downstream river channels when natural high water conditions or water release from floodgates allowed. The introduction of tractors in 1925 accelerated harvest and brought about the building of relatively dense road networks within these watersheds. Loose regulations on harvesting practices had devastating impacts on the landscape, significantly increasing soil erosion within these watersheds (Henry, 1998; Mooney and Dawson, 2016; Stewart et al., 2016). In 1973, the California Forest Practices Act (CFPA) was passed, which required all timber harvest practices to protect public resources and land productivity. Nine years later, the Timberland Productivity Act (1982) amended the CFPA to include sustainable harvest practices. These laws, along with the Porter-Cologne Water Quality Act (1969), the California Environmental Quality Act (1970), and the California Endangered Species Act (1984), have helped protect valuable public resources in the State (Noss, 1999). However, this history of variable timber harvest practices and paucity of data before 1985 complicates an understanding of the natural sediment regimes within these systems.

*Study Watersheds*

All 71 of our study watersheds are grouped within nine river basins located along the upper North Coast of California. Twelve of the watersheds are located in protected

lands: Prairie Creek State Park and Redwood National Park; Headwaters Forest Reserve; and Humboldt Redwood State Park. Thirty-two of the watersheds are currently under commercial timber management, and twenty-seven are managed by US Forest Service within the Caspar Creek Experimental Watershed. Study watersheds range in size from 0.1 to over 100 $km^2$ and are predominantly comprised of coastal redwood (*sequoia sempervirens*) stands with intermixed Douglas-fir, tanoak, and California bay laurel.

Some of the last remaining stands of old-growth redwood forest are located in Prairie Creek State Park, Redwood National Park, Headwaters Forest Reserve, and Humboldt Redwood State Park. Prairie Creek State Park and Redwood National Park were established in 1920 and 1968, respectively, with some areas currently managed for redwood tree establishment (Sawyer et al., 2000; National Park Service, 2018). However, two monitored sub-basins in Prairie Creek State Park contain over 89% old-growth forest (Klein and Ozaki, 2017; Wilzbach and Ozaki, 2017). Further south, the Headwaters Forest Reserve protects 12.5 $km^2$ of old-growth forest surrounded by 18 $km^2$ of second-growth forest and is managed by the Bureau of Land Management (BLM) (Programs: National Conservation Lands: California: Headwaters Forest Reserve, 2019; 34th Annual Salmonid Restoration Conference). The federal government and the State of California purchased the land from a timber management company in 1998 after a violent standoff between environmental activists and the management company (Sawyer et al., 2000). The last study watershed on protected land is Bull Creek, located in Humboldt Redwoods State Park. A tributary to the Eel River, Bull Creek was purchased by the State of California in the 1930s and consists of 16% old-growth forest (Sawyer et al., 2000).

These stands of old-growth forests are important windows into pre-harvest watershed conditions.

Eight commercially managed basins extend south from the Oregon border, with most being in the vicinity of Eureka, California. The watersheds are managed by two timber companies that employ different timber harvest practices that result in various mixes of uneven-aged and even-aged forests after timber harvests. Harvesting practices specifically include individual tree and group selection, variable tree retention and clear-cutting. Timber management plans precede all harvest activity and include wildlife and habitat conservation, old-growth tree and stand protection, and forest regeneration and planting practices (Management Plan, 2016; Responsible Forestry, 2019).

The southernmost study basin is the Caspar Creek Experimental Watershed. The majority of Caspar Creek was harvested and burned by the mid-1890s. The state of California took over management of the property in the 1960s and started harvesting the second-growth redwood stands.

To understand the effects of logging and road-building on aquatic habitat and sedimentation, a series of paired watershed studies was initiated by federal and state agencies (Henry, 1998; Napolitano, 1998). Current research conducted on the watershed has expanded to measure almost 30 hydrologic, geomorphic, and ecological metrics with a focus on streamflow, sedimentation, and erosion (Adams et al., 2004). With various timber harvest rates and practices documented, these long-term datasets provide valuable opportunity to evaluate the impact of both natural and anthropogenic influences on the SRC.

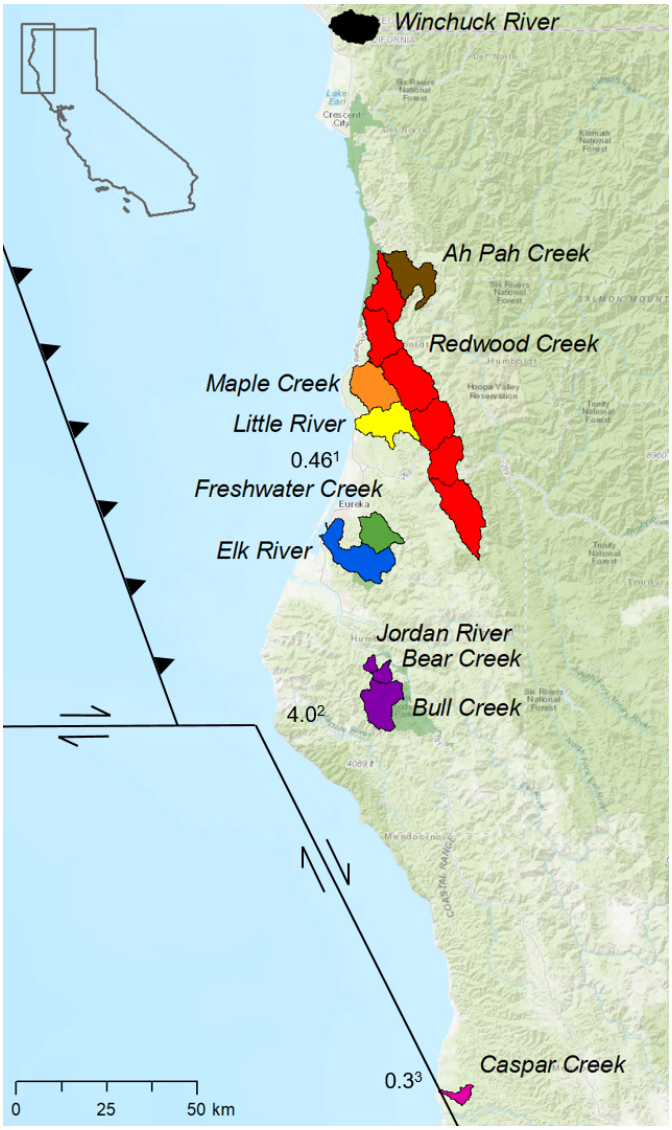


**Figure 1.** Study watersheds are shown along the coast of California. Jordan River, Bear Creek, and Bull Creek are tributaries to the Lower Eel watershed. Tectonic plate boundaries of the Mendocino Triple Junction are depicted in black (Balco et al., 2013). Estimated tectonic uplift rates are shown along the coast (Merritts and Bull, 1989[3]; Merritts et al., 1994[2]; Stallman and Kelsey, 2006[1]). Redwood National Park, Headwaters Forest Reserve, and Humboldt Redwood State Park are shown in green.

*Sediment Rating Curves*

Comprehensive measurement of the wide variety of sediment sources and sinks that exist within a given watershed, many of which vary in both time and space, is often infeasible due to limitations in data, funding, and or logistical constraints. Sediment rating curves (SRC) provide a useful alternative to characterize geomorphic controls on river sediment regimes (Asselman, 2000; Syvitski et al., 2000; Warrick, 2015). The SRC describes the average relationship between suspended sediment concentration (SS) and river discharge (Q), which typically exhibit a power law relationship:

$$SS = aQ^b \quad (1)$$

Parameters *a* and *b* are derived from fitted relationships using least squares regression on log-transformed SS and Q values, where *a* is the vertical offset of the function and *b* is the slope of the function. The simplicity and utility of SRCs have made them popular for characterizing sediment discharge and for trend analysis. Warrick (2015) demonstrated that normalizing discharge by the geometric mean of all sampled discharges reduces the inherent autocorrelation between the offset and slope and allows for basins of different sizes to be directly compared. The adapted version takes the form:

$$SS = \hat{a}(Q/Q_{GM})^b \quad (2)$$

where $\hat{a}$ is the vertical offset parameter and represents the median suspended sediment concentration and $Q_{GM}$ is the geometric mean of the sampled flows.

Vaughan et al. (2017) extended the technique outlined by Warrick (2015) and generated 45 SRCs from stream gages located throughout the state of Minnesota. They

identified three distinct trends that categorize the SRC relationships in log-log space: linear (simple power function), peaked, and threshold relationships (Figure 2). Linear relationships show increasing suspended sediment concentrations with increasing flows. Peaked relationships show an increasing trend up to a certain discharge at which point the trend decreases as a power function. Finally, threshold relationships show a flat or slightly increasing trend up to a discharge threshold, at which point the trend increases as a simple power function.

SRCs contain a considerable amount of information regarding the integrated response of a watershed's sediment sources as a function of flow. For example, a log-log linear trend suggests that a river has continually increased access to sediment sources as flow increases, with the slope of the trend depending on the magnitude of those sources. A peaked relationship suggests a substantial sediment supply limitation above a given flow value. A threshold relationship indicates that a river has access to entrain a fairly consistent concentration of sediment at low flows, and increasing access to sediment

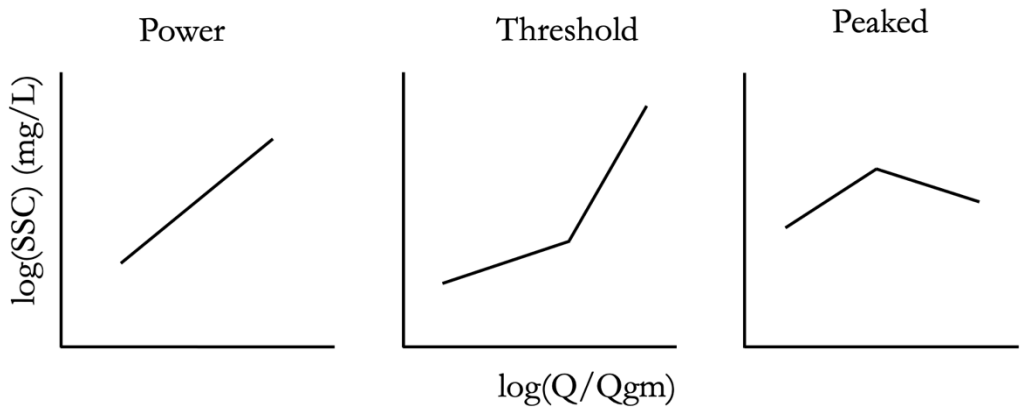


**Figure 2.** Three distinct SRC shapes identified by Vaughan at al., 2017.

sources as flow increases above a certain threshold. Additional information can be extracted from the magnitude of the relationships and the flow values that represent critical thresholds.

Attempts have been made to characterize the physical meaning behind the SRC, including the shape as well as the offset and slope (Asselman, 2000; Syvitski et al., 2000). Vaughan et al. (2017) used a Random Forest statistical model to identify physical factors that control various aspects of the SRC. They showed that the offset and SS concentration under low flow conditions are primarily controlled by land use, whereas the shape and slope are controlled by factors that are indicative of the geomorphic history of the basin, such as near-channel relief, channel gradient, and the number of lakes that exist within the channel-floodplain corridor. Tolorza et al. (2019) also used a Random Forest technique to identify physical factors that regulate changes in SS concentrations following a large tectonic event. They found hillslope gradient and vegetation cover to be the best predictors.

*Random Forest*

Random Forest (RF) models are a machine learning method and can model complex interactions between predictor and response variables (Cutler et al., 2012). RF models use bootstrapping to select training data from randomly selected subsamples of a dataset. The model creates a regression or classification tree from each random sample and combines the predictive accuracy of each tree to create a forest. Observations not selected in the bootstrapping process are used as test datasets and are a measure of the model's overall accuracy, measuring mean squared error (regression) or percent correctly classified (classification) (Cutler et al., 2007).

RF modeling has been shown to demonstrate superior predictive accuracy compared to other conventional statistical models, including classification trees, logistic regression, and linear discriminate analysis (Cutler at al. 2007). Additionally, RF generates both variable importance plots, which assign quantitative values to each of the predictor variables and can be used for variable selection, and partial dependence plots, which allow for visual evaluation between predictor and modeled response variables (Cutler et al., 2012). These tools are used to identify which variables have the most influence on the model. Pairing the statistical power of RF with SRCs is a robust approach to identify and understand environmental and anthropogenic factors influencing SRCs.

## DATA AND METHODS

### *Q/SS Data and Relations*

We compiled discharge and suspended sediment data from a total of 71 watersheds, spanning nine larger river basins (Table 1) from the National Park Service (NPS), U.S. Geological Survey (USGS), U.S. Forest Service (USFS), Green Diamond Resource Company, and Humboldt Redwood Company. Samples were collected using ISCO automated samplers with a discharge or turbidity threshold, above which samples were collected either at 15 to 30-minute intervals or at variable frequencies based on real-time turbidity values (Henry, 1998; Hydrologic Year 2016 Hydrologic Monitoring Submittal Report, 2016; Klein and Ozaki, 2017).

We evaluated each of the datasets for data quality. We date-matched each suspended sediment measurement with the corresponding flow value from high

resolution (10-30 minute) instantaneous discharge data. For data collected by the USGS, we date-matched samples to the mean daily discharge. In total, we synthesized approximately 70,000 paired suspended sediment – discharge measurements, summarized by sampling period and percent area harvested (Figure 3).

We developed an R script (Appendix A) to generate SRCs for each watershed. We also compared two different flow values on which to normalize the SRCs. First, we normalized by the geometric mean of flows that corresponded with each sediment sample, as suggested by Warrick (2015). We also attempted normalizing sample flow values by the geometric mean of the total flow record within the sampling

**Table 1**

*Study watersheds listed with the number of stream gages, the measurement period, and stream impairment as denoted by California EPA (Final 2014/2016 California Integrated Report), and data source.*

| Watershed | Number of Stream Gages | Period of Record | Impairment | Data Source |
|---|---|---|---|---|
| Winchuck River | 1 | 2007-2016 | Not Impaired | Green Diamond Resources Company |
| Ah Pah Creek | 1 | 2007-2016 | Not Impaired | Green Diamond Resource Company |
| Redwood Creek | 9 | 1974-1981/ 1992- 2016 | Sediment | National Park Service, U.S. Geological Survey |
| Maple Creek | 2 | 2004-2016 | Not Impaired | Green Diamond Resource Company |
| Little River | 4 | 2003-2016 | Not Impaired | Green Diamond Resource Company |
| Freshwater Creek | 9 | 2002-2015 | Sediment | Humboldt Redwood Company |
| Elk River | 15 | 2002-2016 | Sediment | Humboldt Redwood Company, Green Diamond Resource Company |
| Lower Eel River | 3 | 1975-1978/ 2003-2016 | Sediment | Humboldt Redwood Company, U.S. Geological Survey |
| Caspar Creek | 27 | 1985-2013 | Not impaired | U.S. Forest Service |

period to better characterize the samples in the context of the complete flow regime. However, normalizing by the geometric mean of flow values associated with the sediment samples substantially reduced the autocorrelation between the offset and slope (from -0.76 to -0.44 $R^2$). All SRC analyses presented are normalized by the mean of the flow values measured at the time the sediment samples were collected. Comparison between the two analyses can be found in Appendix B.

We categorized the SRC relationships following Vaughan et al. (2017), locating any breakpoints in the relationship using the spline interpolation method outlined by Dierckx (1975). We treated data above breakpoints as 'high flows' and data below as 'low flows'. We generated boxplots (Figure 4) summarizing the offset and slope for each SRC shape, separating non-harvested watersheds, grouping by larger basin, and orienting them by latitude (South to North). All SRCs used in this study can be found in Appendix C.

We analyzed the number of SRCs needed in unharvested watersheds to accurately compare SRC relationships between harvested and unharvested watersheds using two statistical analyses. We used 68 of the total SRCs in our dataset, removing SRCs that were only measured for two years. Using our initial findings of power and threshold relationships in harvested and unharvested watersheds, we created a Bernoulli trial and power analysis to model the number of SRCs in unharvested watersheds needed to say that only one relationships exists in that system.

To investigate how these Q/SS relationships have changed over time, we explored SRC records spanning more than 20 years. We generated SRCs for each water year (Oct. – May) and calculated the offset and slope. We removed data for years in which the range

of discharge is less than a half a log cycle because SRCs developed over such small ranges of discharge were deemed unreliable. Furthermore, we split nonlinear relationships at the threshold point located using the cumulative data and calculated the offset and slope for high- and low-flow segments of the annualized data. Lastly, we calculated the suspended sediment concentrations at the $20^{th}$ and $80^{th}$ percentile annual discharges to explore how high- and low-flows changed over time.

*Landscape and Land Management Data and Methods*

**Watershed Characteristics**

We summarized the watershed average topographic, geologic, and climatic setting for each study watershed. We estimated erosion rate using existing cosmogenic $^{10}Be$ measurements (Balco et al., 2013; Ferrier et al., *unpublished data*) and an altered form of the nonlinear hillslope erosion equation (Roaring et al., 1999; Montgomery and Brandon, 2002). We also estimated tectonic uplift rates in the study area using dated marine terraces (Merritts and Bull, 1989; Merritts et al., 1994; Snyder et al., 2000; Stallman and Kelsey, 2006; Padgett, 2013; Moon et al., 2018) and the Mendocino Crustal Conveyer model (Furlong and Govers, 1999; Lock et al., 2006). We summarized data sources and metrics in Table 2 and described them in further detail below.

We extracted elevation, slope, and relief derived from a 10-meter resolution digital elevation model (The National Map; www.usgs.gov/core-science-systems/national-geospatial-program/national-map). We measured drainage density for all study watersheds using the National Hydrography Dataset Plus V2 (NHD) flow lines (National Hydrography Dataset; www.epa.gov/waterdata/nhdplus-national-hydrography-dataset-plus), except for Caspar Creek. NHD flow lines were too coarse to capture the small sub-


**Figure 3.** Suspended sediment measurement periods for study watersheds are plotted. Large basins are denoted by color and name (right) with each watershed labeled on the left. Lighter colors represent nested watersheds. Timber harvest practices within watersheds are represented by black hash marks, scaled to percent area harvested. Study watersheds with no available harvest data are denoted with a star. This figure does not show harvest data for pre-national/state park establishment.

basins in Caspar Creek, so we derived a flow network from lidar with a similar drainage density to the other watersheds. We also extracted soil erodibility, measured as K-factor in soil surveys, using data from the Natural Resource Conservation Service and compiled by Environmental Systems Research Institute (USDA NRCS and Esri; www.arcgis.com/home/item.html?id=28e9f476324b486bacaaee7f9fcb77dc). We extracted hydrologic conductivity (www.sciencebase.gov/catalog/item/552c4877e4b0b22a157f5061) and rock strength (measured as uniaxial compressive strength) (www.sciencebase.gov/catalog/item/552c3b20e4b0b22a157f502d) from Olson and Hawkins (2014). We obtained the mean baseflow index, which is the ratio of baseflow to total flow, for each watershed using data from Howard and Merrifield (2010) (databasin.org/datasets/7169ff643d32429c8a543a9217f59429).

To account for the many landslide inputs into these systems, we extracted mean deep-seated landslide susceptibility from the State of California Geologic Survey Deep-seated Landslide Susceptibility map (Wills et al., 2011; www.arcgis.com/home/item.html?id=3cdc744bec6b45c28206e472e8ad0f89). Essentially, this map is a combination of rock strength and topographic slope, consistent with the assumption that terrain with steeper slopes and weaker rock strength have an increased susceptibility to landslide events. However, because this metric does not account for precipitation, which can also strongly influence landslide susceptibility, we generated an additional metric by normalizing the Landslide Susceptibility map by long-term average precipitation to create a precipitation-sensitive deep-seated landslide susceptibility map.

We quantified three climate metrics: long-term average (30-year normal) mean annual precipitation from Parameter-elevation Relationships on Independent Slopes

Model data (Daly et al., 1994; Daly et a., 2008); 24-hour, 2-year rainfall intensity frequency; and 15-minute, 2-year rainfall intensity frequency. The last two metrics were collected from the National Oceanic and Atmospheric Administration Precipitation Frequency Data Server (NOAA) (Bonnin et al., 2006; https://hdsc.nws.noaa.gov/hdsc/pfds/). We extracted the PRISM data for each study watershed and estimated the centroid of each sub-basin to obtain NOAA data.

To estimate long-term, natural background erosion rates in these watersheds, we created two separate models. We based the first model on erosion rate estimates from cosmogenic Beryllium-10 ($^{10}$Be) samples collected from a variety of watersheds along the North Coast of California, including several of our study basins (Balco et al., 2013, Ferrier et al., *unpublished data*). We plotted the erosion rates against sample latitude and fit a cubic spline through the data (Figure D.1). We estimated erosion rate for each study watershed using the latitude of each gage. Latitude was considered an appropriate scaling factor because it captures the long-wavelength variability that we observe in the tectonics of this area. Table 2 shows the equation for the model.

We based the second model on the nonlinear hillslope erosion rate model outlined in Roering et al. (1999) and adjusted for relief, as suggested by Montgomery and Brandon (2002). Equation 3 shows the relief-adjusted nonlinear hillslope erosion rate model:

$$E = E_0 + KR_z /[1-(R_z/R_c)]^2 \quad (3)$$

where $E_0$ is the background erosion rate from chemical weathering, K is a constant, $R_c$ is the limiting local relief, and $R_z$ is the measured relief. We used $E_0$, K, and $R_c$ values

consistent with Balco et al. (2013): $E_0$ = 0.03 m/yr, K = 1.2 x$10^{-4}$, and $R_c$ = 1000 m and measured relief in each watershed in order to populate Equation 3 to estimate erosion rate.

Tectonic uplift is known to be a strong driver of landscape erosion but can be very difficult to quantify. We estimated uplift rate using two models. We based the first model on dated marine terraces along the coast. The second is derived from the Mendocino Crustal Conveyer (MCC) model which describes crustal deformation and uplift rates along the coast of California associated with the MTJ. To create the first model, we pulled from the literature (Merritts and Bull, 1989; Merritts et al., 1994; Snyder et al., 2000; Stallman and Kelsey, 2006; Padgett, 2013; Moon et al., 2018) estimated uplift rates derived from dated marine terraces along the north coast of California. We then regressed two separate exponential functions through the data with uplift as a function of latitude (Figure E.1). We interpolated uplift rates at our study watersheds using the latitude at each gage. The second model, the MCC model, originally from Furlong and Govers (1999) and modified by Lock et al. (2006), estimates crustal deformation in the North American Plate as a result of the subducting Gorda plate at the MTJ. The model predicts a swath of uplift along the coast, running parallel to the San Andreas Fault, and extending north of San Francisco up through Eureka, CA. To extract estimated uplift rates from the MCC model, we plotted the model predictions against latitude, fit a cubic polynomial through 2/3$^{rds}$ of the data and regressed a linear relationship through the remaining 1/3$^{rd}$. We then estimated the uplift rates at our study watersheds using the latitude at each gage (Figure E.2).

There is some unquantifiable uncertainty in these models at the scales of our sub-watersheds. For example, we have no data to constrain how the marine terrace-derived uplift rates change with distance inland. Uncertainty related to the MCC model stems from the fact that it only predicts uplift associated with the MTJ and our derivative assumes these rates are consistent with rates along the coast. In reality, uplift and subsidence in these watersheds may be driven by local tectonic activity in narrow bands or discrete faults, and may be somewhat independent of regional activity.

**Near-Channel Characteristics**

To account for near-channel sediment sources and mechanisms, we extracted local relief, soil erodibility, and precipitation-sensitive deep-seated landslide susceptibility using methods outlined in Vaughan et al., 2017. To evaluate average channel steepness, we created a MATLAB script (Appendix F) using an adaptation of the TopoToolbox code to extract steepness ($k_s$) values at 50-meter intervals (Schwanghart, 2010; Schwanghart, 2014). We then normalized $k_s$ values by the mean reference concavity for all study basins; 0.48 (Wobus et al., 2006).

**Land Management Metrics**

To evaluate the influence of timber harvest practices on SRC shape, offset, and slope, we computed metrics describing the percentage of watershed harvested since 1985, 1995, 2005, and 2010, road density, and density of road-stream crossings. We categorized watersheds as ‘harvested’ if they were harvested after 1975, and all others ‘unharvested’. We could not obtain harvest histories for the following watersheds: Jordan Creek, South Fork Elk River, Ah Pah Creek, Winchuck River, and the north fork and

main stem of Maple Creek. Furthermore, we were only able to acquire harvest histories for watersheds within the Little River basin back to 2000. To use these watersheds in the RF analysis, we inferred harvest histories using the average area harvested per water year and frequency of harvest from 2000-2015. Only about 1% of each watershed was harvested per water year. A portion of Carson Creek and Railroad Creek were harvested, on average, every two years, while a portion of Lower South Fork and Upper South Fork were harvested every year. The back-calculated harvest rates reflect these values and can be found in Table H.1.

Road construction has been shown to increase peak discharge in watersheds in the study site (Ziemer, 1992). To account for differences between harvested and unharvested watersheds, we calculated road density using data from the timber management companies and Humboldt County. We also calculated the number of stream-road crossings, normalized by watershed area.

*Random Forest Models*

We created four Random Forest models using the R packages randomForest package in R (Liaw and Wiener, 2002). We subset our dataset to include only SRC records spanning at least ten years and harvested watersheds for which we could constrain past harvest activity. Thus, the RF models included a total of 47 SRCs. SRC shape, offset, and slope were used as response variables (Table G.1) and the 31 watershed and near-channel characteristics and land management metrics as predictor variables (Table 2) in the RF models. The exact values for each predictor variable are found in Table H.1. To reduce the dimensionality of the dataset, we created models and included predictor variables informed by the R package VSURF (Figure I.1) (Genuer et at., 2016).

We generated partial dependence plots to understand the relationship between predictor variables and modeled response variables. Lastly, we created multiple linear regression models (also informed by VSURF) to compare to the RF models.

**Table 2**

*Predictor variables in the RF model*

| Metric | Method | Equation | Data Source |
|---|---|---|---|
| Mean Slope | Measured | - | The National Map |
| Drainage Density | Measured | - | National Hydrography Dataset; USFS |
| Mean Elevation | Measured | - | The National Map |
| Relief | Measured | - | The National Map |
| Mean Soil Erodibility | Measured | - | USDA NRCS, Esri |
| Mean Hydrologic Conductivity | Measured | - | Olson and Hawkins, 2014 |
| Mean Rock Strength | Measured | - | Olson and Hawkins, 2014 |
| Mean Baseflow Index | Measured | - | Howard and Merrifield, 2010 |
| Mean Annual Precipitation | Measured | - | Daly et al., 2008; Daly et a., 1994 |
| 5-yr, 24-hr Precipitation Intensity | Measured | - | Bonnin et al., 2006 |
| 2-yr, 24-hr Precipitation Intensity | Measured | - | Bonnin et al., 2006 |
| 2-yr, 15-min Precipitation Intensity | Measured | - | Bonnin et al., 2006 |
| 2-yr, 24-hr Precipitation Depth | Measured | - | Bonnin et al., 2006 |
| Estimated Uplift Rate, Marine Terrace Model | Modeled | $y = 3E\text{-}62e^{3.5544x}$<br>$y = 4E+43e^{-2.465x}$<br>$y = -0.5811x + 24.799$ | Merritts and Bull, 1989; Merritts et al., 1994; Snyder et al., 2000; Stallman and Kelsey, 2006; Padgett, 2013; Moon et al., 2018 |
| Estimated Uplift Rate, MCC Model | Modeled | $y = 0.582x^4 - 62.7x^3 + 1899.8x^2 - 516299.8$ | Furlong and Govers (1999); Lock et al. (2006); Balco et al., 2013 |
| Long-term Erosion Rate | Modeled | $y = 0.35x^3 + -0.2x^2 + 0.03^x + 0.32$ | Balco et al., 2013; Moon et al., 2018; Ferrier et al., *unpublished data* |
| Nonlinear Hillslope Erosion Rate | Modeled | $E = E_0 + KR_z/[1-(R_z/R_c)]^2$ | Roering et al. (1999); Montgomery and Brandon (2002) |
| Deep-seated Landslide Susceptibility | Measured | - | Wills et al., 2011 |
| Precipitation Sensitive Deep-seated Landslide Susceptibility | Measured | - | Daly et al., 1994; Daly et a., 2008; Wills et al., 2011 |
| Near-channel Local Relief | Measured | - | The National Map |
| Mean Normalized Channel Steepness | Measured | - | The National Map |
| Near-channel Deep-seated Landslide Susceptibility | Measured | - | Wills et al., 2011 |
| Near-channel Precipitation Sensitive Deep-seated Landslide Susceptibility | Measured | - | Daly et al., 1994; Daly et a., 2008; Wills et al., 2011 |
| Near-channel Soil Erodibility | Measured | - | USDA NRCS, Esri |
| Harvest Status | Measured | - | USFS; Green Diamond Resource Co.; Humboldt Redwood Co. |
| Road Density | Measured | - | Humboldt County; Green Diamond Resource Co.; Humboldt Redwood Co. |
| Density of Road/Stream Crossings | Measured | - | Humboldt County; Green Diamond Resource Co.; Humboldt Redwood Co. |
| Percent Watershed Harvested since 2010 | Measured | - | USFS; Green Diamond Resource Co.; Humboldt Redwood Co. |
| Percent Watershed Harvested since 2005 | Measured | - | USFS; Green Diamond Resource Co.; Humboldt Redwood Co. |
| Percent Watershed Harvested since 1995 | Measured | - | USFS; Green Diamond Resource Co.; Humboldt Redwood Co. |
| Percent Watershed Harvested since 1985 | Measured | - | USFS; Green Diamond Resource Co.; Humboldt Redwood Co. |

# RESULTS

## *Spatial Distribution of Sediment Rating Curves*

Sediment rating curves fell into two categories: simple power functions and threshold relationships. Of the 64 sediment rating curves analyzed, 53 were characterized as simple power functions and 11 were characterized as threshold relationships. The slope and vertical offset parameters for each watershed are summarized in boxplots, ordered South to North, grouped by watershed, and separated by harvested or unharvested where appropriate.

In the figure below, SRC offsets in harvested watersheds initially increase from south to north and peak around the MTJ, located between the Lower Eel and Elk River watersheds, with Elk River having an anomalously large range of values. Offset values then decrease in watersheds to the north of Elk River and remain constant north of Little River. SRC offsets in unharvested watersheds are typically within the range, if slightly lower, than their harvested watershed counterparts. The one exception to this observation is the unharvested sub-watershed in the Elk River Basin, which exhibits an offset value that is considerably lower than most other harvested sub-watersheds within Elk River, though two harvested sub-watersheds in the Elk River Basin contain similarly low offset values.

The SRC slope for harvested watersheds decrease around the MTJ and then increase northward. Unharvested watersheds in Elk River (the Forest Headwaters Reserve) and Redwood Creek (Redwood National Park) both have a much lower slope than their harvested watershed counterparts and neighboring watersheds. However, SRC slopes in unharvested watersheds of Caspar Creek and the Lower Eel River are

commensurate with their harvested counterparts. SRC power relationships show a similar trend (Figure J.1).

We further investigated threshold relationships by separating the SRC into high flows and low flows, with high flows defined as above the discharge threshold value and low flows falling below the discharge threshold value. Of the 64 SRCs created, only 11 exhibit a threshold relationship. For high flow SRC threshold relationships (Figure 5), offsets are quite low and exhibit little variability. High flow SRC slopes fall within a

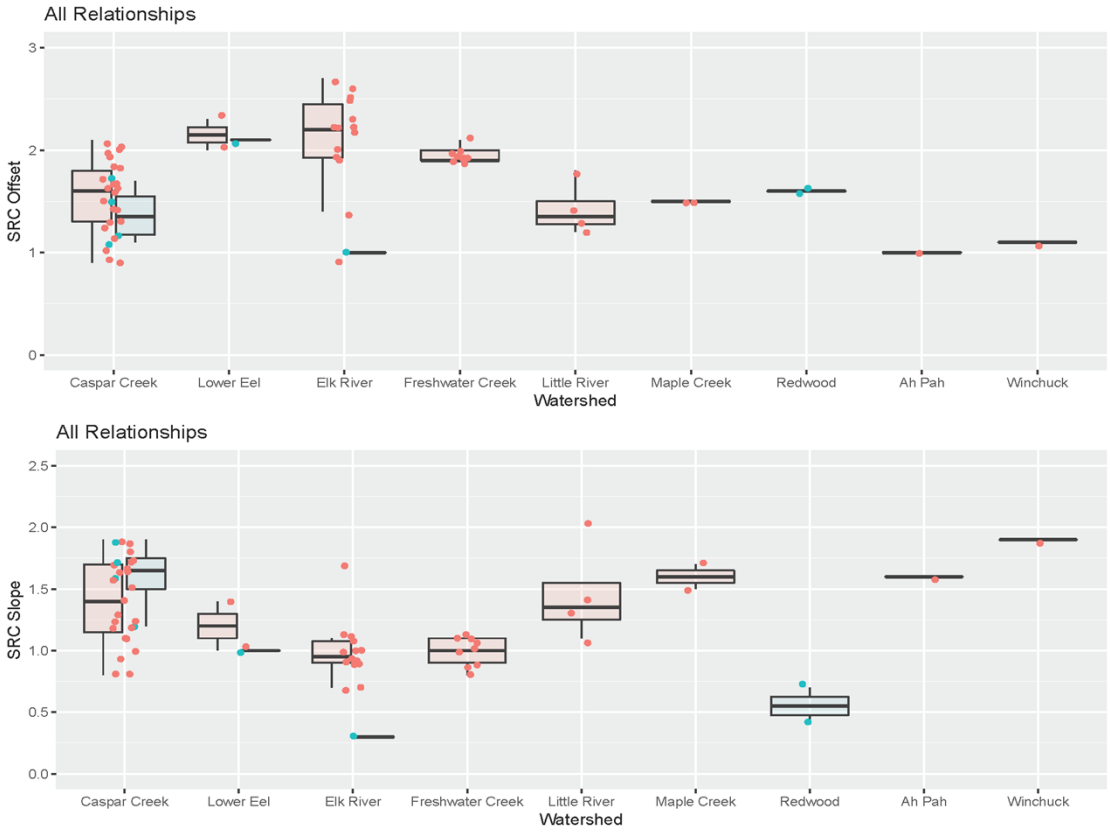


**Figure 4.** The SRC offset and slope for each gage are summarized by watershed and ordered by latitude with Caspar Creek being the furthest South and Winchuck being the furthest North. Harvested catchments are shown in orange (ordered left) and unharvest catchments are shown in green (ordered right). SRC offset values are plotted on a log axis.

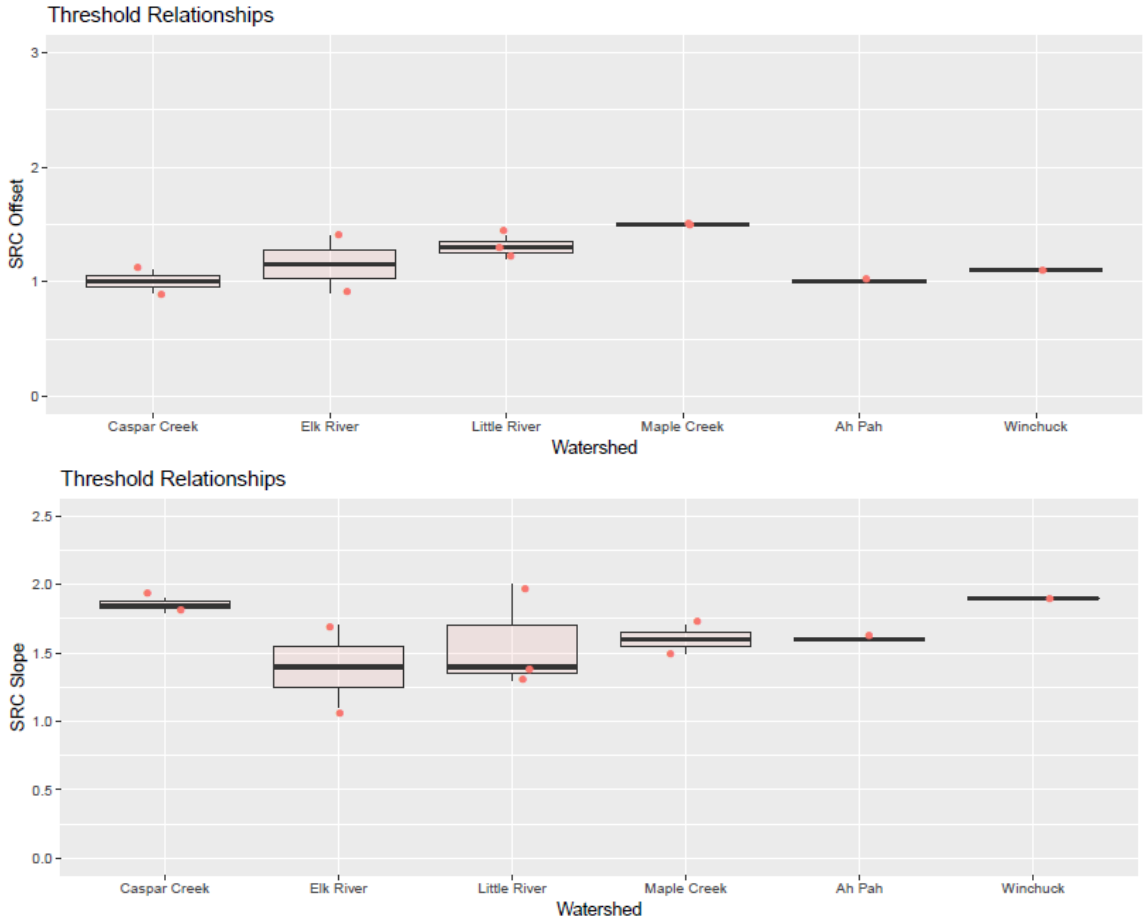


**Figure 5.** SRC offset and slope for only threshold relationships. The high flow SRC offset (top panel) and slope (bottom panel) are summarized by watershed and ordered by latitude with Caspar Creek being the furthest South and Winchuck being the furthest North. All watersheds in this figure have been harvested. SRC offset values are plotted on a log axis.

relatively tight range, with catchments in the Caspar Creek watershed having the highest values. Low flow SRC threshold relationships exhibit a similar geographic trend to high flow SRC slopes (Figure J.2).

The results of our unharvested watershed sample size analyses conclude that only power relationships are found in unharvested watersheds. We informed the Bernoulli trial and power analysis using the ratio of SRC power to threshold relationships found in all

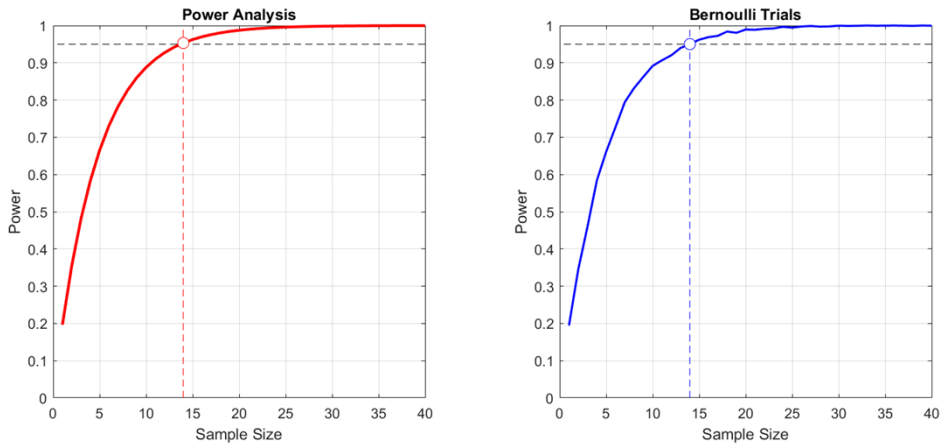


**Figure 6.** The results of the Bernoulli trial and power analysis. Both conclude that a sample size of 14 is needed to say with 95% confidence that only power relationships are found in unharvested watersheds.

harvested watersheds (0.2) to determine the SRC sample size needed in unharvested watersheds to observe only one relationship. Both analyses conclude that 14 SRCs are needed to state with 95% confidence, that only power relationships are found in unharvested watersheds. Figure 6 shows the results of these analyses.

*Temporal Trends in Sediment Rating Curves*

Time series plots of SRC offset and slopes show long-term trends in harvested watersheds (Figure 7). In harvested watersheds, the SRC offsets have increased over the last 20 years, while slopes have decreased. Furthermore, the 20$^{th}$ percentile (i.e. low flow) sediment concentration values have increased faster than then 80$^{th}$ percentile values (i.e. high flow). The four unharvested watersheds (Henningson, Iverson, Little Lost Man, and Munn) display much variability in both parameters and no systematic trends, except for a possible decrease in SRC slope in the Munn watershed.

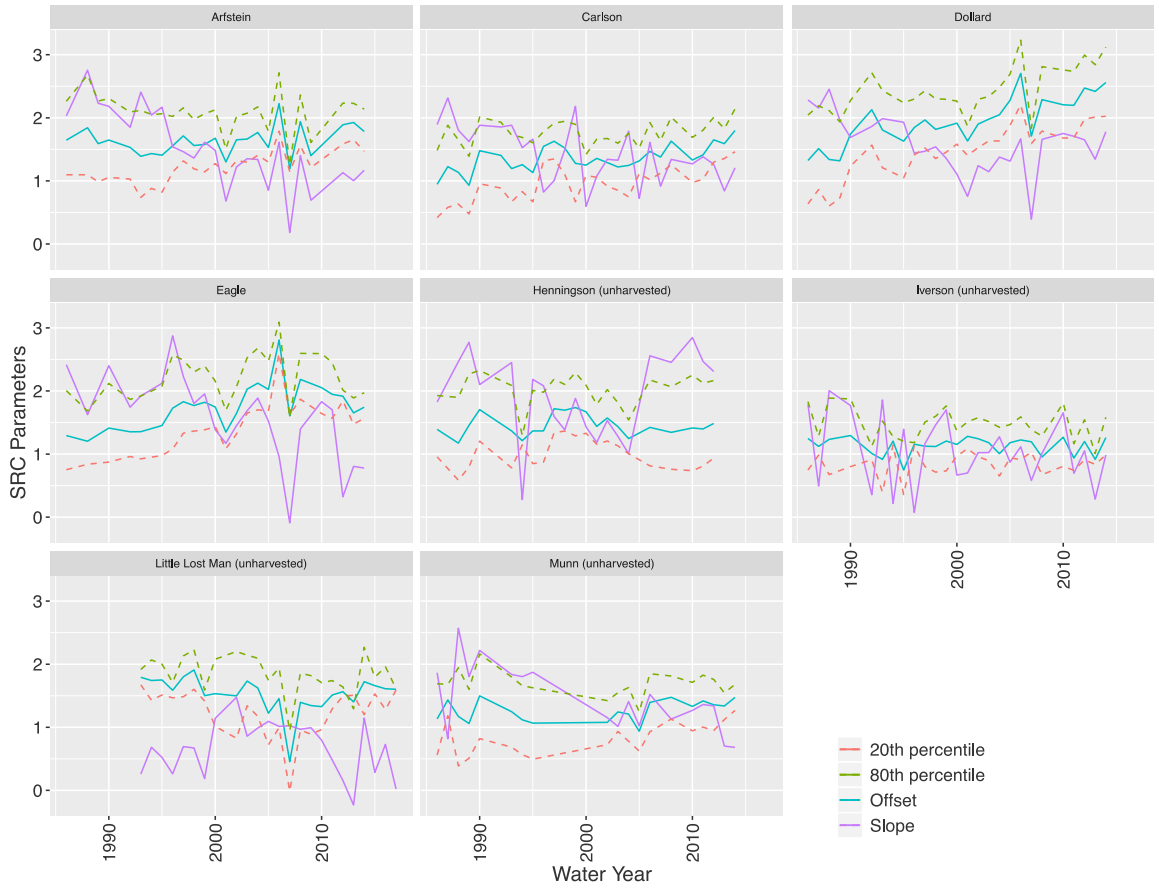


**Figure 7.** SRC offsets and slope time series plots for eight watersheds. Eagle watershed is nested in the Dollard watershed. Eagle, Dollard, Carlson, Henningson, Iverson, and Munn are all nested in the Arfstein watershed. The Little Lost Man, Henningson, Iverson, and Munn watersheds are reference watersheds. The SRC offset is plotted on a log axis.

*Random Forest Model*

Results of the RF models are described below and in Table 2. The model correctly classified 96% of SRC shapes. The model did best at classifying power relationships, correctly classify 98% of them, and moderately well at classifying threshold relationships, correctly classifying 83% of them. The kappa statistic for the model, which adjusts the percent correctly classified for random chance (ranging from 0-1), measures well, at 0.8. Overall, the SRC shape model performs remarkably well. The predictor

variables found to be most important in the model are near-channel precipitation-sensitive deep-seated landslide susceptibility, and near-channel soil erodibility. Partial dependence plots (Figure 8) show the complex relationship between each predictor variable and the probability of the SRC being classified as having a power relationship.

The RF model exploring SRC offset can explain 40% of the variance within the dataset using only two predictor variables, namely percent area harvested since 2010 and near-channel local relief. The partial dependence plots (Figure 9) generally show a linear relationship with SRC offset and percent area harvested since 2010 and a nonlinear relationship with SRC offset and near-channel local relief.

Watershed characteristics explain a moderate amount of the variance in the SRC slope. The RF model explains 39% of the variance in the dataset with estimated uplift based on dated marine terraces along the coast, mean annual precipitation, and the 2-yr, 15-minute precipitation intensity. Partial dependence plots (Figure 10) generally show an inverse linear relationship between estimated uplift and SRC slope, an inverse linear relationship between mean annual precipitation and SRC slope, and a linear relationship between precipitation intensity and SRC slope.

The multiple linear regression models, with predictor variables informed by VSURF, had an adjusted $R^2$ below 0.2 (Figure K.1). The deficient predictive power exhibited by these models, compared with the RF models, is consistent with the notion that predictor variables exhibit nonlinear relationships to the SRC parameters.

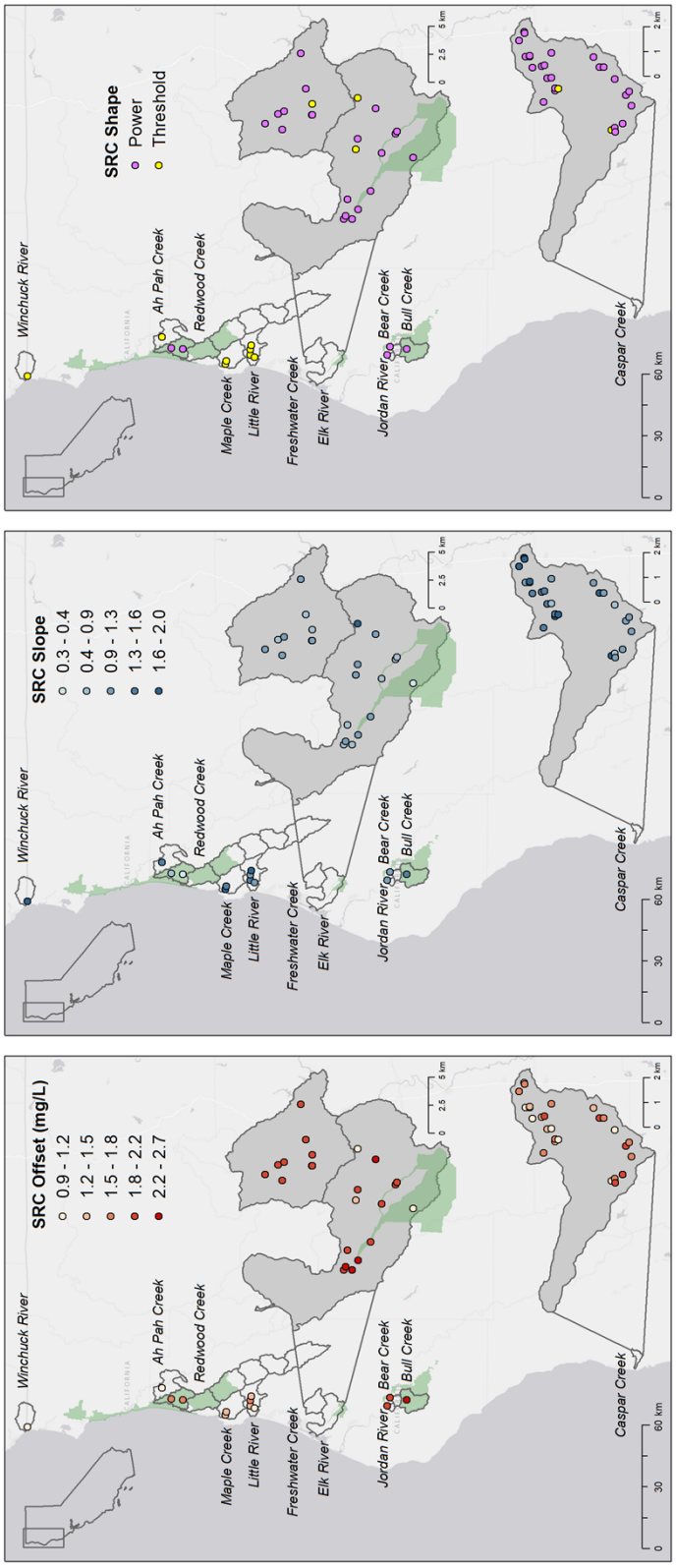


**Figure 8.** Maps showing the spatial distributions of the SRC offset (a), slope (b), and shape (c).

**Table 3**

*Predicted accuracy for the SRC Shape model is measured in Percent Correctly Classified and Percent Variance Explained for the two SRC Parameter models. Near-channel characteristics are shown in bold and land management metrics are shown in italics.*

| SRC Response Variable | Model Accuracy | Predictor Variables |
|---|---|---|
| SRC Shape | 96% | **Near-channel Precipitation Sensitive Deep-Seated Landslide Susceptibility, Near-channel Soil Erodibility** |
| SRC Offset | 40% | *Percent Area Harvested since 2010*, **Near-channel Local Relief** |
| SRC Slope | 39% | Estimated Uplift (marine terrace model), Average Precipitation (30-year normal), 2-year, 15-minute precipitation Intensity |

**Table 4**

*Confusion matrix for the RF model predicting SRC shape*

| | | Predicted Class | | | |
|---|---|---|---|---|---|
| | | Power | Threshold | % Correctly Classified | Kappa |
| Actual Class | Power | 40 | 1 | 98% | 0.8 |
| | Threshold | 1 | 5 | 83% | |

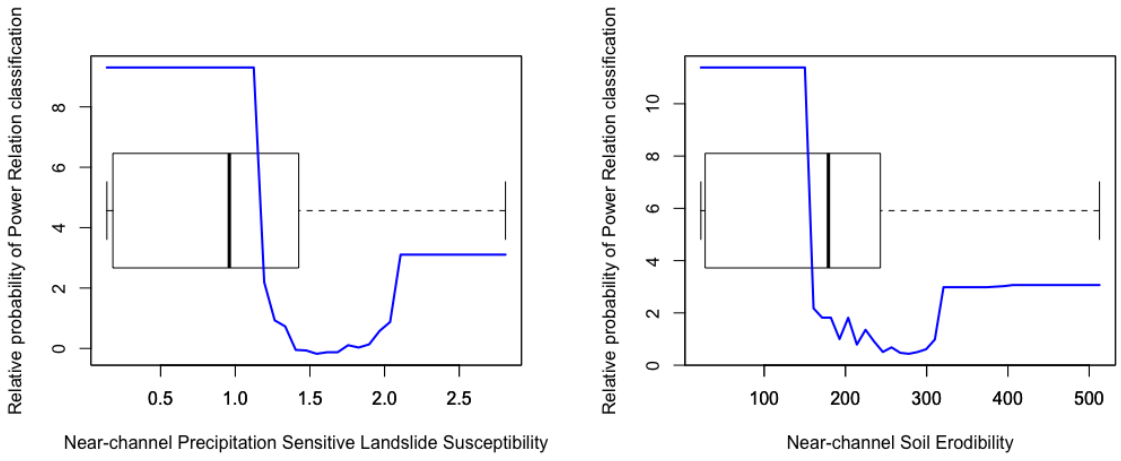


**Figure 9.** Partial dependence plots from the RF classification model for SRC shape. The y-axis shows the relative probability of SRC power relationship classification. Box-and-whisker plots show the distribution of the predictor variables.

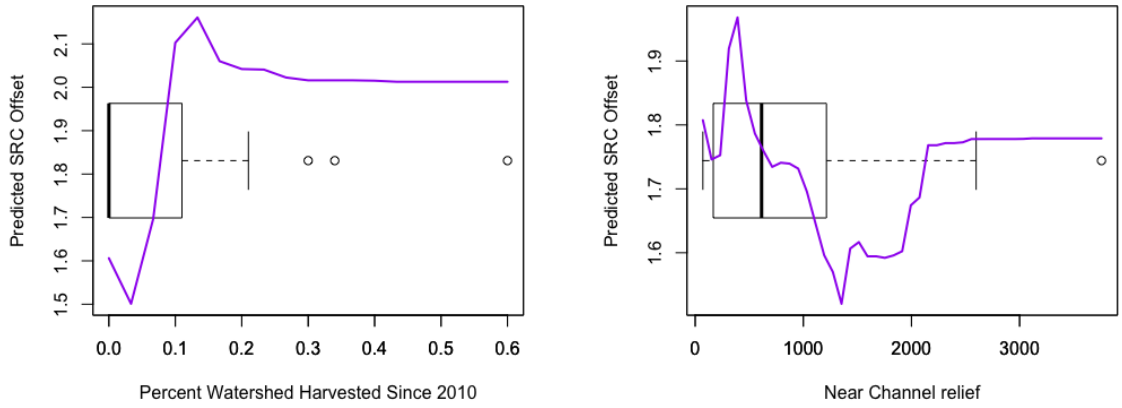


**Figure 10.** Partial dependence plots from the RF model for SRC offset. The y-axis shows the predicted offset value. Box-and-whisker plots show the distribution of the predictor variables.

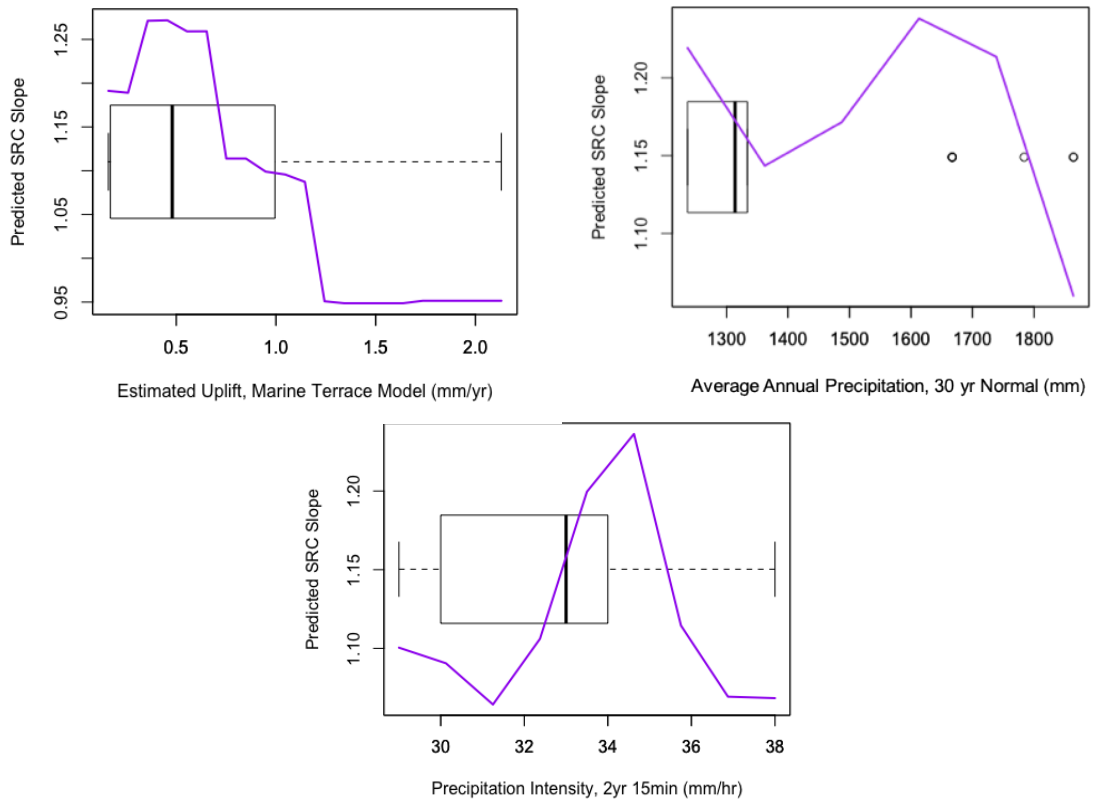


**Figure 11.** Partial dependence plots from the RF model for SRC slope. The y-axes show the predicted slope value. The x-axes show the three predictor variables used in the model. Box-and-whisker plots show the distribution of the predictor variables.

# DISCUSSION

This research aims to understand controls on discharge-suspended sediment dynamics in rivers that drain redwood forests along the northern coast of California. We find SRC relationships fall into two categories: simple power functions and threshold relationships. The absence of peaked relationships, as documented in Minnesota by Vaughan et al. (2017), indicates that sediment supply is not a strongly limiting factor at any flow rate in any of these watersheds, whether harvested or unharvested. This result is consistent with the notion that natural processes continually generate sediment through tectonic uplift and relatively erodible rock types, regardless of harvest history.

We find a latitudinal spatial pattern in the SRC parameters with the highest offset values and lowest slope values in drainages nearest the MTJ. We attribute this pattern to the rapid rates of tectonic uplift associated with the MTJ. High uplift rates create sediment sources that are easily accessed and transported at all flows, which increases the SRC offset and reduces the SRC slope. We observe a similar reduction in SRC slopes in response to extensive timber harvest in our temporal trend analysis. Specifically, sediment concentrations at low flows disproportionately increased compared to concentrations at high flows over a 20 years after timber harvest (dashed lines in Figure 6), causing SRC offsets to increase and SRC slopes to be reduced. However, this pattern could only be observed in the harvested watersheds of Casper Creek, where the sediment and flow records are sufficiently long and the experimental harvesting practices allow for us to observe the watershed response to a deliberate, punctuated disturbance. These findings are consistent with Cafferata and Reid (2013), which observed changes in in-channel geomorphic processes following timber harvest in Caspar Creek watersheds.

Furthermore, Tolorza et al. (2019) observed an increase in SRC offset and decrease in SRC slope values after an earthquake, a similar trend to what we see in harvested watersheds, possibly signaling that SRCs respond to strong tectonic activity and intense timber harvest management in similar ways.

Near-channel geomorphology strongly controls SRC shape. Specifically, near-channel precipitation-sensitive landslide susceptibility and near-channel soil erodibility were determined to be the most important predictor variables in our RF analysis. This finding supports the notion that the structural strength of the near-channel environment can strongly influence the watershed sediment regime, consistent with the findings of Vaughan et al. (2017). In our case, the structurally weak near-channel environments found in many of our watersheds establishes conditions amenable to accelerated erosion by both natural and anthropogenic processes.

The RF results of the SRC shape model do not include management or road metrics. This seems contradictory to our analysis on SRC shapes in unharvested watersheds (Bernoulli trial and power analysis), where we conclude that only power relationships are observed in unharvested watersheds, i.e. threshold relationships are only observed in harvested watershed. However, management may be a necessary but insufficient criterion for the development of a threshold relationship. Additionally, the SRC shape analysis does not address the uncertainties of spatial autocorrelation or non-stationarity within the dataset.

Although threshold SRC relationships are located throughout our study region, the majority of them are observed in Little River and Maple Creek, two neighboring watersheds. Moreover, the majority of unharvest watersheds are located in the Redwood

Creek river basin, which the Prairie Creek and Little Lost Man watersheds drain into. Neighboring watersheds are more likely to have similar geologic and soil properties, experience the same tectonic drivers, and share precipitation patterns. Additionally, the analysis does not account for nested watersheds, which experience more spatial autocorrelation than neighboring basins. Therefore, a deeper analysis of SRC shape is needed to make a non-conditional conclusion.

Uplift rates and precipitation patterns were the most important predictor variables found to influence SRC slope. Increased uplift rates amplify hillslope erosion processes, which respond to precipitation patterns in highly nonlinear ways, making sediment more available through surface erosion and landslides. Notably, none of the timber harvest, road, or land management practice predictor variables appear to be relevant to predicting SRC slope, again consistent with the findings of Vaughan et al. (2017).

Timber harvest activity and near-channel local relief were the two most important predictor variables found to influence SRC offset values. Timber harvest activity removes vegetation from the landscape and may increase erosion and sediment delivery through decreased interception, soil-water plant uptake, slope stability, and root cohesion. These processes alter sediment supplies and change the SRC. Again, these findings are consistent with Vaughan et al. (2017), who found that SRC offset and suspended sediment concentration under low flow conditions were the only aspects of the SRC that were influenced by land use.

Our RF model can predict SRC shape with 96% accuracy. Our other models for SRC slope and offset explain about 40% of the variance in the dataset, which are in the range of previous studies (Syvitski et al., 2000; Vaughan et al., 2017; Tolorza et al.,

2019). Several factors may contribute to this moderate model accuracy value, including errors in water or sediment measurements, errors or biases in how the extracted predictor metrics characterize the relevant processes or environmental conditions, or lack of data to represent factors that we know to be important. Additionally, some error could be introduced from spatial autocorrelation among watersheds within the same larger basin with some watersheds nested in another. Other errors include slight variations in sampling methods between data sources and legacy timber harvest effects on watersheds classified as unharvested.

Our data sources have similar suspended sediment data collection methods which differ slightly. Samples were collected using ISCO automated samplers with a discharge or turbidity threshold, collected at varying intervals. Differing threshold values between data sources can lead to inaccurate comparisons of data.

Another sources of error could be accounted for by our classification of 'unharvested' watersheds. All but one of our 'unharvested' watersheds have been harvested by some measure, at some time. The only watershed within our study that contains 100% old-growth is the Little South Fork (Elk River) located in the Headwaters Forest Reserve. The two watersheds in Redwood National Park used in the RF model consist of 89% and 90% old-growth forest and the Bull creek watershed, protected in the Humboldt Redwood State Park, consists of 16% old-growth forest. The classified 'unharvested' watersheds in Caspar Creek were harvested in the mid-1980s and consist of second-growth forest. Legacy sediment sources from past harvest activity may still be in these watersheds and influencing sediment regimes. However, these watersheds are the clearest windows we have to pre-harvest watershed conditions.

Perhaps the most challenging predictor variable to constrain is uplift rates throughout the study area. The tectonic setting of our study watersheds is highly complex and challenging to model at the small spatial scale that is relevant for our watersheds. For this reason, we attempted to use two different models of uplift along the Coast Range, both of which are relatively coarse in resolution. The model that provided the most useful predictor variable estimated uplift rates based on dated marine terraces along the coast (Merritts and Bull, 1989; Merritts et al., 1994; Snyder et al., 2000; Stallman and Kelsey, 2006; Padgett, 2013; Moon et al., 2018). However, we have no way of knowing how well these rates represent tectonic activity further inland. Additionally, multiple regional tectonic drivers are influencing different watersheds within this study, with uplift in Caspar Creek likely driven by a lingering portion of the Farallon Plate and uplift in the Lower Eel effected by complex interactions between the Gorda and North American plates (Lock et al., 2006). Moreover, these systems may be responding to movement on individual faults or local tectonic forces, which may not follow the broader regional trend. Further exploration of tectonic activity is needed to better understand the complex dynamics of this landscape.

Timber harvest activity is difficult to constrain and represent accurately. This is especially true for timber harvest prior to 1985. We calculated the percent area harvested as a metric for harvest activity. However, we were not able to decipher between harvesting methods, some of which may impact erosional and sediment delivery more than others. Additionally, we could not account for timber harvest activity before 1985 due to lack of available detailed data. This limits our study to focus on current management practices and not account for historic timber activity that influenced these

systems. An in-depth, large-scale exploration of these factors within this study site would greatly inform these uncertainties but is beyond the scope of this study.

## POLICY AND MANAGEMENT IMPLICATIONS

The North Coast of California is highly erodible due to structurally weak geology and constant tectonic activity. Discharge-suspended sediment relationships with these watersheds are strongly controlled by these factors, and regulations regarding sediment need to account for them. Furthermore, an unconstrainable amount of geomorphic uncertainty is inherently present within these systems due to the long history of timber harvest practices. Legacy sediments within these systems need to be noted and addressed when making policy and managing these watersheds.

## CONCLUSION

No previous studies have considered both timber harvest practices and tectonic forcing in attempting to explain the observed spatial patterns in sediment production. Our research explores these high-order controls on sediment production through SRC exploration. We did not find any sediment limited watersheds within our study sites. Additionally, we find suspended sediment concentrations at low flows disproportionately adjusting to harvest activity compared to concentrations at higher flows. Furthermore, we find near-channel morphology to be a strong predictor of SRC shape; land management, and near-channel metrics control SRC offset; and uplift and precipitation patterns control SRC slope. Our findings further the understanding of controls on discharge-suspended sediment relationships and can inform policymakers and land managers.

# REFERENCES

"34th Annual Salmonid Restoration Conference." *Salmon Creek Watershed, from Headwaters Forest Reserve to Humboldt Bay National Wildlife Refuge | Salmonid Restoration Federation*, www.calsalmon.org/programs/events/salmon-creek-watershed-headwaters-forest-reserve-humboldt-bay-national-wildlife.

Adams, M. B., Loughry, L., Plaugher, L. (2004). Experimental Forests and Ranges of the USDA Forest Service. Gen. Tech. Rep. NE-321. Newtown Square, PA: U.S. Department of Agriculture, Forest Service, Northeastern Research Station. www.fs.fed.us/psw/ef/caspar_creek/index.shtml.

Ahnert, F. (1970). Functional relationships between denudation, relief, and uplift in large, mid-latitude drainage basins. American Journal of Science, 268(3), 243-263.

Asselman, N. E. M. (2000). Fitting and interpretation of sediment rating curves. Journal of Hydrology, 234(3-4), 228-248.

Balco, G., Finnegan, N., Gendaszek, A., Stone, J. O., & Thompson, N. (2013). Erosional response to northward-propagating crustal thickening in the coastal ranges of the US Pacific Northwest. American Journal of Science, 313(8), 790-806.

Belmont, P. (2011). Floodplain width adjustments in response to rapid base level fall and knickpoint migration. Geomorphology, 128(1-2), 92-102.

Bilotta, G. S., & Brazier, R. E. (2008). Understanding the influence of suspended solids on water quality and aquatic biota. Water Research, 42(12), 2849-2861.

Bonnin, G. M., Martin, D., Lin, B., Parzybok, T., Yekta, M., & Riley, D. (2006). Precipitation-frequency atlas of the United States. NOAA atlas, 14(2), 1-65.

Cafferata, P. H., & Reid, L. M. (2013). Applications of long-term watershed research to forest management in California: 50 years of learning from the Caspar Creek experimental watersheds. State of California, The Natural Resources Agency, Department of Forestry & Fire Protection.

Cashman, S. M., Kelsey, H. M., & Harden, D. R. (1995). Geology of the Redwood Creek Basin, Humboldt County, California. Geomorphic processes and aquatic habitat in the Redwood Creek basin, northwestern California. US Geol. Surv. Prof. Pap, 1454.

Cutler, A., Cutler, D. R., & Stevens, J. R. (2012). Random forests. In Ensemble machine learning (pp. 157-175). Springer, Boston, MA.

Cutler, D. R., Edwards, T. C., Beard, K. H., Cutler, A., Hess, K. T., Gibson, J., & Lawler, J. J. (2007). Random forests for classification in ecology. Ecology, 88(11), 2783-2792.

Daly, C., Halbleib, M., Smith, J. I., Gibson, W. P., Doggett, M. K., Taylor, G. H., ... & Pasteris, P. P. (2008). Physiographically sensitive mapping of climatological temperature and precipitation across the conterminous United States. International Journal of Climatology: a Journal of the Royal Meteorological Society, 28(15), 2031-2064.

Daly, C., Neilson, R. P., & Phillips, D. L. (1994). A statistical-topographic model for mapping climatological precipitation over mountainous terrain. Journal of applied meteorology, 33(2), 140-158.

Dierckx, P. (1975). An algorithm for smoothing, differentiation and integration of experimental data using spline functions. Journal of Computational and Applied Mathematics, 1(3), 165-184.

Donovan, M., Miller, A., Baker, M., & Gellis, A. (2015). Sediment contributions from floodplains and legacy sediments to Piedmont streams of Baltimore County, Maryland. Geomorphology, 235, 88-105.

Ferrier, Ken L., *unpublished data*

Ferrier, Ken L., James W. Kirchner, and Robert C. Finkel. 2005. "Erosion rates over millennial and decadal timescales at Caspar Creek and Redwood Creek, northern California Coast Ranges." Earth Surface Processes and Landforms 30, no. 8 (2005): 1025-1038.

Final 2014/2016 California Integrated Report (Clean Water Act Section 303(d) List / 305(b) Report (2016). Impaired Water Bodies, State Water Resource Control Board, California Environmental Protection Agency. https://www.waterboards.ca.gov/water_issues/programs/tmdl/integrated2014_2016.shtm Accessed July 7, 2018.

Furlong, K. P., & Govers, R. (1999). Ephemeral crustal thickening at a triple junction: The Mendocino crustal conveyor. Geology, 27(2), 127-130.

Genuer, R., Poggi, J. M., & Tuleau-Malot, C. (2016). VSURF: variable selection using random forests. R package version, 1(3).

Graham, R. & O'Green, T. (2016) Geomorphology and Soils (Chapter Four). In: Mooney, H., & Zavaleta, E. (eds) Ecosystems of California (pp. 47-73). Univ of California Press.

Harden, D. R. (1998). California geology. Prentice Hall.

Henley, W. F., Patterson, M. A., Neves, R. J., & Lemly, A. D. (2000). Effects of sedimentation and turbidity on lotic food webs: a concise review for natural resource managers. Reviews in Fisheries Science, 8(2), 125-139.

Henry, N. (1998). Overview of the Caspar Creek watershed study. In: Ziemer, Robert R., technical coordinator. Proceedings of the conference on coastal watersheds: the Caspar Creek story, 6 May 1998; Ukiah, California. General Tech. Rep. PSW GTR-168. Albany, California: Pacific Southwest Research Station, Forest Service, US Department of Agriculture: 1-9 (Vol. 168).

Howard, J. & Merrifield, M. (2010). Mapping Groundwater Dependent Ecosystems in California. PLoS One, 5, e11249. http://dx.plos.org/10.1371/journal.pone.0011249.

Hydrologic Year 2016 Hydrology Monitoring Submittal Report. Humboldt Redwood Company, 2016.

Iacobellis, S. F., et al., (2016) Climate (Chapter Two). In: Mooney, H., & Zavaleta, E. (eds) Ecosystems of California (pp. 9-25). Univ of California Press.

Keppeler, E. T., & Ziemer, R. R. (1990). Logging effects on streamflow: water yield and summer low flows at Caspar Creek in northwestern California. Water resources research, 26(7), 1669-1679

Klein, R. D., Lewis, J., & Buffleben, M. S. (2012). Logging and turbidity in the coastal watersheds of northern California. Geomorphology, 139, 136-144.

Klein, R. D., & Ozaki, V. (2017). Effects of logging road removal on suspended sediment loads and turbidity. Gen. Tech. Rep. PSW-GTR-258. Albany, CA: US Department of Agriculture, Forest Service, Pacific Southwest Research Station: 203-214, 258, 203-214.

Lane, B. A., Dahlke, H. E., Pasternack, G. B., & Sandoval-Solis, S. (2017). Revealing the diversity of natural hydrologic regimes in California with relevance for environmental flows applications. Journal of the American Water Resources Association, 53(2), 411-430.

Langbein, W. B., & Schumm, S. A. (1958). Yield of sediment in relation to mean annual precipitation. Eos, Transactions American Geophysical Union, 39(6), 1076-1084.

Lewis, J. (1998). Evaluating the impacts of logging activities on erosion and suspended sediment transport in the Caspar Creek watersheds. In: Ziemer, Robert R., technical coordinator. Proceedings of the conference on coastal watersheds: The Caspar Creek story, 6 May 1998; Ukiah, California. General Tech. Rep. PSW GTR-168. Albany, California: Pacific Southwest Research Station, Forest Service, US Department of Agriculture: 55-69 (Vol. 168).

Liaw, A., & Wiener, M. (2002). Classification and regression by randomForest. R news, 2(3), 18-22.

Lock, J., Kelsey, H., Furlong, K., & Woolace, A. (2006). Late Neogene and Quaternary landscape evolution of the northern California Coast Ranges: Evidence for Mendocino triple junction tectonics. Geological Society of America Bulletin, 118(9-10), 1232-1246.

"Management Plan." *Management Plan*, Humboldt Redwood Company, 2016, https://www.hrcllc.com/sites/default/files/inline-files/HRC-Management-Plan_7_2016.pdf

The National Map. *National Geospatial Program*. 19 Aug. 2019 <https://www.usgs.gov/core-science-systems/national-geospatial-program/national-map>.

Merritts, D., & Bull, W. B. (1989). Interpreting Quaternary uplift rates at the Mendocino triple junction, northern California, from uplifted marine terraces. Geology, 17(11), 1020-1024.

Merritts, D. J., Vincent, K. R., & Wohl, E. E. (1994). Long river profiles, tectonism, and eustasy: A guide to interpreting fluvial terraces. Journal of Geophysical Research: Solid Earth, 99(B7), 14031-14050.

Moon, S., Merritts, D. J., Snyder, N. P., Bierman, P., Sanquini, A., Fosdick, J. C., & Hilley, G. E. (2018). Erosion of coastal drainages in the Mendocino Triple Junction region (MTJ), northern California. Earth and Planetary Science Letters, 502, 156-165.

Mooney, H., & Dawson, T. E. (2016) Coast Redwood Forests (Chapter Twenty-Six). In: Mooney, H., & Zavaleta, E. (eds) Ecosystems of California (pp. 535-552). Univ of California Press.

Montgomery, D. R., & Brandon, M. T. (2002). Topographic controls on erosion rates in tectonically active mountain ranges. Earth and Planetary Science Letters, 201(3-4), 481-489.

Mueller, E. R., & Pitlick, J. (2013). Sediment supply and channel morphology in mountain river systems: 1. Relative importance of lithology, topography, and climate. Journal of Geophysical Research: Earth Surface, 118(4), 2325-2342.

Napolitano, M. B. (1998). Persistence of historical logging impacts on channel form in mainstem North Fork Caspar Creek. In: Ziemer, Robert R., technical coordinator. Proceedings of the conference on coastal watersheds: The Caspar Creek story, 6 May 1998; Ukiah, California. General Tech. Rep. PSW GTR-168. Albany,

California: Pacific Southwest Research Station, Forest Service, US Department of Agriculture: 97-101 (Vol. 168).

National Hydrography Dataset, U.S. Geological Survey, Reston, Virginia. 2002-2016, https://www.epa.gov/waterdata/nhdplus-national-hydrography-dataset-plus.

National Park Service (2018). Restoration Through Selective Thinning. U.S. Department of the Interior, www.nps.gov/redw/learn/nature/forestthinning.htm.

Norris, R. M., & Webb, R. W. (1990). Geology of California. New York: J. Wiley.

Noss, R. F. (1999). The redwood forest: history, ecology, and conservation of the coast redwoods. Island Press.

Olson, J.R. and Hawkins, C.P., 2014, Geochemical Characteristics of the Conterminous United States: U.S. Geological Survey data release, http://dx.doi.org/10.5066/F7X0653P.

Ouimet, W. B., Whipple, K. X., & Granger, D. E. (2009). Beyond threshold hillslopes: Channel adjustment to base-level fall in tectonically active mountain ranges. Geology, 37(7), 579-582.

Power, M. E., Kupferberg, S. J., Cooper, S. D., & Deas, M. L. (2016) Rivers (Chapter Thirty-Three). In: Mooney, H., & Zavaleta, E. (eds) Ecosystems of California (pp. 713-752). Univ of California Press.

"Programs: National Conservation Lands: California: Headwaters Forest Reserve." *Headwaters Forest Reserve | Bureau of Land Management*, 15 Aug. 2019, www.blm.gov/programs/national-conservation-lands/california/headwaters-forest-reserve.

"Responsible Forestry." *Responsible Forestry*, Green Diamond Resource Company, 2019, www.greendiamond.com/responsible-forestry/.

Riebe, C. S., Kirchner, J. W., Granger, D. E., & Finkel, R. C. (2001). Strong tectonic and weak climatic control of long-term chemical weathering rates. Geology, 29(6), 511-514.

Roering, J. J., Kirchner, J. W., & Dietrich, W. E. (1999). Evidence for nonlinear, diffusive sediment transport on hillslopes and implications for landscape morphology. Water Resources Research, 35(3), 853-870.

Sawyer, J. O., Gray, J., West, J. G., Thornburgh, D. A., Noss, R. F., Engbeck, J. H. Jr., Marcot, B. G., & Raymond, R. (2000). History of Redwood and Redwood Forests (Chapter Two). In: Noss, R. F. (ed) The Redwood Forest. Washington, DC: IslandPress.

Snyder, N. P., Whipple, K. X., Tucker, G. E., & Merritts, D. J. (2000). Landscape response to tectonic forcing: Digital elevation model analysis of stream profiles in the Mendocino triple junction region, northern California. Geological Society of America Bulletin, 112(8), 1250-1263.

Stallman, J.D.; Kelsey, H. 2006. Transient geomorphic response to late Pleistocene baselevel change and climate forcing in the southern Cascadia thrust-and-fold belt, north central California. Handout for Friends of the Pleistocene Guidebook, 6 pp. plus figures and tables.

Stewart, W., Sharma, B., York, R., Diller, L., Hamey, N., Powell, R., Swiers, R. (2016) Forestry (Chapter Thirty-Six). In: Mooney, H., & Zavaleta, E. (eds) Ecosystems of California (pp. 817-833). Univ of California Press.

Schwanghart, W., Scherler, D. (2014): TopoToolbox 2 – MATLAB-based software for topographic analysis and modeling in Earth surface sciences. Earth Surface Dynamics, 2, 1-7. [DOI: 10.5194/esurf-2-1-2014]

Schwanghart, W., Kuhn, N. J. (2010): TopoToolbox: a set of Matlab functions for topographic analysis. Environmental Modelling & Software, 25, 770-781. [DOI: 10.1016/j.envsoft.2009.12.002]

Schwartz, J. S., Simon, A., & Klimetz, L. (2011). Use of fish functional traits to associate in-stream suspended sediment transport metrics with biological impairment. Environmental Monitoring and Assessment, 179(1-4), 347-369.

Syvitski, J. P., Morehead, M. D., Bahr, D. B., & Mulder, T. (2000). Estimating fluvial sediment transport: the rating parameters. Water Resources Research, 36(9), 2747-2760.

Tolorza, V., Mohr, C. H., Carretier, S., Serey, A., Sepúlveda, S. A., Tapia, J., & Pinto, L. (2019). Suspended Sediments in Chilean Rivers Reveal Low Postseismic Erosion After the Maule Earthquake (Mw 8.8) During a Severe Drought. Journal of Geophysical Research: Earth Surface.

USDA NRCS and Esri, USA Soils Erodibility Factor. Created: 2015, Updated: 2019. https://www.arcgis.com/home/item.html?id=28e9f476324b486bacaaee7f9fcb77dc

Vaughan, A.A., Belmont, P., Hawkins, C.P., Wilcock, P.R., (2017) Near-channel versus watershed controls on sediment rating curves. Journal of Geophysical Research – Earth Surface. 122. https://doi.org/10.1002/2016JF004180.

Walter, R. C., & Merritts, D. J. (2008). Natural streams and the legacy of water-powered mills. Science, 319(5861), 299-304.

Warrick, J. A. (2015). Trend analyses with river sediment rating curves. Hydrological Processes, 29(6), 936-949.

Willett, S. D., S. W. McCoy, J. Taylor Perron, L. Goren, and C. -Y Chen. (2014), Dynamic reorganization of river basins. Science 343 (6175). doi:10.1126/science.1248765.

Wills C.J., Perez, F., Gutierrez, C., 2011, Susceptibility to deep-seated landslides in California: California Geological Survey, Map Sheet 58, http://www.conservation.ca.gov/cgs/Documents/library-publications/MS58.pdf. https://www.arcgis.com/home/item.html?id=3cdc744bec6b45c28206e472e8ad0f89

Wilzbach, P., & Ozaki, V. (2017). Fisheries and aquatic resources of Prairie Creek, Redwood National Park (No. NPS/REDW/NRR—2017/1492). National Park Service.

Wobus, C., Whipple, K. X., Kirby, E., Snyder, N., Johnson, J., Spyropolou, K., ... & Willett, S. D. (2006). Tectonics from topography: Procedures, promise, and pitfalls. Special papers-geological society of america, 398, 55.

Wood, P. J., & Armitage, P. D. (1997). Biological effects of fine sediment in the lotic environment. Environmental management, 21(2), 203-217.

Ziemer, R. R. (1992). Effect of logging on subsurface pipeflow and erosion: coastal northern California, USA. In: Erosion, Debris Flows and Environment in Mountain Regions, Proceedings of the Chendu Symposium, July 1992, Chendu, China. International Association of Hydrological Sciences Publication no. 209. Wallingford, UK; 187-197.

# APPENDICES

Appendix A. Sediment Rating Curve Code

```
# written in R
# code to plot SRC and calculate slope and vertical offset

# created 1/16/2019 - way too late into my thesis...but what the hell
# created by Adam Fisher

#####

## install packages
# install.packages("readxl")
# install.packages("ggplot2")
# install.packages("Scale")
# install.packages('EnvStats')

library(readxl)
library(ggplot2)
library(scales)
library(EnvStats)

# sediment rating curve function

sed.rc <- function(wd, wtshd, fn){ # inputs: working directory (QSS_data_and_Analysis), watershed name, and file name - NO underscores
  # setwd(wd) # Need to set working directory

  # read in file from wd, wtshd, and fn
  fn.spl <- strsplit(fn, ' ')[[1]]

  if (length(fn.spl) == 1){
    ff <- paste(wd, wtshd, fn, sep = "/")
    fp <- paste0(paste(wd,  wtshd, fn, fn, sep='/'), '.xlsx')

  } else if (length(fn.spl) == 2){
    fn.under <- paste0(fn.spl[1], '_', fn.spl[2])
    ff <- paste(wd, wtshd, fn.under, sep = "/")
    fp <- paste0(paste(wd, wtshd, fn.under, fn.under, sep = "/"), '.xlsx') # filepath to excel file

  } else if (length(fn.spl) == 3){
    fn.under <- paste0(fn.spl[1], '_', fn.spl[2], '_', fn.spl[3])
    ff <- paste(wd, wtshd, fn.under, sep = "/")
    fp <- paste0(paste(wd, wtshd, fn.under, fn.under, sep = "/"), '.xlsx') # filepath to excel file
```

```
  } else if (length(fn.spl) == 4){
    fn.under <- paste0(fn.spl[1], '_', fn.spl[2], '_', fn.spl[3], '_', fn.spl[4])
    ff <- paste(wd, wtshd, fn.under, sep = "/")
    fp <- paste0(paste(wd, wtshd, fn.under, fn.under, sep = "/"), '.xlsx') # filepath to excel
file
  }

  df <- read_xlsx(fp, col_names = TRUE) # read in excel file information
  sub.df <- df[,2:4] #subset df to only include timestamp, Q, and SS
  names(sub.df) <- c('timestamp','Sample Discharge','ss (mg/L)') # remove cfs or cms
from Sample Discharge column

  low <- as.numeric(df[5,9]) # extract low flow number
  samQ <- sub.df$'Sample Discharge' # creat sample discharge matrix
  samQ <- samQ[!is.na(samQ)] # remove NAs

  # extract geomean of SAMPLE FLOW
  geomean <- geoMean(samQ)

  log_Qgm <- sapply(samQ/geomean, log10) # log transform Q/Qgm
  log_ss <- sapply(df$`SS (mg/L)`, log10) # log transform ss
  Qgm <- samQ/geomean # non-log transform Q/Qgm
  ss <- df$`SS (mg/L)` # non-log transform ss

  # remove na from lists
  log_Qgm <- log_Qgm[!is.na(log_Qgm)]
  log_ss <- log_ss[!is.na(log_ss)]
  Qgm <- Qgm[!is.na(Qgm)]
  ss <- ss[!is.na(ss)]

  # merge
  log_t <- as.data.frame(cbind(log_Qgm, log_ss)) # merge log_Qgm and log_ss
  t <- as.data.frame(cbind(Qgm,ss))

  # weight values for high and low flows
  for (i in 1:nrow(log_t)){
    if (log_t$log_Qgm[i] <= low){
      log_t[i,3] <- 1  # low flows are weighted 1
      log_t[i,4] <- 0  # high flows are weighted 0 so they are not counted toward low flow
regression

    } else {
      log_t[i,3] <- 0
      log_t[i,4] <- 1
    }
  }
```

```
  # combine indicated high and lowflows to non-transformed data
  t <- cbind(t, log_t$V3, log_t$V4)
  colnames(t) <- c('qgm','ss','low', 'high')

  # convert to facors to be able to seporate by color (plot)
  t$low <- as.factor(t$low)
  t$high <- as.factor(t$high)

  # generate regression equations: code edited from
https://stackoverflow.com/questions/7549694/adding-regression-line-equation-and-r2-on-
graph
  lf.m <- lm(log_ss~log_Qgm, log_t, weights = V3); # LOW FLOW regression
  lf.eq <- substitute(SS == a %*% (Q/Qgm)**b,
                      list(a = round(coef(lf.m)[1],1),
                           b = round(coef(lf.m)[2],1)))

  hf.m <- lm(log_ss~log_Qgm, log_t, weights = V4); # HIGH FLOW regression
  hf.eq <- substitute(SS == a %*% (Q/Qgm)**b,
                      list(a = round(coef(hf.m)[1],1),
                           b = round(coef(hf.m)[2],1)))

  #### plot using ggplot2 with non-transformed values
  g <- ggplot(t, aes(x=Qgm, y=ss, color=low)) +
    geom_point(alpha=0.2) +
    geom_smooth(method=lm, se=FALSE)+
    labs(title = fn, x='Q/Qgm', y='SS (mg/L)') + # add axis labels and title
    theme(plot.title = element_text(face ='bold', size=30),
          axis.title = element_text(size=15),
          axis.text = element_text(size = 13))+
    scale_x_continuous(trans = log10_trans(), # add log x axis indices
                       breaks = trans_breaks("log10", function(x) 10^x),
                       labels = trans_format("log10", math_format(10^.x)),
                       limits = c(.0001,1000)) +
    scale_y_continuous(trans = log10_trans(), # add log y axis indices
                       breaks = trans_breaks("log10", function(x) 10^x),
                       labels = trans_format("log10", math_format(10^.x)),
                       limits = c(.1,100000)) +
    theme(legend.position="none") # remove legend

  if (low == -10){
    g.power <- g + annotate('text', x = .0001, y = 40000, # add TEXT
                            label = "F:",
                            color = '#F8766D',
                            hjust = 0, size = 7) +
      annotate('text', x = 0.0005, y = 40000, # add FLOW equation on plot
```

```
            label = as.character(as.expression(hf.eq)),
            color = '#F8766D',
            hjust = 0, size = 7, parse = TRUE)

   g.power # view power trend SRC
   ggsave(filename = 'SRC.sam.png', width = 7, height = 7, path = ff) # save fdc to
propper file path

  } else {

   g.thresh <- g + annotate('text', x = .0001, y = 40000, # add TEXT
                        label = "HF:",
                        color = '#F8766D',
                        hjust = 0, size = 7) +
     annotate('text', x = .0001, y = 20000, # add TEXT
            label = "LF:",
            color = '#00BFC4',
            hjust = 0, size = 7) +
     annotate('text', x = 0.0005, y = 40000, # add HIGH FLOW equation on plot
            label = as.character(as.expression(hf.eq)),
            color = '#F8766D',
            hjust = 0, size = 7, parse = TRUE) +
     annotate('text', x = 0.0005, y = 20000, # add LOW FLOW equation on plot
            label = as.character(as.expression(lf.eq)),
            color = '#00BFC4',
            hjust = 0,size = 7, parse = TRUE)

   g.thresh # view threshold trend SRC
   ggsave(filename = 'SRC.sam.png', width = 7, height = 7, path = ff) # save fdc to
propper file path
  }
}

# filepath to working directory
# Watershed name (NO spaces)
# gage name (no underscores)

sed.rc(wd = '/Volumes/ACNF2/GSchool/NorCal/QSS_Data_and_Analysis',
       wtshd = 'CasparCreek', fn = 'South Fork')
```

# Appendix B. Discharge Normalization Comparison

We compared normalizing SRC discharge by two values, the geometric mean of the suspended sediment sample discharge and the total measured flow within the sampling period (Figure E.1). The autocorrelation between the SRC offset and slope parameters for all watersheds, when normalized by the geometric mean of the sample discharge, is -0.44. And the autocorrelation between the parameters when normalized by the geometric mean of the total discharge is -0.76. We proceeded with the method that reduced the autocorrelation between the parameters.

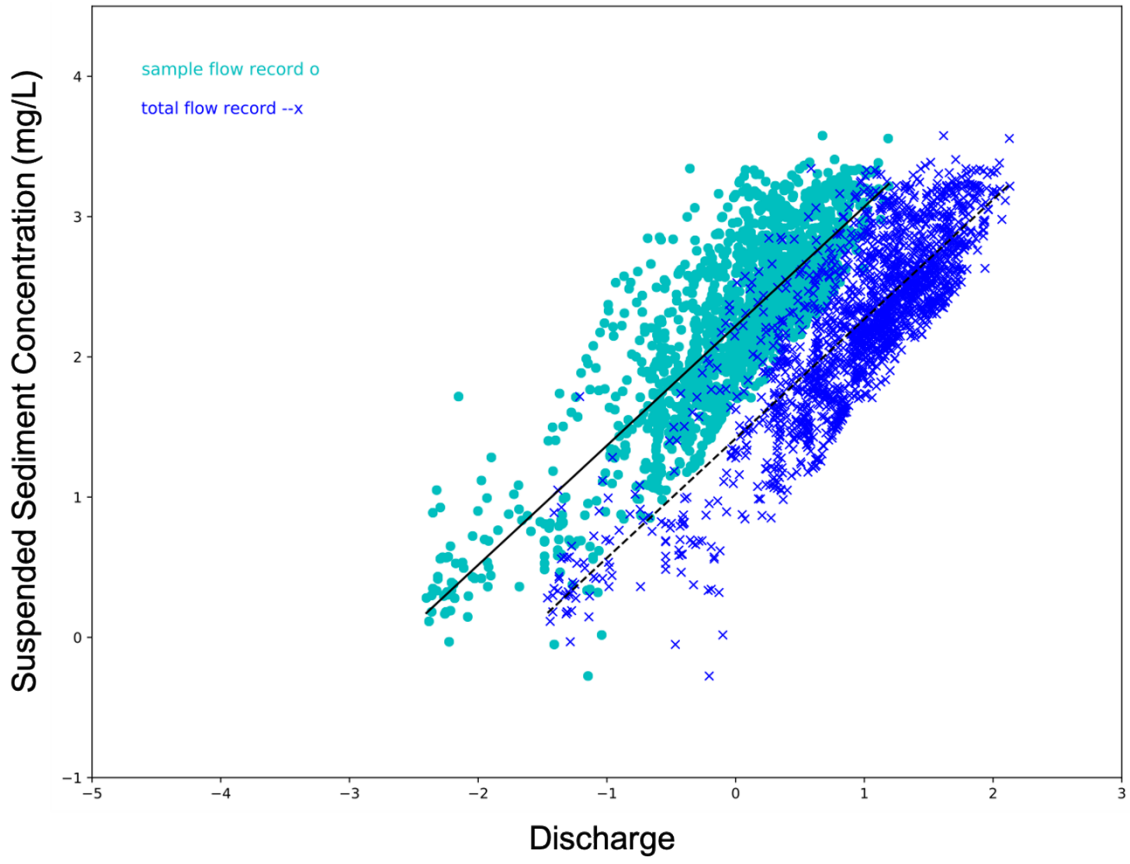


**Figure B.1.** A SRC normalized by the geometric mean of the suspended sediment sample discharge and the total measured flow within the sampling period.

Appendix C. Sediment Rating Curves for All Study Watersheds

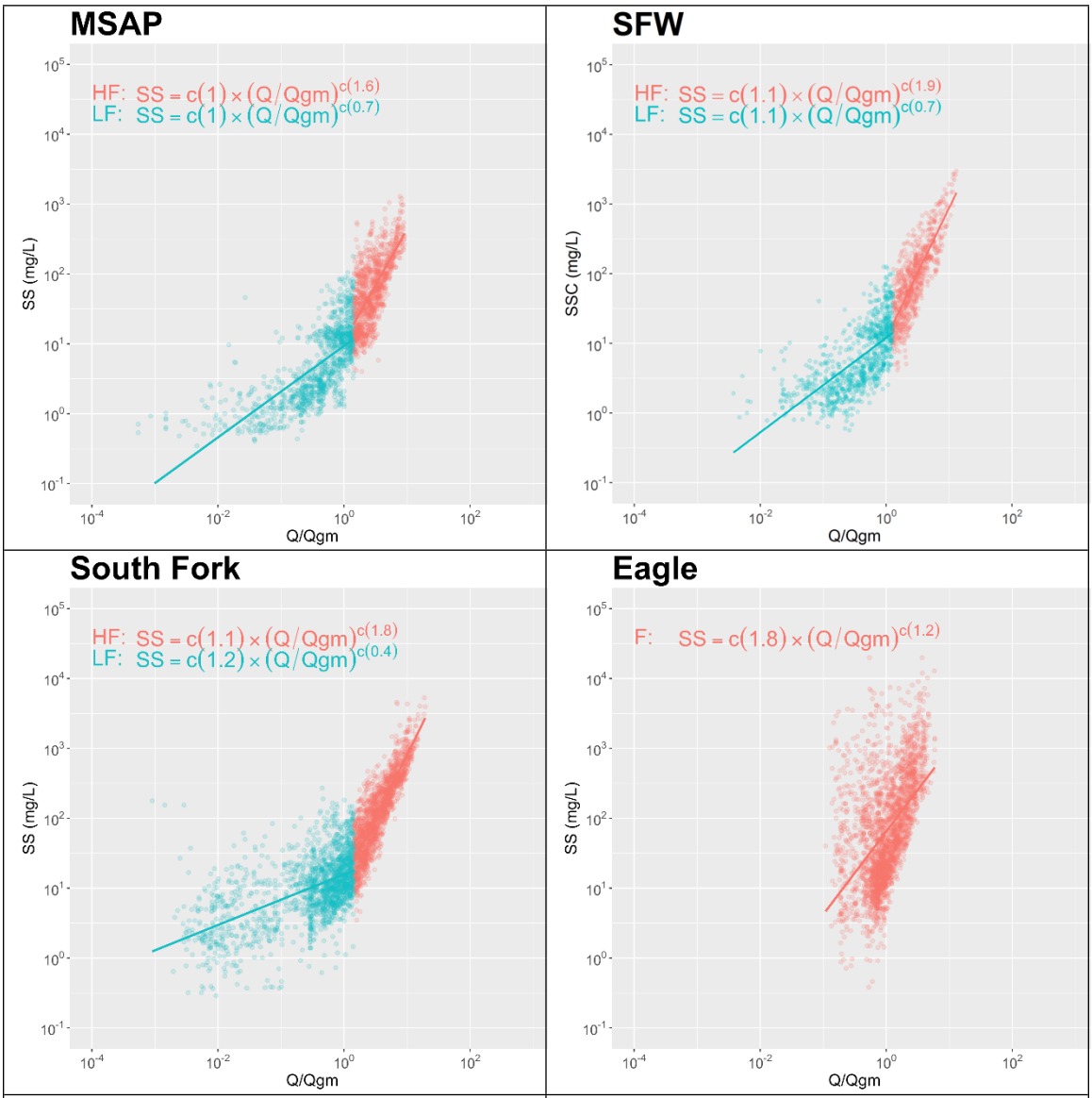


**Figure C.1.** All SRC used in this study,

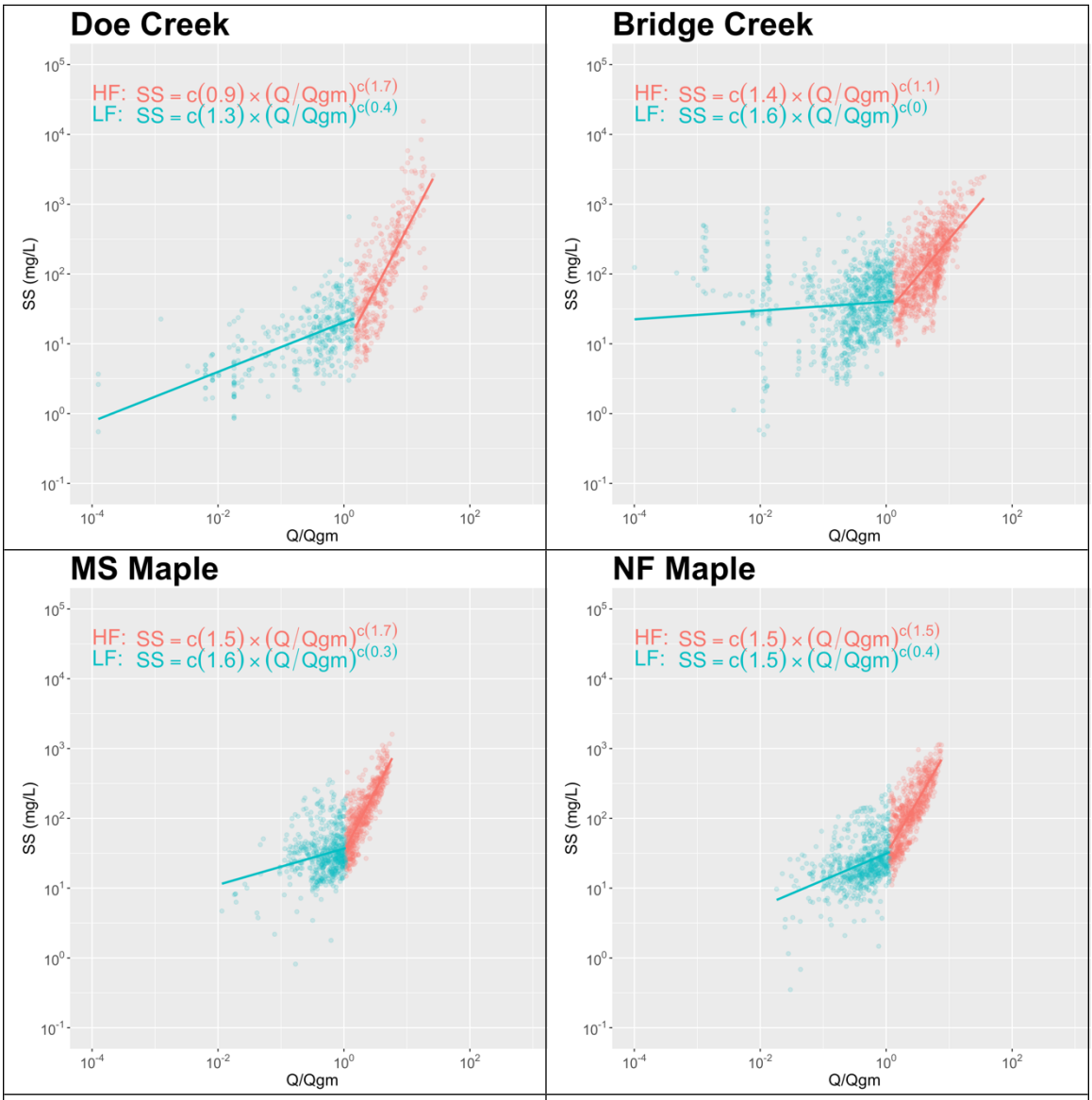


**Figure C.1.** (cont.)

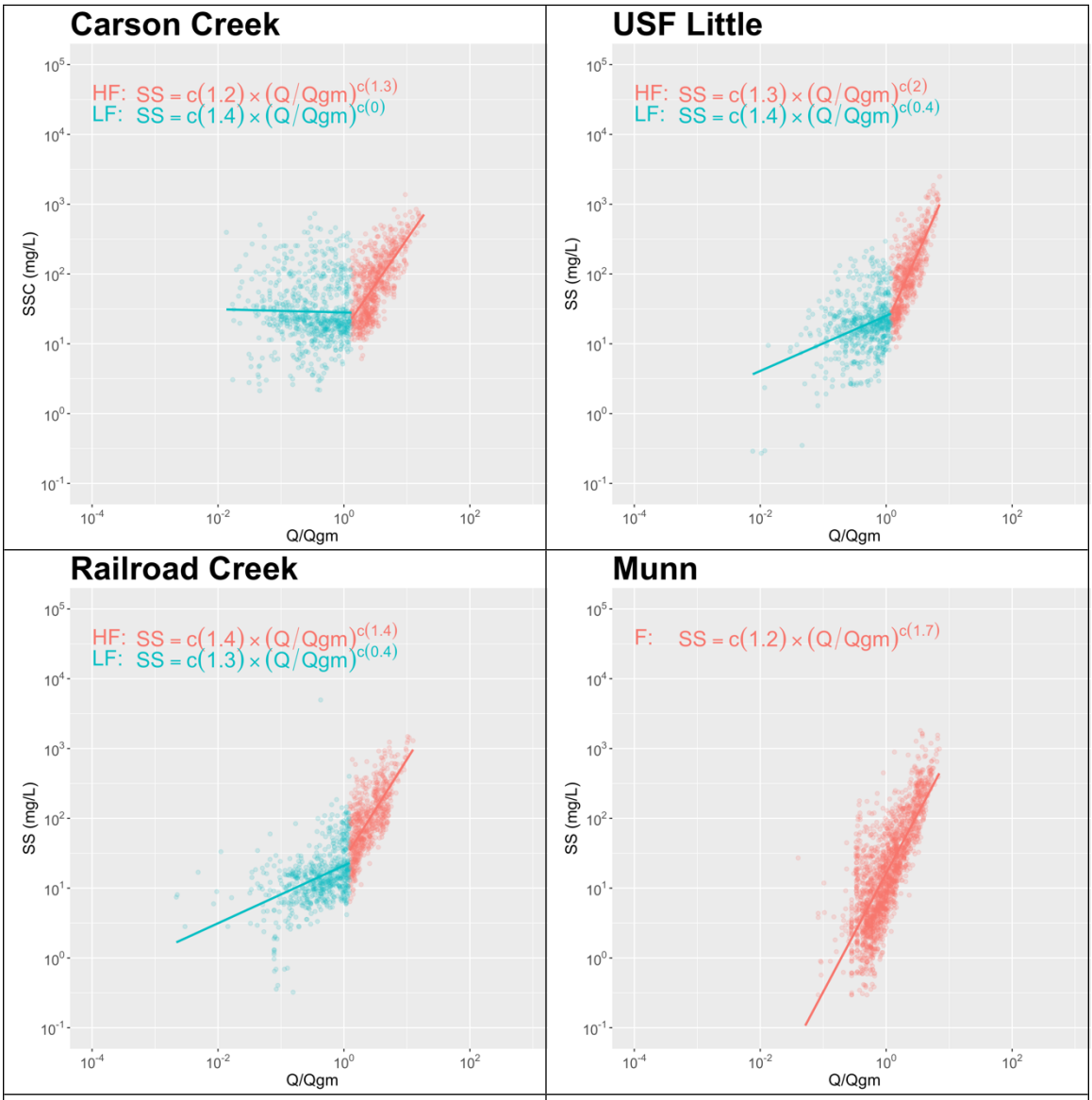


**Figure C.1.** (cont.)

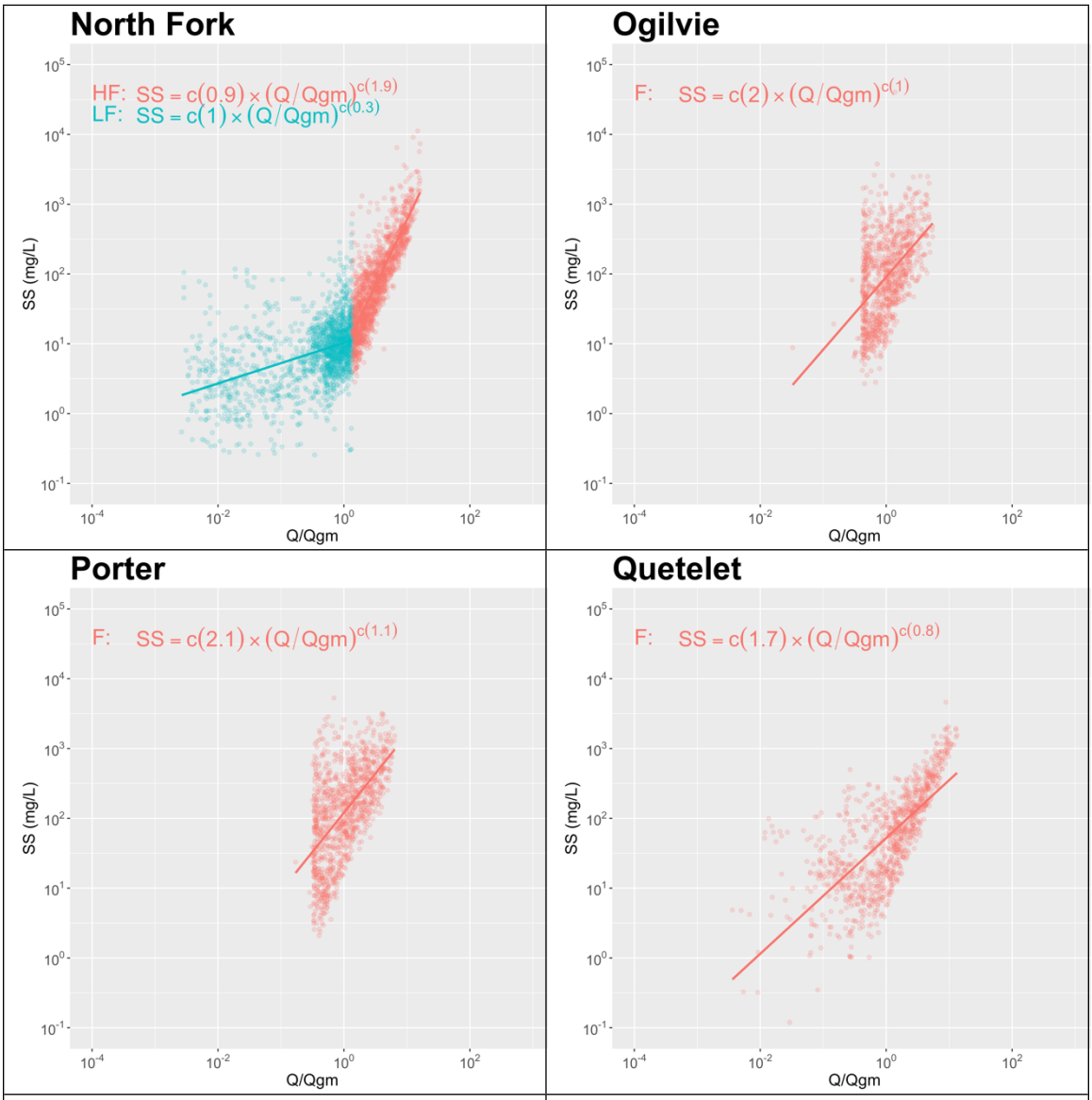


**Figure C.1.** (cont.)

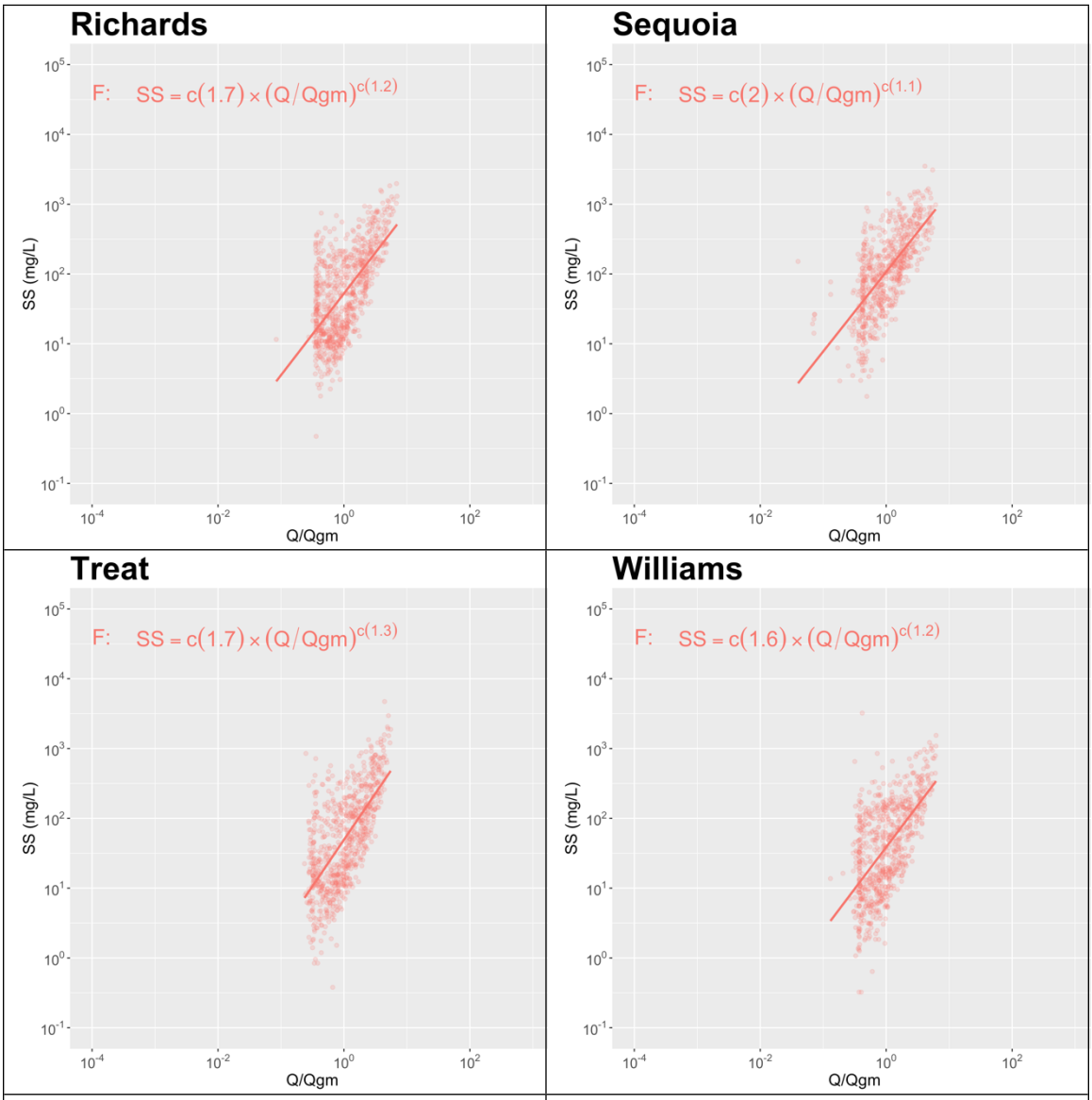


**Figure C.1.** (cont.)

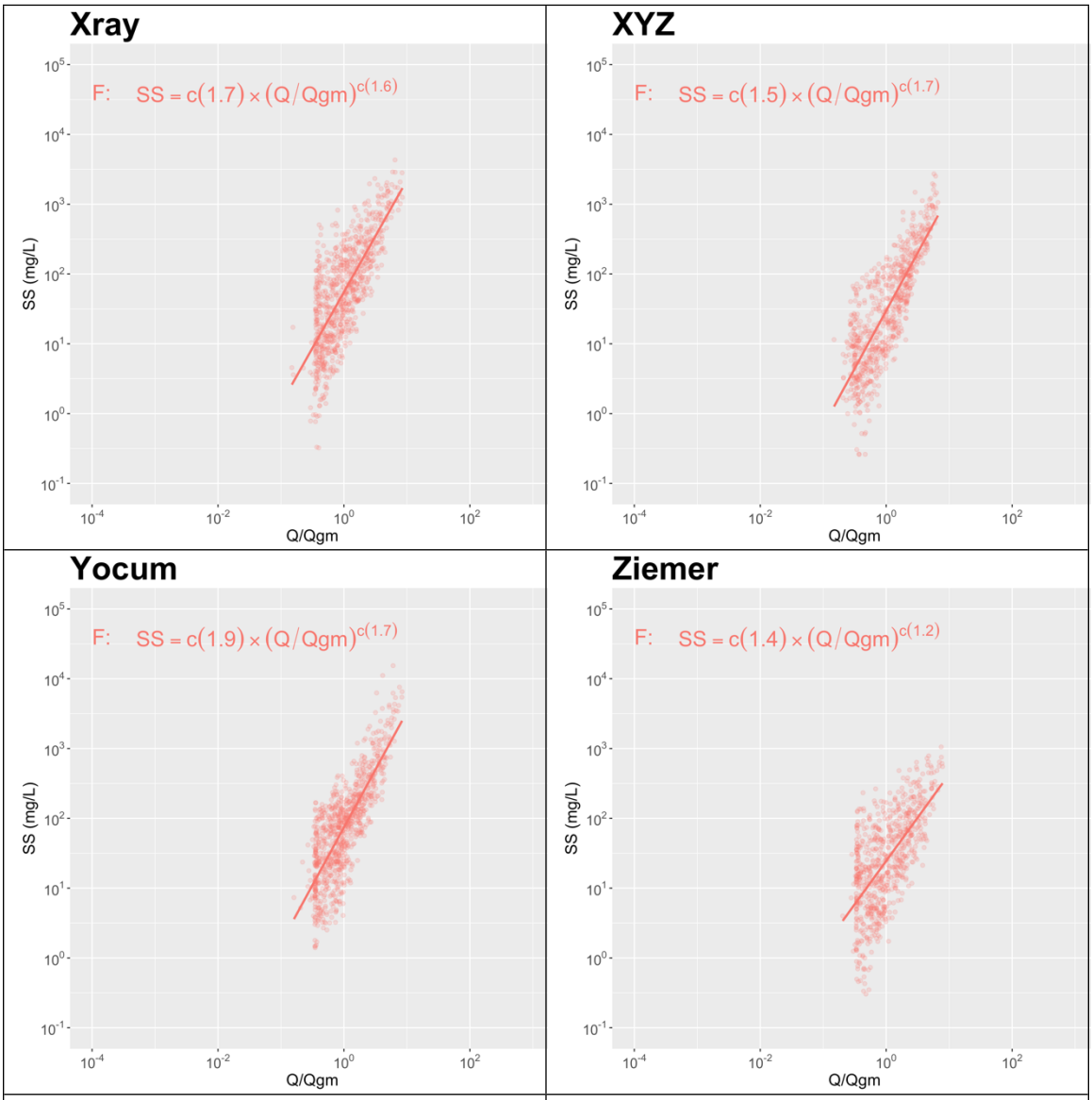


**Figure C.1.** (cont.)

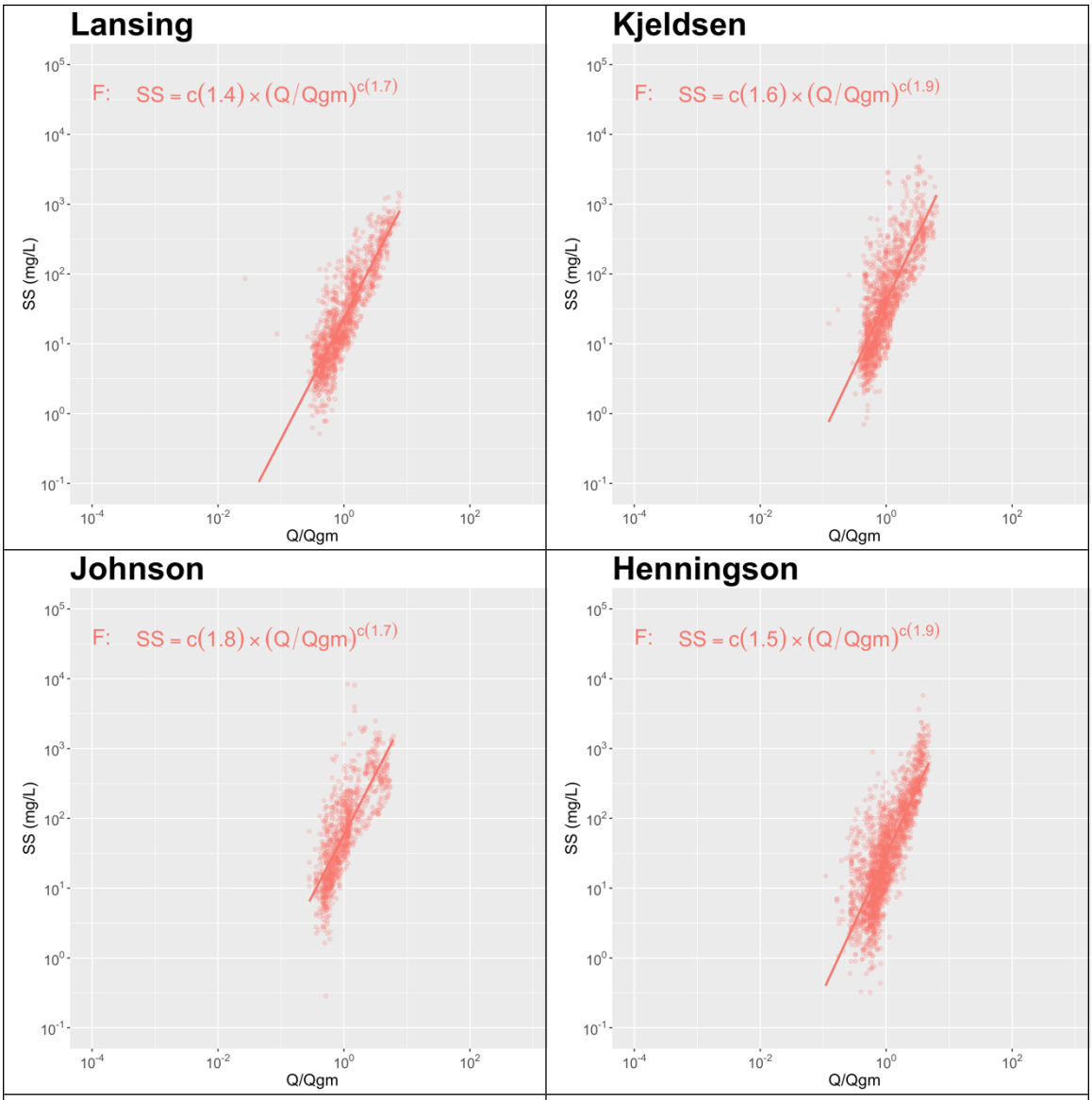


**Figure C.1.** (cont.)

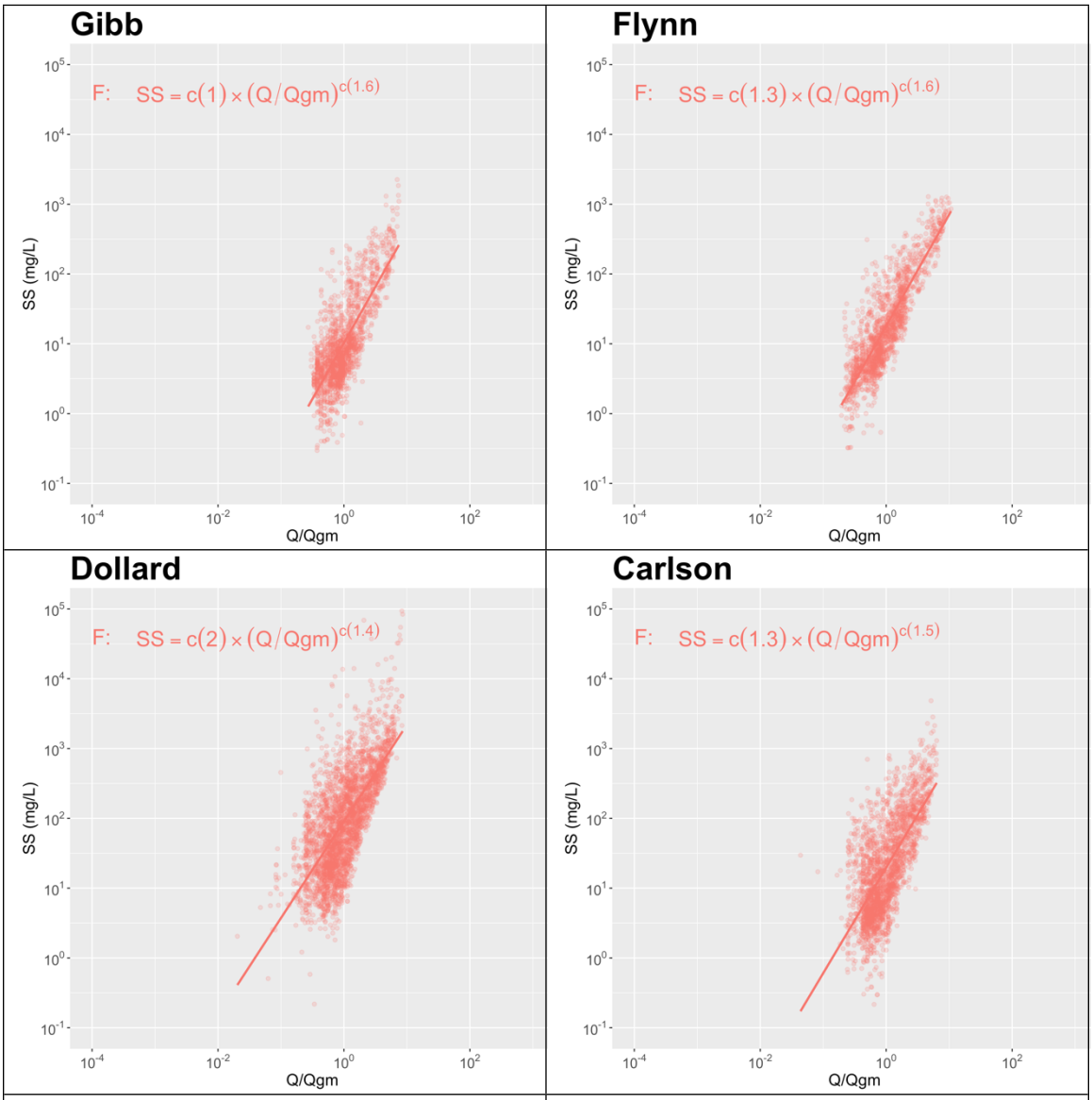


**Figure C.1.** (cont.)

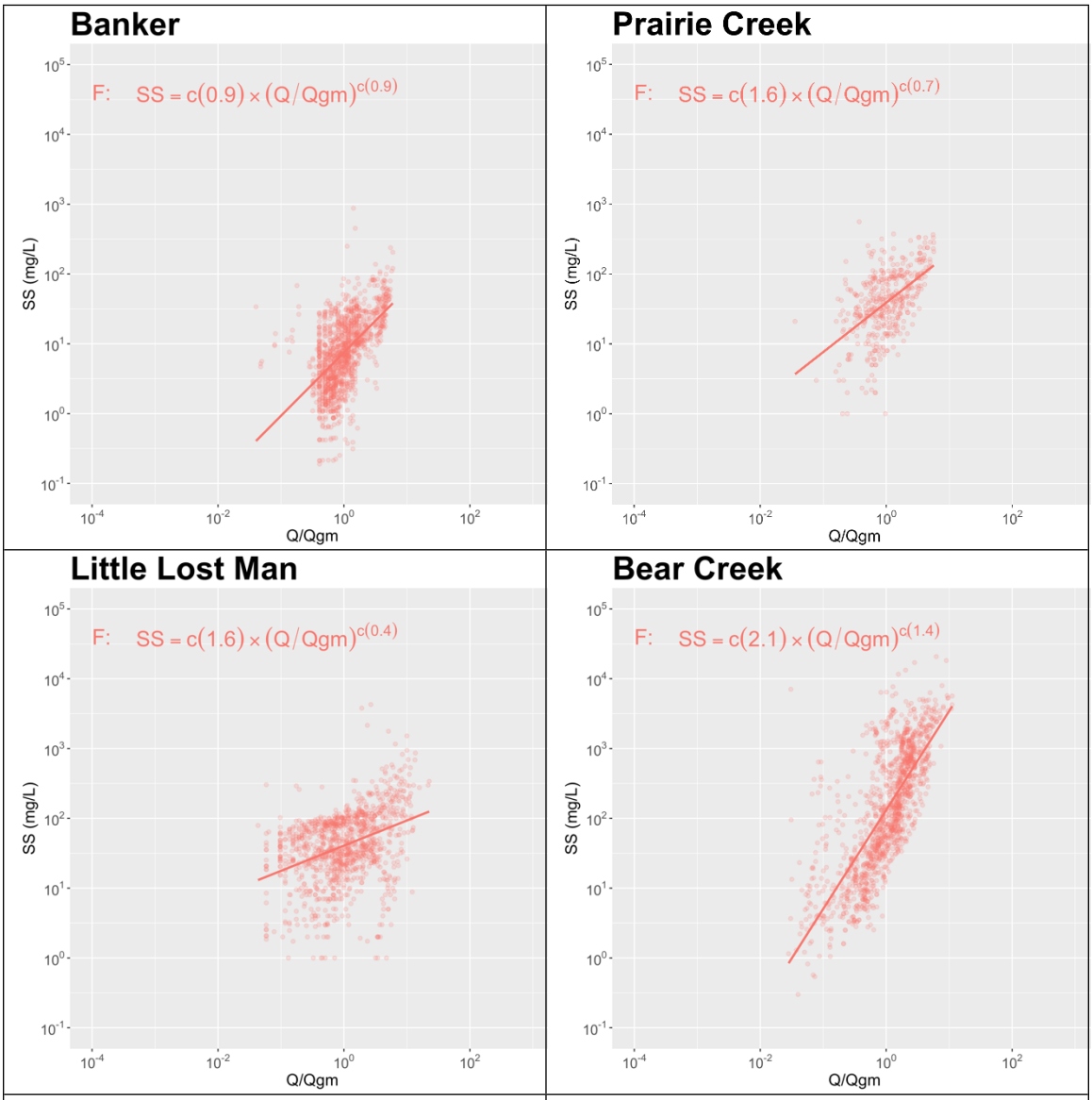


**Figure C.1.** (cont.)

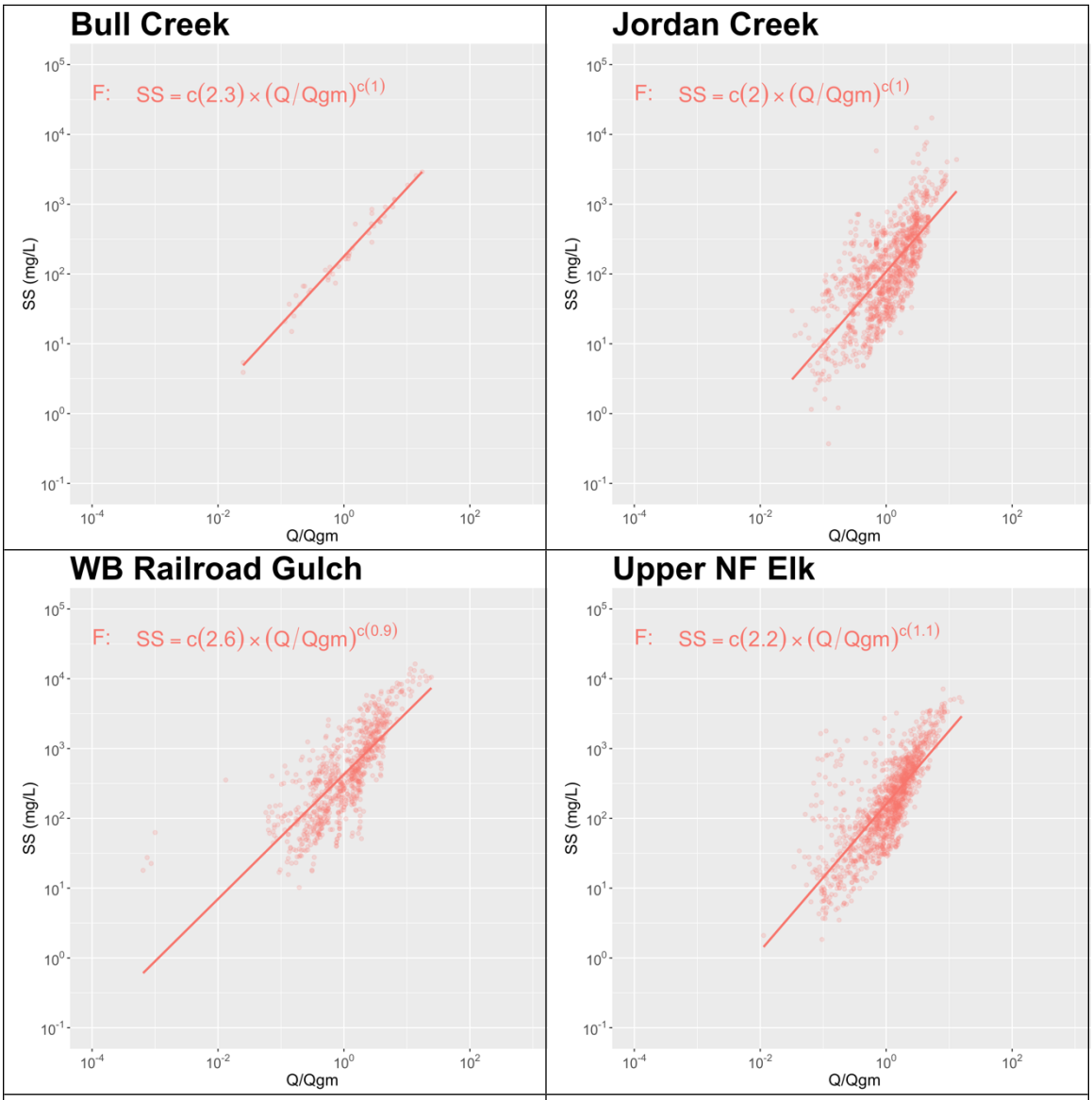


**Figure C.1.** (cont.)

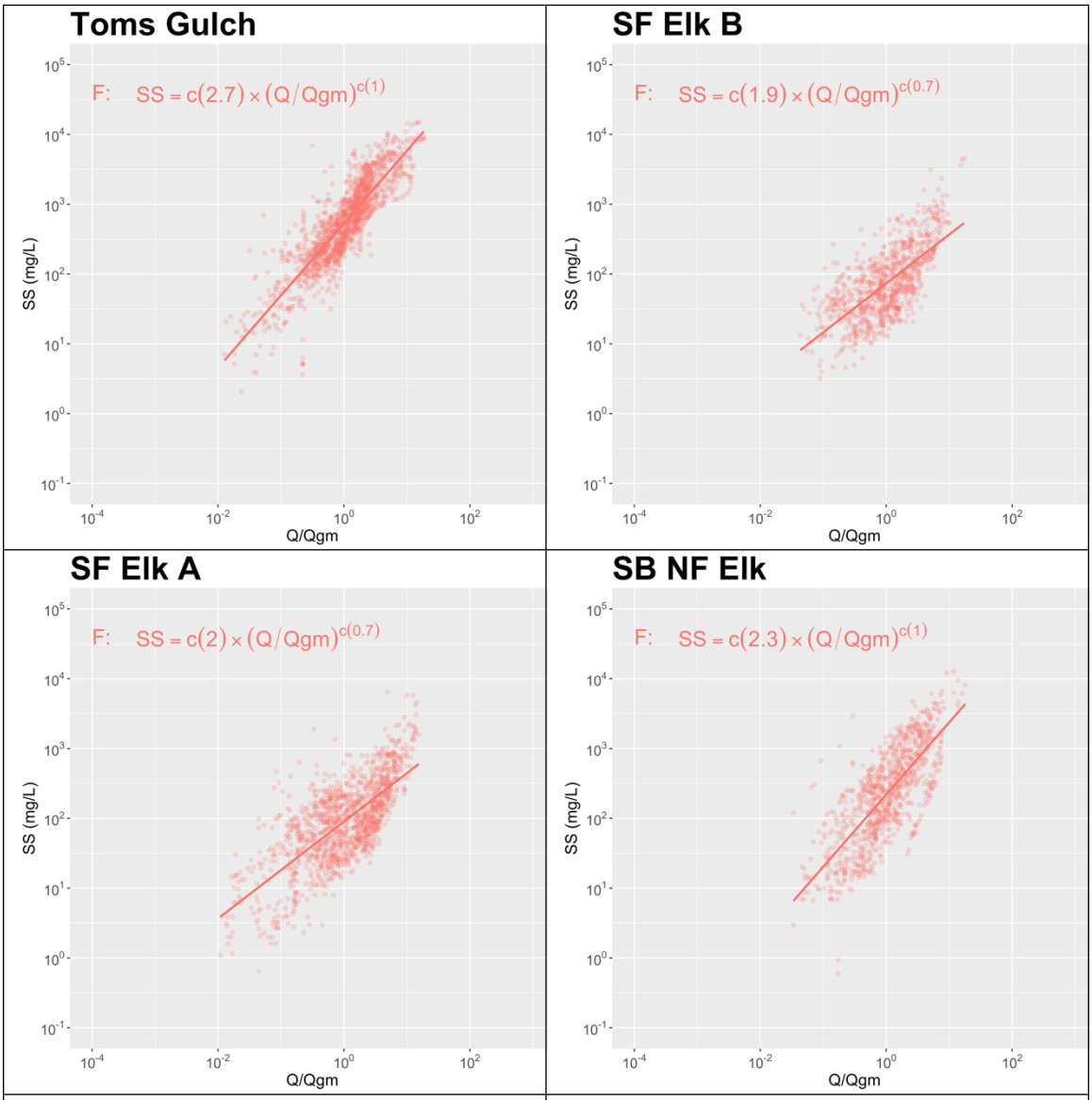


**Figure C.1.** (cont.)

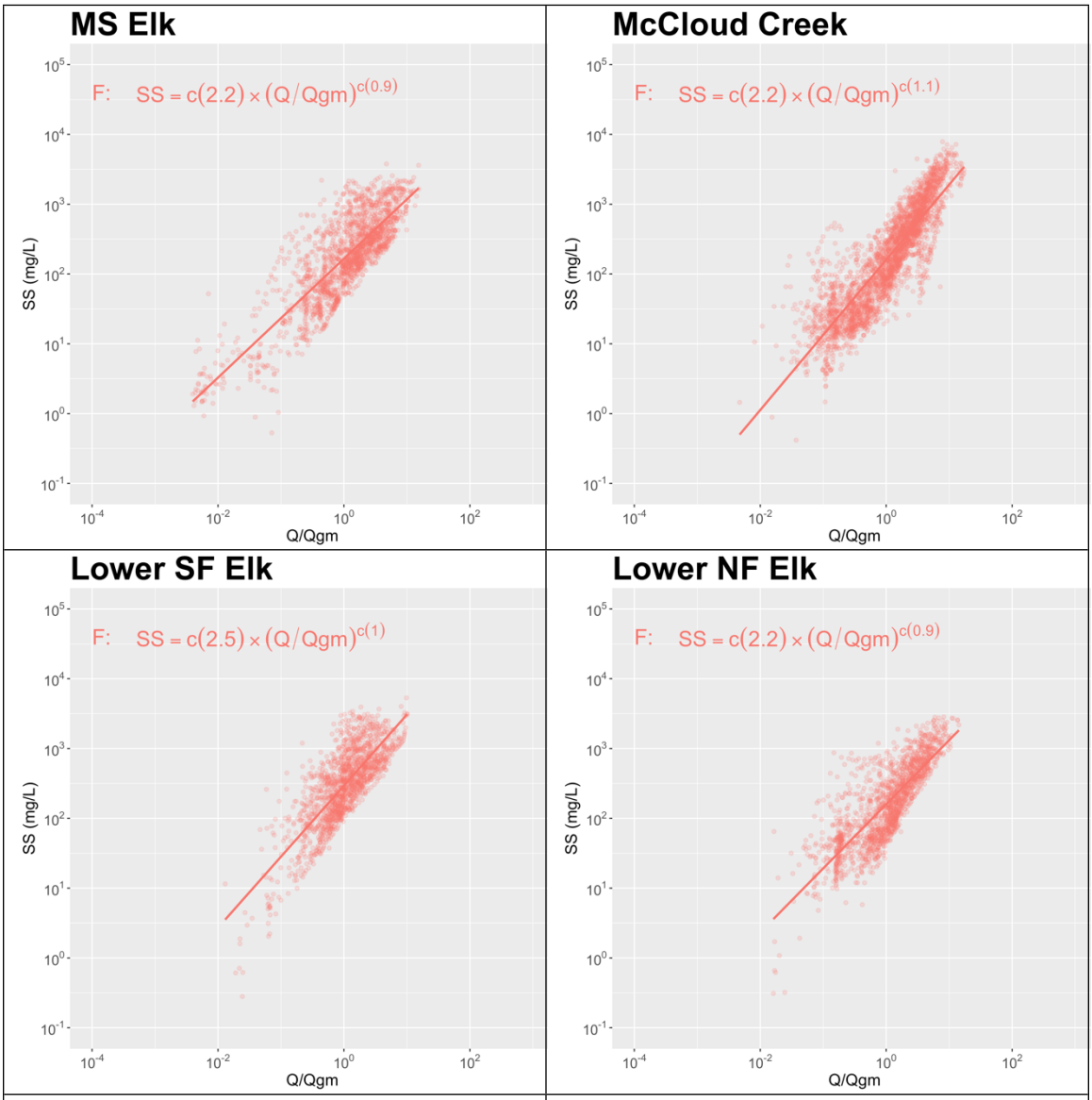


**Figure C.1.** (cont.)

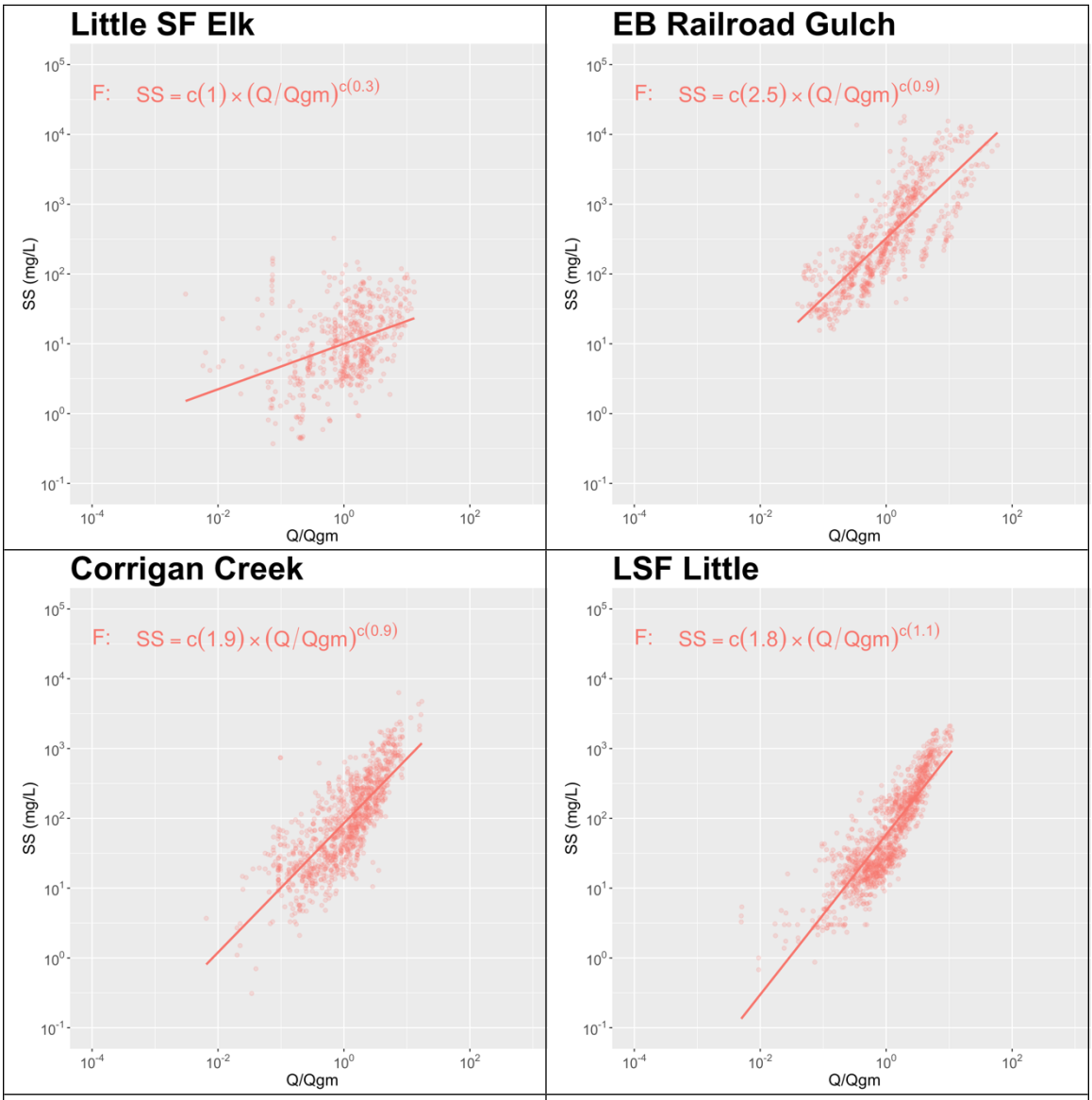


**Figure C.1.** (cont.)

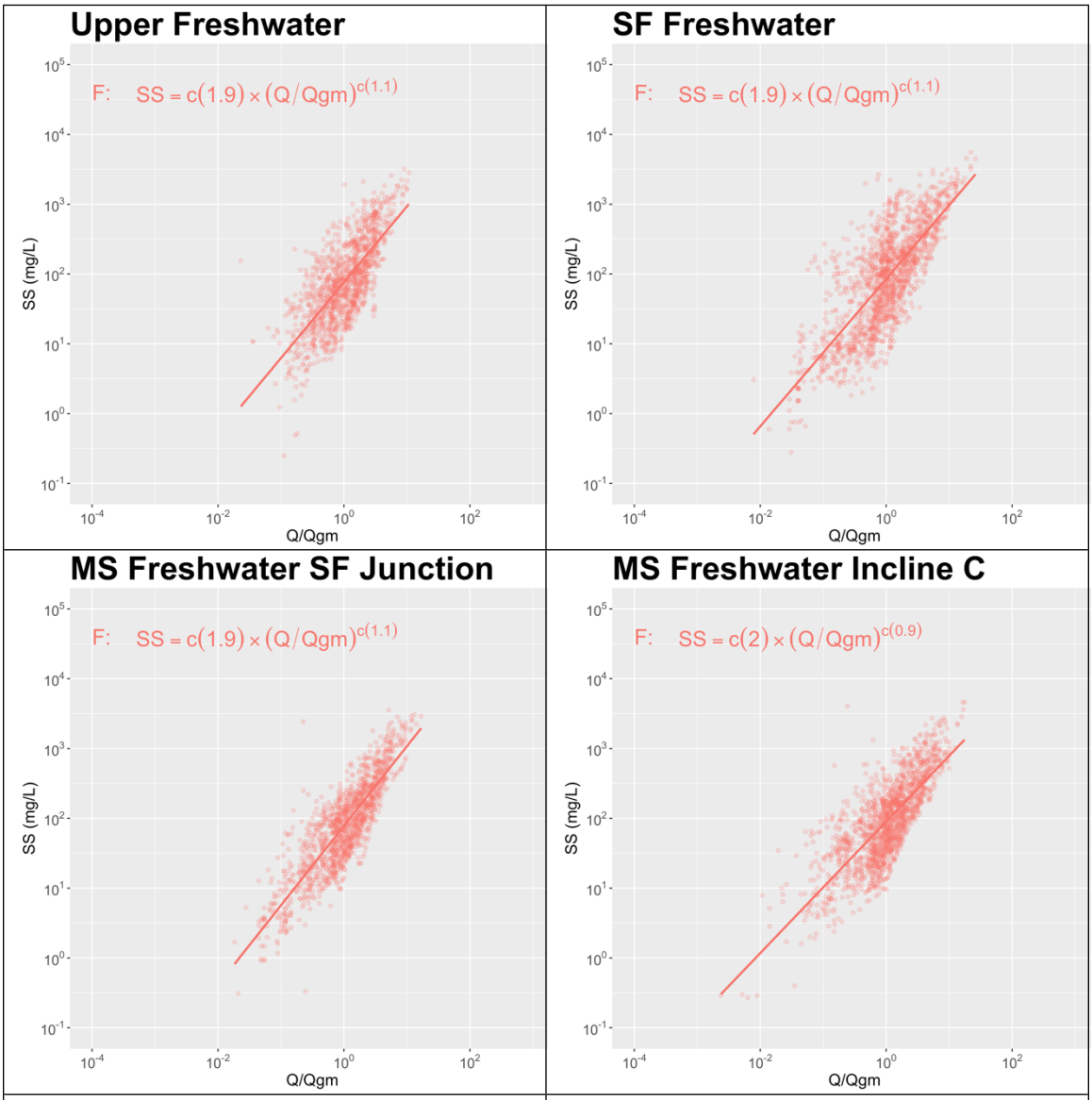


**Figure C.1.** (cont.)

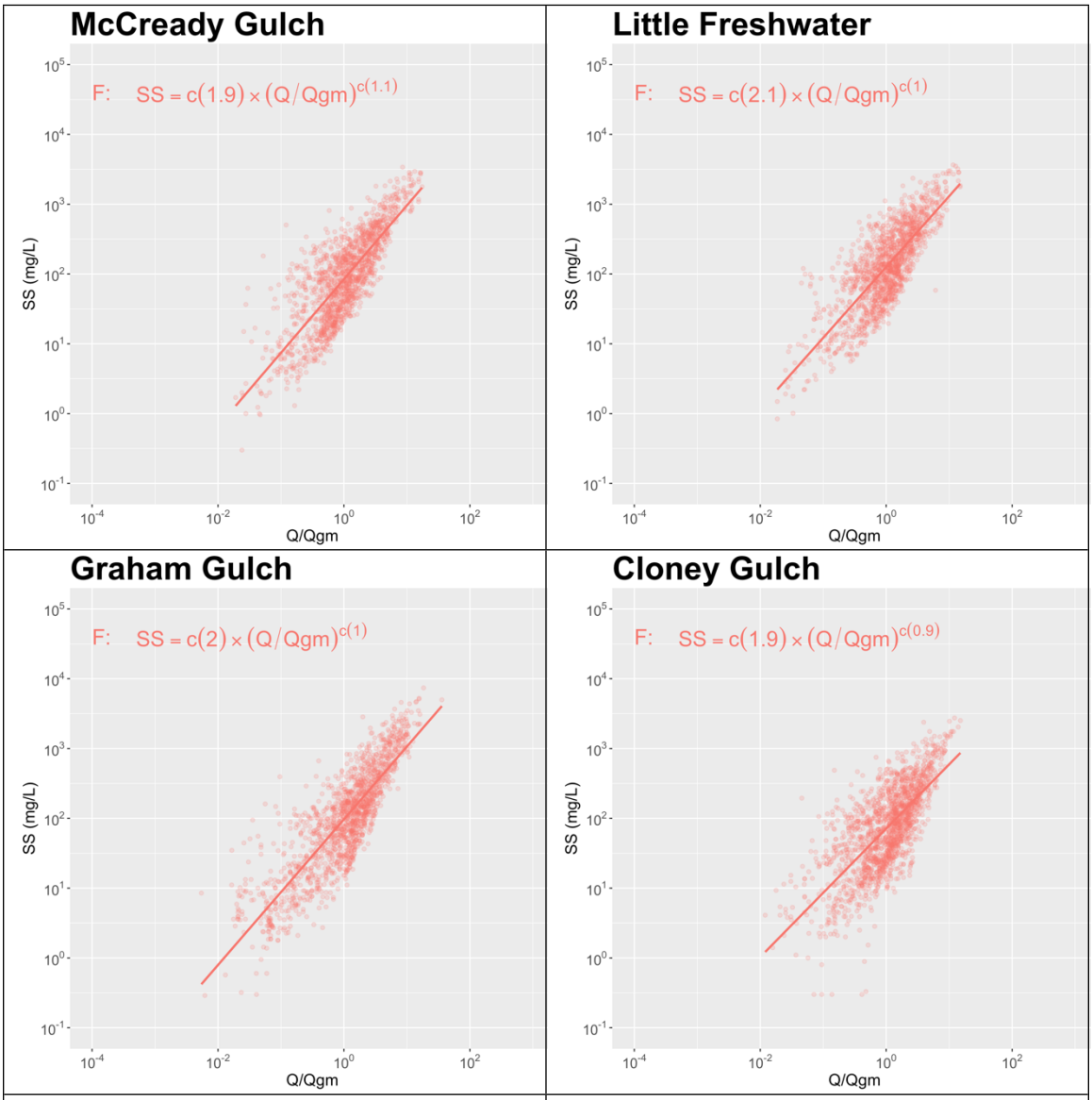


**Figure C.1.** (cont.)

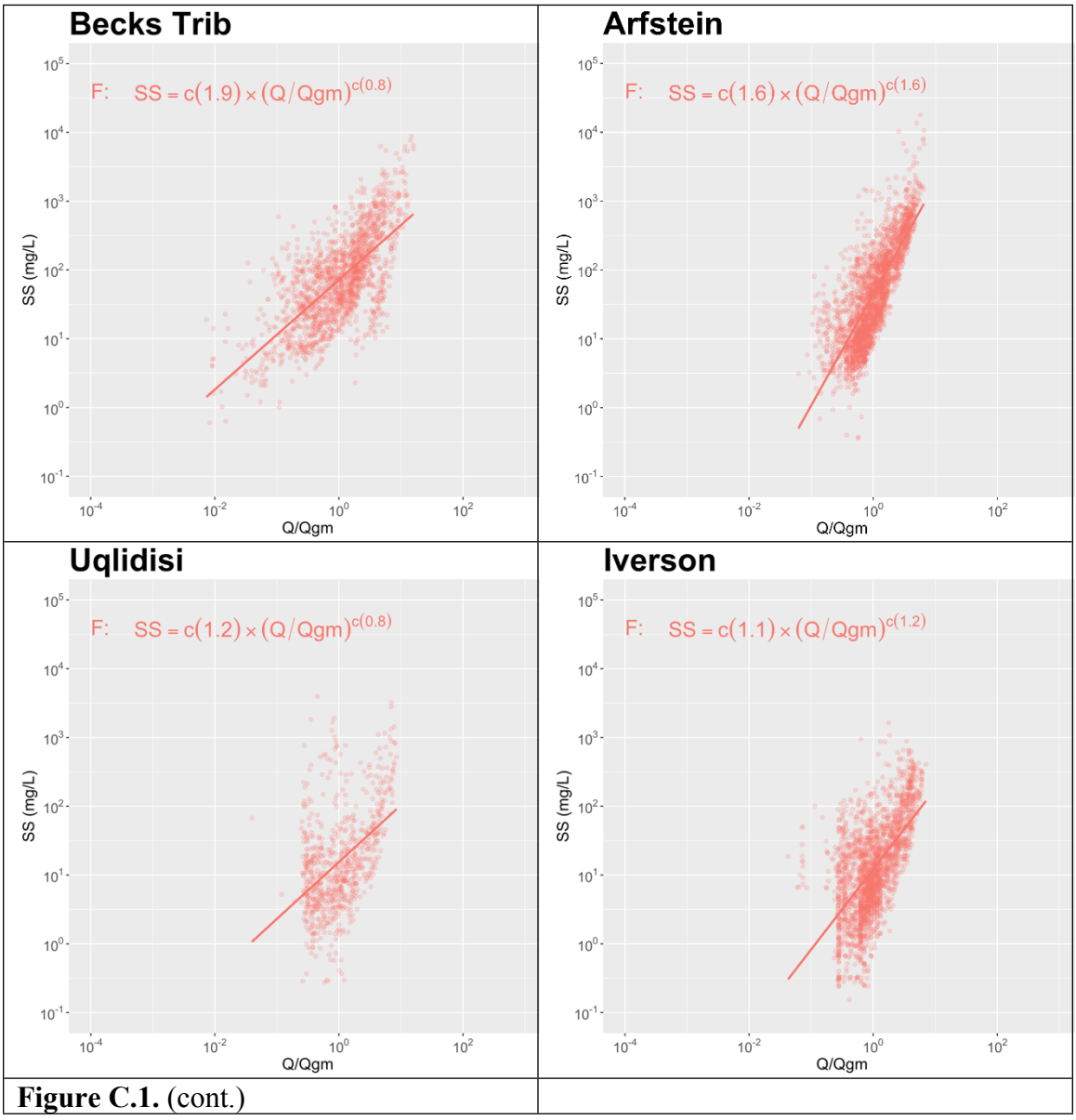


**Figure C.1.** (cont.)

# Appendix D. Cosmogenic Beryllium-10 Erosion Rate Model

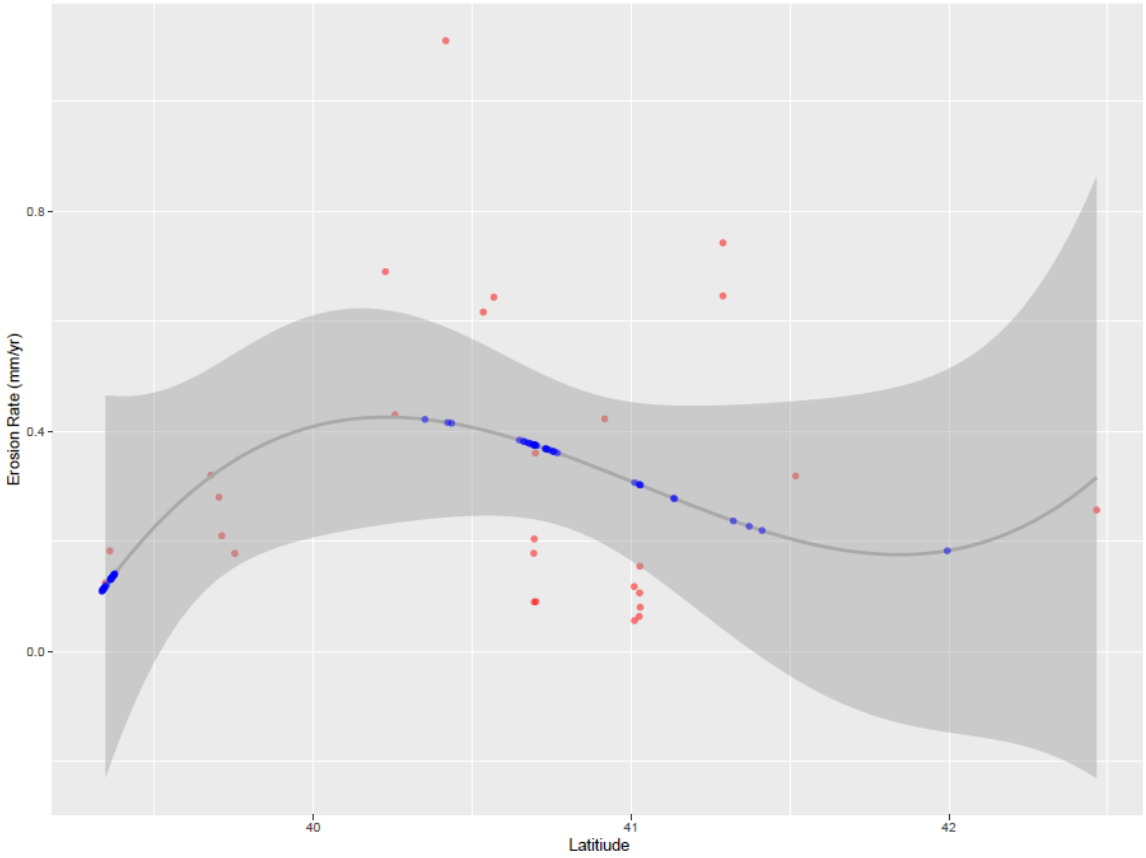


**Figure D.1.** Estimated erosion rates from cosmogenic $BE^{10}$ samples and their respective latitudes are plotted in red. The cubic spline model is shown by the dark grey line with 90% confidence intervals. Modeled erosion rates are shown in blue.

# Appendix E. Estimated Uplift Models

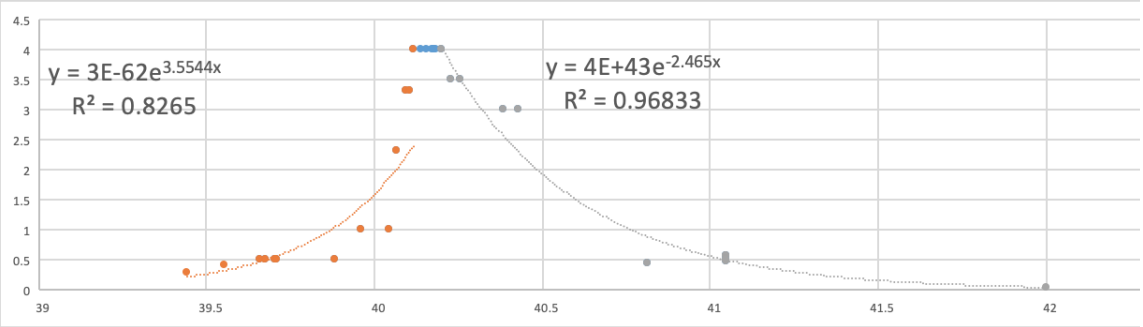


**Figure E.1.** Estimated uplift rates derived from dated marine terraces.

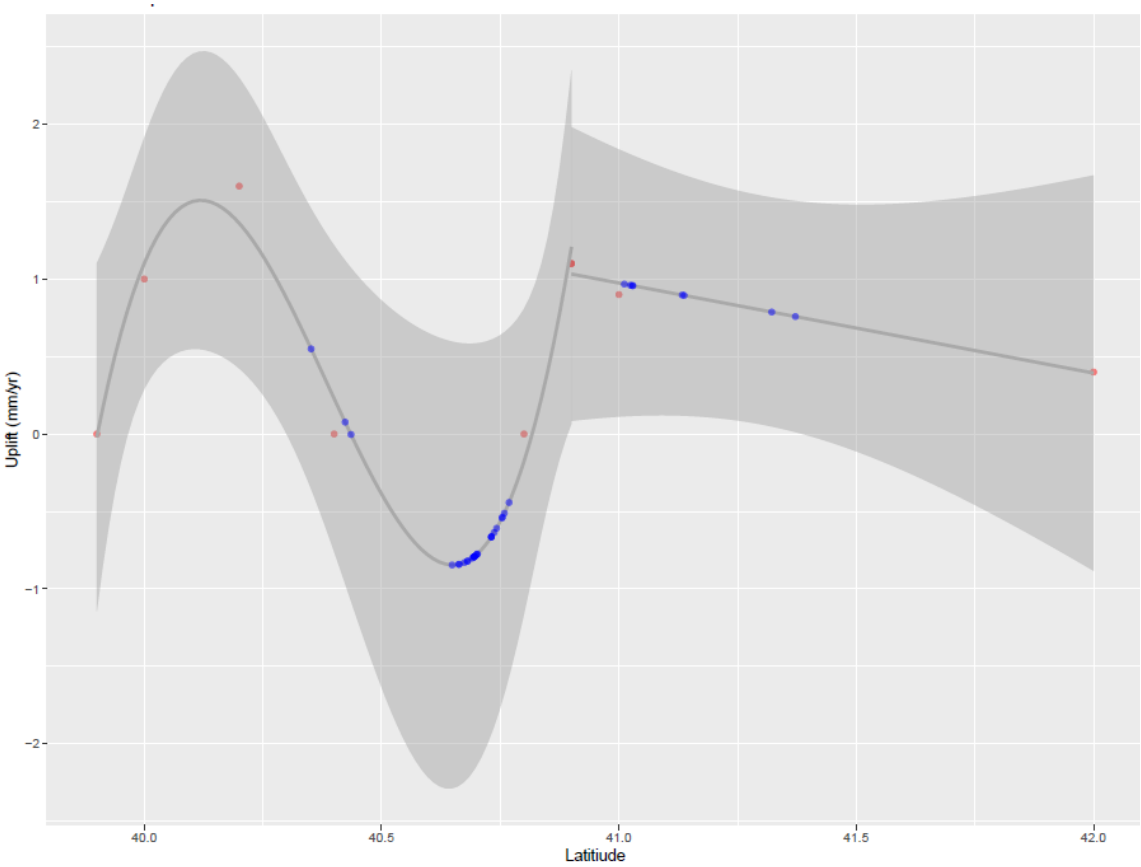


**Figure E.2.** Modeled uplift rates derived from the MCC model.

# Appendix F. Normalized Channel Steepness Code

```
% Written in MATLAB
%% TopoToolbox_Profiler_Master:
% Master code to run Topotoolbox functions for long profiles, slope-
area,
% chi analysis, channel steepness analysis, and output ksn values as
% shapefile. You must define the projection after importing into ArcGIS
%
% Written by Brendan Murphy and Adam Fisher, 2017

% Parent Directory Folder Must Contain:
% 1) TopoToolbox_Profiler_Master.m
% 2) 'DEM' folder with DEM formatted as an ESRI Ascii grid or Geotiff
% 3) Unzipped topotoolbox download: wschwanghart-topotoolbox-79648a2

% Inputs:
% DEM formatted as an ESRI Ascii grid or Geotiff

% Outputs:
% Optionally selected figures of:
% 1) mainstem long profiles and slope-area plot
% 2) stream network highlighting mainstem
% 3) chi profiles (all and limited network)
% 4) chi plan view map (all)
% 5) channel steepness, ksn, profiles & plan view map

% References:
% TopoToolbox: https://topotoolbox.wordpress.com

clear
close all

%%

% Inputs & Outputs:
input_dem = 'Caspar_dem.tif'; % Input DEM file
outputfolder = 'CasparRiverFigs_Amin_1e4'; % Output folder for figures
topotoolbox_folder =
'G:\GSchool\NorCal\Chi_and_Ksn_Analysis\StreamProfileAnalysis\wschwangh
art-topotoolbox-79648a2'; % Topotoolbox folder full path
dem_folder = 'DEM';


% Analysis Options:
mainstem = 1; % Plot the mainstem of the watershed, 1 = on, 0 = off
chi = 1; % Run Chi Plot Analysis, 1 = on, 0 = off
k_sn = 1; % Run Channel Steepness Analysis, 1 = on, 0 = off
theta_opt = 2;  % 0 = m/n standard reference (default = 0.45),
                % 1 = m/n based on mainstem slope-area analysis,
                % 2 = m/n based on optimization for chi_plot_all
profiles
ksn_shapeup = 1; % export ksn shapefile, 1 = on, 0 = off
```

```
% Input Parameters:
main_Amin = 1e6; % Select minimum drainage area for mainstem analysis
ksn_Amin = 1e6; % Select minimum drainage area for ksn analysis
chi_Amin_all = 1e4; % Select minimum drainage area for chi analysis
chi_Amin_lim = 1e6; % Select minimum drainage area for chi analysis
"limited network"
chi_A0 = 1e6; % chiplot reference area
ref_theta = 0.48; % Standard reference theta

% Make and Call Output Folder
addpath(topotoolbox_folder);
addpath(strcat(cd,'/',dem_folder))


if exist(outputfolder,'dir') == 7
    parentfolder = cd(outputfolder);
else
    mkdir(outputfolder)
    parentfolder = cd(outputfolder);
end

% Prep Input Data
DEM = GRIDobj(input_dem); % Load input DEM
FD = FLOWobj(DEM, 'preprocess','carve'); % Derive flow direction
FA = flowacc(FD); % Derive flow accumulation

% Parameter Mismatch Error
if mainstem == 0 && theta_opt == 1
    error('mainstem must = 1 to use theta_opt = 1')
end


%% Option to plot mainstem of watershed
if mainstem == 1

    S_main = STREAMobj(FD,'minarea',main_Amin,'unit','map'); % Create a
flow network at ksn minimum drainage area
    S_main = klargestconncomps(S_main,1); % Retain larger connected
component in the stream network
    ZS_main = crs(S_main, DEM,'K',2,'tau',0.5); % Smooth river profile
using the crs function

    St = trunk(S_main); % Extract mainstem
    ZSt = crs(St, DEM,'K',2,'tau',0.5); % Smooth river profile using
the crs function

    figure('Name','Mainstem - Plan View',...
        'units','normalized',...
        'position',[.1 .1 .8 .8])
    plot(S_main); % Plot stream network
    hold on
    plot(St); % Plot mainstem
    title('Mainstem - Plan View','FontSize',16) % Add title
```

```
    print('Mainstem_PanView','-dtiff','-r300')

    figure('Name','Mainstem Profile',...
        'units','normalized',...
        'position',[.1 .1 .9 .9])
    pos1 = [0.05 0.2 0.5 0.6];
    pos2 = [0.65 0.3 0.3 0.4];
    subplot('Position',pos1)
        plotdz(St,ZSt) % Plot mainstem long profile
    subplot('Position',pos2)
        main_sa = slopearea(St,ZSt,FA); % Plot slope-area analysis
    text(max(main_sa.hLine.XData),min(main_sa.hLine.YData),['   m/n  =
',num2str(-1*main_sa.theta,2)],'FontSize',16)
    print('Mainstem_LongProfile','-dtiff','-r300')
%     saveas(gcf,'Mainstem_LongProfile','pdf') % Save figure as .tif

end


%% Chi Analysis
if chi == 1
    S_chi = STREAMobj(FD,'minarea',chi_Amin_all,'unit','map'); % Create
a flow network at chi minimum drainage area (chi_Amin_all)
    S_chi = klargestconncomps(S_chi,1); % Retain larger connected
component in the stream network
    ZS_chi = crs(S_chi, DEM,'K',2,'tau',0.5); % Smooth river profile
using the crs function

    if theta_opt == 0
        chi_plot_all = chiplot(S_chi,ZS_chi,FA,'mn',ref_theta); % Plot
chi vs elevation using standard reference theta
    elseif theta_opt == 1
        chi_plot_all = chiplot(S_chi,ZS_chi,FA,'mn',-1*main_sa.theta);
% Plot chi vs elevation using slope-area derived theta
    elseif theta_opt == 2
        chi_plot_all = chiplot(S_chi,ZS_chi,FA,'mnoptim','nlinfit'); %
Plot chi vs elevation using the optimal theta found by chiplot.m
    end

    title(['m/n = ',num2str(chi_plot_all.mn,2)],'FontSize',16) % Add
title
    set(gcf,'Name','Chi Plot Profiles - All Drainages',...
        'units','normalized',...
        'position',[.1 .1 .8 .8])
    print('ChiPlot','-dtiff','-r300')
%     saveas(gcf,'ChiPlot','tif') % Save figure as .tif

    figure('Name','Chi Plot Plan View - All Drainages',...
        'units','normalized',...
        'position',[.1 .1 .8 .8])
    imageschs(DEM,[],'colormap',[1 1 1],
'colorbar',false,'ticklabel','nice'); % Plot basin hillshade
    title(['m/n = ',num2str(chi_plot_all.mn,2)],'FontSize',16) % Add
title
    hold on
```

```
    chi_trans = chitransform(S_chi,FA,'a0',chi_A0,'mn',-
1*main_sa.theta,'plot',1); % Planform view of chi using slope-area
theta
    colormap(jet)
    hx = colorbar;
    hx.Label.String = '\chi'; % Label scale
    hx.FontSize = 12;
    print('Chi_Transform','-dtiff','-r300')
%     saveas(gcf,'Chi_Transform','tif') % Save figure as .tif

    % Limited Network Chi Analysis
    S_chi_lim = STREAMobj(FD,'minarea',chi_Amin_lim,'unit','map'); %
Create a flow network at chi minimum drainage area "limited network"
(chi_Amin_lim)
    S_chi_lim = klargestconncomps(S_chi_lim,1); % Retain larger
connected component in the stream network
    ZS_chi_lim = crs(S_chi_lim, DEM,'K',2,'tau',0.5); % Smooth river
profile using the crs function

    if theta_opt == 0
        chi_plot_lim = chiplot(S_chi_lim,ZS_chi_lim,FA,'mn',ref_theta);
% Plot chi vs elevation using standard reference theta
    elseif theta_opt == 1
        chi_plot_lim = chiplot(S_chi_lim,ZS_chi_lim,FA,'mn',-
1*main_sa.theta); % Plot chi vs elevation using slope-area derived
theta
    elseif theta_opt == 2
        chi_plot_lim =
chiplot(S_chi_lim,ZS_chi_lim,FA,'mnoptim','nlinfit');  % Plot chi vs
elevation using the optimal theta found by chiplot.m
    end

    title(['m/n = ',num2str(chi_plot_lim.mn,2)],'FontSize',16) % Add
title
    set(gcf,'Name','Chi Plot Profiles - Limited Drainages',...
        'units','normalized',...
        'position',[.1 .1 .8 .8])
    print('ChiPlotLimited','-dtiff','-r300')
%     saveas(gcf,'ChiPlotLimited','tif') % Save figure as .tif

end

%% Steepness Analysis
if (k_sn == 1) && (chi == 1)

    S_ksn = STREAMobj(FD,'minarea',ksn_Amin,'unit','map'); % Create a
flow network at ksn minimum drainage area (ksn_Amin)
    S_ksn = klargestconncomps(S_ksn,1); % Retain larger connected
component in the stream network
    ZS_ksn = crs(S_ksn, DEM,'K',2,'tau',0.5); % Smooth river profile
using the crs function

    if theta_opt == 0
        k = ksn(S_ksn,ZS_ksn,FA,ref_theta); % Calculate steepness using
smoothed river profile using standard reference theta
```

```
    elseif theta_opt == 1
        k = ksn(S_ksn,ZS_ksn,FA,-1*main_sa.theta); % Calculate
steepness using smoothed river profile and slope-area derived theta
    elseif theta_opt == 2
        k = ksn(S_ksn,ZS_ksn,FA,chi_plot_all.mn); % Calculate steepness
using smoothed river profile using the optimal theta found by chiplot.m
    end

    figure('Name','Channel Steepness, Ksn',...
        'units','normalized',...
        'position',[.1 .1 .9 .9])
    pos1 = [0.05 0.2 0.5 0.6];
    pos2 = [0.575 0.3 0.4 0.4];
    subplot('Position',pos1)

plotdz(S_ksn,ZS_ksn,'color',k,'linewidth',2,'colormap','jet','colormeth
od','surface','colorbar',true,'cbarlabel','k_{sn}'); % Plot long
profiles with ksn



    if theta_opt == 0
        title(['m/n = ',num2str(ref_theta)],'FontSize',16) % Add title
    elseif theta_opt == 1
        title(['m/n = ',num2str(-1*main_sa.theta,2)],'FontSize',16) %
Add title
    elseif theta_opt == 2
        title(['m/n = ',num2str(chi_plot_all.mn,2)],'FontSize',16) %
Add title
    end



    subplot('Position',pos2)
    imageschs(DEM,[],'colormap',[1 1 1],
'colorbar',false,'ticklabel','nice'); % Plot basin hillshade

    if theta_opt == 0
        title(['m/n = ',num2str(ref_theta)],'FontSize',16) % Add title
    elseif theta_opt == 1
        title(['m/n = ',num2str(-1*main_sa.theta,2)],'FontSize',16) %
Add title
    elseif theta_opt == 2
        title(['m/n = ',num2str(chi_plot_all.mn,2)],'FontSize',16) %
Add title
    end

    hold on
    plotc(S_ksn,k); % Planform view of ksn
    colormap(jet)
    hx = colorbar;
    hx.Label.String = 'k_{sn}'; % Label the scale
    hx.FontSize = 12;
    print('Ksn_Analysis','-dtiff','-r300')
%     saveas(gcf,'Ksn_Analysis','tif') % Save figure as .tif

elseif (k_sn == 1) && (chi == 0)
```

```
    S_ksn = STREAMobj(FD,'minarea',ksn_Amin,'unit','map'); % Create a
flow network at ksn minimum drainage area (ksn_Amin)
    S_ksn = klargestconncomps(S_ksn,1); % Retain larger connected
component in the stream network
    ZS_ksn = crs(S_ksn, DEM,'K',2,'tau',0.5); % Smooth river profile
using the crs function

    if theta_opt == 0
        k = ksn(S_ksn,ZS_ksn,FA,ref_theta); % Calculate steepness using
smoothed river profile using standard reference theta
    elseif theta_opt == 1
        k = ksn(S_ksn,ZS_ksn,FA,-1*main_sa.theta); % Calculate
steepness using smoothed river profile and slope-area derived theta
    elseif theta_opt == 2
        S_chi = STREAMobj(FD,'minarea',chi_Amin_all,'unit','map'); %
Create a flow network at chi minimum drainage area (chi_Amin_all)
        S_chi = klargestconncomps(S_chi,1); % Retain larger connected
component in the stream network
        ZS_chi = crs(S_chi, DEM,'K',2,'tau',0.5); % Smooth river
profile using the crs function
        chi_plot_all =
chiplot(S_chi,ZS_chi,FA,'mnoptim','nlinfit','plot',false); % Calculate
optimal theta

        k = ksn(S_ksn,ZS_ksn,FA,chi_plot_all.mn); % Calculate steepness
using smoothed river profile using the optimal theta found by chiplot.m
    end

    figure('Name','Channel Steepness, Ksn',...
        'units','normalized',...
        'position',[.1 .1 .8 .8])
    pos1 = [0.05 0.2 0.5 0.6];
    pos2 = [0.65 0.3 0.3 0.4];
    subplot('Position',pos1)

plotdz(S_ksn,ZS_ksn,'color',k,'linewidth',2,'colormap','jet','colormeth
od','surface','cbarlabel','k_{sn}'); % plot long profiles with ksn

    if theta_opt == 0
        title(['m/n = ',num2str(ref_theta)],'FontSize',16) % Add title
    elseif theta_opt == 1
        title(['m/n = ',num2str(-1*main_sa.theta,2)],'FontSize',16) %
Add title
    elseif theta_opt == 2
        title(['m/n = ',num2str(chi_plot_all.mn,2)],'FontSize',16) %
Add title
    end

    subplot('Postion',pos2)
    imageschs(DEM,[],'colormap',[1 1 1],
'colorbar',false,'ticklabel','nice'); % Plot basin hillshade

    if theta_opt == 0
        title(['m/n = ',num2str(ref_theta)],'FontSize',16) % Add title
    elseif theta_opt == 1
```

```
        title(['m/n = ',num2str(-1*main_sa.theta,2)],'FontSize',16) %
Add title
    elseif theta_opt == 2
        title(['m/n = ',num2str(chi_plot_all.mn,2)],'FontSize',16) %
Add title
    end

    hold on
    plotc(S_ksn,k); % Planform view of ksn
    colormap(jet)
    hx = colorbar;
    hx.Label.String = 'k_{sn}'; % Label the scale
    hx.FontSize = 12;
    print('Ksn_Analysis','-dtiff','-r300')
%     saveas(gcf,'Ksn_Analysis','tif') % Save figure as .tif

end
%% ksn shapefile export
% Output shapefile does not include a projected spatial reference -
must
% define projection in GIS.

ksn_shp = STREAMobj2mapstruct(S_ksn, 'seglength',500,'attributes',
{'ksn' k @mean}); % convert streamobj to map structure
shapewrite(ksn_shp,'ksn_network.shp');

%%
disp("Don't fogret to define your projection.");

%% Go back to parent folder
cd(parentfolder)
```

# Appendix G. Table of Sediment Rating Curve Parameters

**Table G.1.**
*Table of Sediment Rating Curve Parameters*

| Watershed | Larger Basin | SRC Offset (mg/L) | SRC Slope | SRC Shape |
|---|---|---|---|---|
| Prairie | Prairie Creek | 1.6 | 0.7 | Power |
| Little Lost Man | Prairie Creek | 1.6 | 0.4 | Power |
| Railroad | Little River | 1.4 | 1.4 | Threshold |
| Lower South Fork | Little River | 1.8 | 1.1 | Power |
| Upper South Fork | Little River | 1.3 | 2 | Threshold |
| Carson | Little River | 1.2 | 1.3 | Threshold |
| McCready | Freshwater Creek | 1.9 | 1.1 | Power |
| Cloney | Freshwater Creek | 1.9 | 0.9 | Power |
| Little Freshwater | Freshwater Creek | 2.1 | 1 | Power |
| Graham | Freshwater Creek | 2 | 1 | Power |
| Upper | Freshwater Creek | 1.9 | 1.1 | Power |
| Mainstem Incline C (Middle Freshwater) | Freshwater Creek | 2 | 0.9 | Power |
| Mainstem South Fork Junction (Lower Freshwater) | Freshwater Creek | 1.9 | 1.1 | Power |
| Becks | Freshwater Creek | 1.9 | 0.8 | Power |
| South Fork | Freshwater Creek | 1.9 | 1.1 | Power |
| Mainstem | Elk River | 2.2 | 0.9 | Power |
| Lower South Fork | Elk River | 2.5 | 1 | Power |
| Lower North Fork | Elk River | 2.2 | 0.9 | Power |
| Bridge | Elk River | 1.4 | 1.1 | Threshold |
| Upper North Fork | Elk River | 2.2 | 1.1 | Power |
| Toms | Elk River | 2.7 | 1 | Power |
| McCloud | Elk River | 2.2 | 1.1 | Power |
| South Branch A | Elk River | 2 | 0.7 | Power |
| Corrigan | Elk River | 1.9 | 0.9 | Power |
| Little South Fork (Headwaters Reserve) | Elk River | 1 | 0.3 | Power |
| Bear | Lower Eel | 2.1 | 1 | Power |
| Munn | Caspar Creek | 1.2 | 1.7 | Power |
| Iverson | Caspar Creek | 1.1 | 1.2 | Power |
| Henningson | Caspar Creek | 1.5 | 1.9 | Power |
| Dollard | Caspar Creek | 2 | 1.4 | Power |

**Table G.1.** (cont.)

| | | | | |
|---|---|---|---|---|
| Xray | Caspar Creek | 1.7 | 1.6 | Power |
| Carlson | Caspar Creek | 1.3 | 1.5 | Power |
| Eagle | Caspar Creek | 1.8 | 1.2 | Power |
| XYZ | Caspar Creek | 1.5 | 1.7 | Power |
| Arfstein | Caspar Creek | 1.6 | 1.6 | Power |
| North Fork | Caspar Creek | 0.9 | 1.9 | Threshold |
| Ziemer | Caspar Creek | 1.4 | 1.2 | Power |
| Yocom | Caspar Creek | 1.9 | 1.7 | Power |
| Williams | Caspar Creek | 1.6 | 1.2 | Power |
| South Fork | Caspar Creek | 1.1 | 1.8 | Threshold |
| Uqlidisi | Caspar Creek | 1.2 | 0.8 | Power |
| Quetelet | Caspar Creek | 1.7 | 0.8 | Power |
| Ogilvie | Caspar Creek | 2 | 1 | Power |
| Porter | Caspar Creek | 2.1 | 1.1 | Power |
| Sequoyah | Caspar Creek | 2 | 1.1 | Power |
| Treat | Caspar Creek | 1.7 | 1.3 | Power |
| Richards | Caspar Creek | 1.7 | 1.2 | Power |

# Appendix H. Table of Predictor Variables

**Table H.1.** Table of Predictor Variables

| Watershed | Mean Slope (degrees) | Drainage Density (km/km2) | Mean Elevation (m) | Mean Relief (m) | Mean Soil Erodibility (k factor) | Mean Hydraulic Conductivity (µm/s) | Mean Rock Strength (MPa) | Baseflow Index | 30-yr normal (mm) | 5yr-24hr Precipitation Intensity (mm/hr) |
|---|---|---|---|---|---|---|---|---|---|---|
| Prairie | 29.9 | 1.3 | 241.5 | 436.8 | 29.8 | 0.2 | 83.3 | 0.3 | 1864.1 | 6.0 |
| Little Lost Man | 29.1 | 1.0 | 404.0 | 628.7 | 29.5 | 0.2 | 83.3 | 0.3 | 1864.1 | 7.0 |
| Railroad | 28.7 | 1.4 | 261.0 | 400.1 | 30.3 | 0.2 | 101.8 | 0.4 | 1667.0 | 6.0 |
| Lower South Fork | 30.0 | 0.9 | 312.8 | 526.5 | 30.2 | 0.2 | 101.8 | 0.4 | 1667.0 | 6.0 |
| Upper South Fork | 31.9 | 1.0 | 369.9 | 573.9 | 31.2 | 0.3 | 97.8 | 0.4 | 1667.0 | 6.0 |
| Carson | 24.1 | 1.2 | 153.8 | 401.0 | 30.9 | 36.1 | 73.8 | 0.4 | 1667.0 | 5.0 |
| McCready | 28.9 | 1.5 | 196.7 | 376.3 | 36.4 | 0.2 | 66.4 | 0.4 | 1333.7 | 5.0 |
| Cloney | 28.7 | 0.9 | 282.1 | 587.9 | 30.6 | 0.2 | 92.6 | 0.4 | 1333.7 | 5.0 |
| Little Freshwater | 36.4 | 1.3 | 163.4 | 290.1 | 40.0 | 2.3 | 61.3 | 0.4 | 1333.7 | 5.0 |
| Graham | 30.9 | 1.3 | 309.0 | 632.4 | 31.1 | 0.2 | 91.0 | 0.4 | 1333.7 | 5.0 |
| Upper | 31.3 | 1.2 | 711.2 | 399.8 | 30.8 | 0.2 | 101.8 | 0.4 | 1333.7 | 6.0 |
| Mainstem Incline C (Middle Freshwater) | 30.0 | 1.2 | 538.7 | 748.9 | 30.0 | 0.2 | 101.8 | 0.4 | 1333.7 | 6.0 |
| Mainstem South Fork Junction (Lower Freshwater) | 30.9 | 1.3 | 459.7 | 811.3 | 31.1 | 0.2 | 97.7 | 0.4 | 1333.7 | 6.0 |
| Becks | 33.3 | 1.2 | 296.4 | 480.8 | 33.3 | 0.2 | 87.6 | 0.4 | 1333.7 | 5.0 |
| South Fork | 38.2 | 1.5 | 288.2 | 650.6 | 37.6 | 0.2 | 73.9 | 0.4 | 1333.7 | 5.0 |
| Mainstem | 31.6 | 1.3 | 273.3 | 701.0 | 38.7 | 1.1 | 65.8 | 0.2 | 1313.8 | 5.0 |
| Lower South Fork | 28.6 | 1.1 | 301.3 | 639.4 | 38.2 | 0.6 | 63.5 | 0.2 | 1313.8 | 5.0 |
| Lower North Fork | 34.7 | 1.4 | 261.0 | 695.8 | 39.2 | 0.2 | 68.9 | 0.2 | 1313.8 | 5.0 |
| Bridge | 40.5 | 1.3 | 158.5 | 251.8 | 40.9 | 0.2 | 62.3 | 0.2 | 1313.8 | 5.0 |
| Upper North Fork | 34.2 | 1.4 | 331.3 | 666.6 | 38.6 | 0.2 | 73.0 | 0.2 | 1313.8 | 5.0 |
| Toms | 24.7 | 0.8 | 156.4 | 358.4 | 39.2 | 0.2 | 62.3 | 0.2 | 1313.8 | 5.0 |
| McCloud | 29.8 | 0.7 | 225.0 | 475.2 | 38.9 | 0.2 | 62.3 | 0.2 | 1313.8 | 5.0 |

**Table H.1.** (cont.)

| | | | | | | | | | | |
|---|---|---|---|---|---|---|---|---|---|---|
| South Branch A | 28.1 | 1.1 | 414.6 | 489.2 | 35.8 | 0.2 | 66.3 | 0.2 | 1313.8 | 6.0 |
| Corrigan | 31.9 | 1.0 | 401.2 | 389.2 | 37.9 | 0.2 | 65.1 | 0.2 | 1313.8 | 5.0 |
| Little South Fork (Headwaters Reserve) | 22.5 | 0.9 | 510.1 | 232.9 | 39.9 | 0.2 | 62.3 | 0.2 | 1313.8 | 6.0 |
| Bear | 51.3 | 1.4 | 432.9 | 799.8 | 31.2 | 0.2 | 81.2 | 0.4 | 1784.0 | 6.0 |
| Munn | 24.1 | 0.5 | 253.1 | 115.0 | 29.0 | 0.2 | 81.2 | 0.3 | 1236.7 | 6.0 |
| Iverson | 33.2 | 1.5 | 227.6 | 170.5 | 29.0 | 0.2 | 81.2 | 0.3 | 1236.7 | 6.0 |
| Henningson | 34.5 | 1.0 | 229.8 | 194.4 | 29.0 | 0.2 | 81.2 | 0.3 | 1236.7 | 6.0 |
| Dollard | 39.9 | 1.3 | 214.1 | 199.2 | 29.0 | 0.2 | 81.2 | 0.3 | 1236.7 | 6.0 |
| Xray | 26.9 | 1.5 | 251.4 | 128.4 | 28.7 | 0.2 | 81.2 | 0.3 | 1236.7 | 6.0 |
| Carlson | 37.9 | 1.7 | 227.7 | 201.1 | 29.0 | 0.2 | 81.2 | 0.3 | 1236.7 | 6.0 |
| Eagle | 38.3 | 0.7 | 241.5 | 168.7 | 29.0 | 0.2 | 81.2 | 0.3 | 1236.7 | 6.0 |
| XYZ | 32.5 | 1.3 | 232.2 | 218.7 | 28.9 | 0.2 | 81.2 | 0.3 | 1236.7 | 6.0 |
| Arfstein | 36.7 | 1.6 | 208.4 | 234.9 | 28.9 | 0.2 | 81.2 | 0.3 | 1236.7 | 6.0 |
| North Fork | 36.0 | 1.6 | 212.0 | 237.3 | 29.9 | 0.2 | 81.2 | 0.3 | 1236.7 | 6.0 |
| Ziemer | 27.6 | 1.0 | 274.5 | 115.1 | 28.0 | 0.2 | 81.2 | 0.3 | 1236.7 | 6.0 |
| Yocom | 31.9 | 1.4 | 253.4 | 179.4 | 27.7 | 0.2 | 81.2 | 0.3 | 1236.7 | 6.0 |
| Williams | 35.5 | 0.7 | 245.2 | 173.4 | 28.0 | 0.2 | 81.2 | 0.3 | 1236.7 | 6.0 |
| South Fork | 33.0 | 1.6 | 171.1 | 291.1 | 27.2 | 2.2 | 79.9 | 0.3 | 1236.7 | 6.0 |
| Uqlidisi | 34.4 | 0.0 | 212.4 | 161.8 | 27.6 | 0.2 | 81.2 | 0.3 | 1236.7 | 6.0 |
| Quetelet | 33.7 | 1.6 | 173.2 | 288.6 | 27.3 | 0.5 | 81.0 | 0.3 | 1236.7 | 6.0 |
| Ogilvie | 14.4 | 0.5 | 158.6 | 93.3 | 24.0 | 44.9 | 53.5 | 0.3 | 1236.7 | 6.0 |
| Porter | 17.5 | 1.0 | 151.3 | 111.3 | 27.6 | 0.2 | 81.2 | 0.3 | 1236.7 | 6.0 |
| Sequoyah | 24.8 | 1.0 | 163.6 | 127.3 | 25.5 | 0.2 | 81.2 | 0.3 | 1236.7 | 6.0 |
| Treat | 36.2 | 1.0 | 170.9 | 131.7 | 27.4 | 0.2 | 81.2 | 0.3 | 1236.7 | 6.0 |
| Richards | 32.1 | 1.0 | 162.1 | 144.0 | 28.1 | 0.2 | 81.2 | 0.3 | 1236.7 | 6.0 |

**Table H.1.** (cont.)

| Watershed | 2yr-15mn Precipitation Intensity (mm/hr) | 2yr-24hr Precipitation Intensity (mm/hr) | 2yr-24hour (cm) Precipitation Depth | Est. Uplift Rate (marine terrace model)(mm/yr) | Est. Uplift Rate (MCC model)(mm/y) | Cosmogenic Beryllium-10 Erosion Rate Model (mm/y) | Nonlinear Hillslope Erosion Rate Model (mm/y) | Deep-Seated Landslide Susceptibility (LSS) (unitless) | Precipitation Sensitive LSS (unitless) | Mean Upstream Normalized Steepness Index (ksn) |
|---|---|---|---|---|---|---|---|---|---|---|
| Prairie | 36.0 | 5.0 | 11.8 | 0.2 | 0.8 | 0.2 | 0.1 | 8.1 | 32.2 | 40.3 |
| Little Lost Man | 38.0 | 5.0 | 11.0 | 0.2 | 0.8 | 0.2 | 0.2 | 7.9 | 31.4 | 104.9 |
| Railroad | 32.0 | 4.0 | 10.7 | 0.5 | 1.0 | 0.3 | 0.1 | 7.8 | 27.8 | 62.9 |
| Lower South Fork | 32.0 | 5.0 | 11.0 | 0.5 | 1.0 | 0.3 | 0.1 | 7.9 | 28.1 | 52.1 |
| Upper South Fork | 33.0 | 5.0 | 11.5 | 0.5 | 1.0 | 0.3 | 0.1 | 8.2 | 29.2 | 71.1 |
| Carson | 31.0 | 4.0 | 10.1 | 0.5 | 1.0 | 0.3 | 0.1 | 7.3 | 26.0 | 24.3 |
| McCready | 30.0 | 4.0 | 9.0 | 0.9 | -0.4 | 0.4 | 0.1 | 7.8 | 22.2 | 47.1 |
| Cloney | 30.0 | 4.0 | 10.0 | 0.9 | -0.5 | 0.4 | 0.1 | 8.0 | 22.8 | 80.6 |
| Little Freshwater | 29.0 | 4.0 | 8.8 | 0.9 | -0.5 | 0.4 | 0.1 | 8.3 | 23.6 | 33.9 |
| Graham | 30.0 | 4.0 | 10.1 | 0.9 | -0.5 | 0.4 | 0.2 | 8.1 | 23.1 | 98.1 |
| Upper | 32.0 | 4.0 | 12.0 | 1.0 | -0.6 | 0.4 | 0.1 | 7.8 | 22.2 | 87.2 |
| Mainstem Incline C (Middle Freshwater) | 32.0 | 5.0 | 11.6 | 1.0 | -0.6 | 0.4 | 0.2 | 8.1 | 23.1 | 129.6 |
| Mainstem South Fork Junction (Lower Freshwater) | 31.0 | 5.0 | 10.5 | 1.0 | -0.7 | 0.4 | 0.3 | 8.3 | 23.6 | 123.5 |
| Becks | 30.0 | 4.0 | 9.8 | 1.0 | -0.7 | 0.4 | 0.1 | 8.8 | 25.1 | 79.4 |
| South Fork | 29.0 | 4.0 | 9.6 | 1.0 | -0.7 | 0.4 | 0.2 | 8.6 | 24.5 | 68.5 |
| Mainstem | 30.0 | 4.0 | 9.3 | 1.1 | -0.8 | 0.4 | 0.2 | 8.8 | 24.7 | 53.7 |
| Lower South Fork | 30.0 | 4.0 | 9.8 | 1.1 | -0.8 | 0.4 | 0.2 | 8.8 | 24.7 | 67.0 |
| Lower North Fork | 29.0 | 4.0 | 9.4 | 1.1 | -0.8 | 0.4 | 0.2 | 8.7 | 24.4 | 48.2 |
| Bridge | 29.0 | 4.0 | 8.9 | 1.1 | -0.8 | 0.4 | 0.1 | 8.8 | 24.7 | 26.5 |
| Upper North Fork | 30.0 | 4.0 | 9.9 | 1.1 | -0.8 | 0.4 | 0.2 | 8.9 | 25.0 | 64.8 |
| Toms | 29.0 | 4.0 | 9.1 | 1.1 | -0.8 | 0.4 | 0.1 | 8.9 | 25.0 | 26.6 |
| McCloud | 30.0 | 4.0 | 8.3 | 1.1 | -0.8 | 0.4 | 0.1 | 9.2 | 25.8 | 49.6 |
| South Branch A | 31.0 | 4.0 | 10.5 | 1.2 | -0.8 | 0.4 | 0.1 | 8.8 | 24.7 | 77.3 |

**Table H.1.** (cont.)

| | | | | | | | | | | |
|---|---|---|---|---|---|---|---|---|---|---|
| Corrigan | 30.0 | 4.0 | 10.3 | 1.2 | -0.8 | 0.4 | 0.1 | 7.7 | 21.6 | 94.2 |
| Little South Fork (Headwaters Reserve) | 31.0 | 5.0 | 10.8 | 1.2 | -0.8 | 0.4 | 0.1 | 8.2 | 23.0 | 78.0 |
| Bear | 35.0 | 5.0 | 12.5 | 2.1 | 0.1 | 0.4 | 0.3 | 8.8 | 33.5 | 92.5 |
| Munn | 34.0 | 4.0 | 10.6 | 0.2 | 0.0 | 0.1 | 0.0 | 7.6 | 20.1 | 41.3 |
| Iverson | 34.0 | 4.0 | 10.7 | 0.2 | 0.0 | 0.1 | 0.1 | 8.1 | 21.4 | 48.1 |
| Henningson | 34.0 | 4.0 | 10.7 | 0.2 | 0.0 | 0.1 | 0.1 | 8.6 | 22.7 | 44.2 |
| Dollard | 34.0 | 4.0 | 10.7 | 0.2 | 0.0 | 0.1 | 0.1 | 8.6 | 22.7 | 45.5 |
| Xray | 34.0 | 4.0 | 10.7 | 0.2 | 0.0 | 0.1 | 0.0 | 7.1 | 18.7 | 37.1 |
| Carlson | 34.0 | 4.0 | 10.7 | 0.2 | 0.0 | 0.1 | 0.1 | 8.3 | 21.9 | 55.3 |
| Eagle | 34.0 | 4.0 | 10.7 | 0.2 | 0.0 | 0.1 | 0.1 | 8.5 | 22.4 | 50.4 |
| XYZ | 34.0 | 4.0 | 10.7 | 0.2 | 0.0 | 0.1 | 0.1 | 7.4 | 19.5 | 53.9 |
| Arfstein | 34.0 | 4.0 | 10.7 | 0.2 | 0.0 | 0.1 | 0.1 | 8.4 | 22.2 | 42.5 |
| North Fork | 34.0 | 4.0 | 10.8 | 0.2 | 0.0 | 0.1 | 0.1 | 8.2 | 21.7 | 44.8 |
| Ziemer | 34.0 | 4.0 | 10.6 | 0.2 | 0.0 | 0.1 | 0.0 | 7.7 | 20.3 | 32.7 |
| Yocom | 34.0 | 4.0 | 10.7 | 0.2 | 0.0 | 0.1 | 0.1 | 8.0 | 21.1 | 38.3 |
| Williams | 33.0 | 4.0 | 10.5 | 0.2 | 0.0 | 0.1 | 0.1 | 8.5 | 22.4 | 47.7 |
| South Fork | 34.0 | 4.0 | 10.6 | 0.2 | 0.0 | 0.1 | 0.1 | 7.7 | 20.3 | 40.8 |
| Uqlidisi | 33.0 | 4.0 | 10.5 | 0.2 | 0.0 | 0.1 | 0.0 | 8.6 | 22.7 | 50.0 |
| Quetelet | 34.0 | 4.0 | 10.6 | 0.2 | 0.0 | 0.1 | 0.1 | 7.9 | 20.9 | 40.1 |
| Ogilvie | 33.0 | 4.0 | 10.4 | 0.2 | 0.0 | 0.1 | 0.0 | 4.5 | 11.9 | 50.1 |
| Porter | 33.0 | 4.0 | 10.4 | 0.2 | 0.0 | 0.1 | 0.0 | 5.5 | 14.5 | 42.2 |
| Sequoyah | 34.0 | 4.0 | 10.6 | 0.2 | 0.0 | 0.1 | 0.0 | 6.9 | 18.2 | 39.3 |
| Treat | 33.0 | 4.0 | 10.4 | 0.2 | 0.0 | 0.1 | 0.0 | 8.4 | 22.2 | 43.9 |
| Richards | 33.0 | 4.0 | 10.4 | 0.2 | 0.0 | 0.1 | 0.0 | 7.5 | 19.8 | 43.8 |

**Table H.1.** (cont.)

| Watershed | Near-channel Local Relief (m) | Near-channel LSS (unitless) | Near-channel Precipitation Sensitive LSS (unitless) | Near-channel Soil Erodibility (k factor) | Harvested | Watershed Area (km2) | Road Density (km/km2) | Number of Stream/Road Crossings | Density of Stream/Road Crossing (crossing/km2) | Percent Harvested since 2010 |
|---|---|---|---|---|---|---|---|---|---|---|
| Prairie | 245.7 | 76.6 | 20965.8 | 318.0 | Unharvested | 19.8 | 1.0 | 14.0 | 0.7 | 0.0 |
| Little Lost Man | 124.9 | 34.8 | 9534.5 | 122.9 | Unharvested | 9.0 | 0.6 | 0.0 | 0.0 | 0.0 |
| Railroad | 1314.1 | 63.6 | 15566.3 | 241.4 | Harvested | 6.9 | 5.1 | 12.0 | 1.7 | 0.0 |
| Lower South Fork | 997.8 | 47.3 | 11570.5 | 185.0 | Harvested | 14.1 | 6.0 | 10.0 | 0.7 | 0.1 |
| Upper South Fork | 1707.2 | 59.3 | 14513.8 | 217.9 | Harvested | 14.0 | 5.9 | 16.0 | 1.1 | 0.1 |
| Carson | 696.6 | 50.1 | 12276.0 | 244.6 | Harvested | 9.5 | 6.4 | 8.0 | 0.8 | 0.0 |
| McCready | 704.0 | 49.7 | 9727.6 | 226.4 | Harvested | 4.7 | 9.0 | 9.0 | 1.9 | 0.0 |
| Cloney | 828.9 | 50.6 | 9915.6 | 199.4 | Harvested | 11.9 | 7.0 | 11.0 | 0.9 | 0.0 |
| Little Freshwater | 1194.4 | 96.6 | 18919.7 | 452.1 | Harvested | 11.9 | 5.6 | 0.0 | 0.0 | 0.2 |
| Graham | 1305.4 | 57.4 | 11236.3 | 207.2 | Harvested | 6.3 | 7.6 | 11.0 | 1.8 | 0.2 |
| Upper | 2469.3 | 34.4 | 6742.2 | 125.3 | Harvested | 5.1 | 4.7 | 4.0 | 0.8 | 0.0 |
| Mainstem Incline C (Middle Freshwater) | 3757.1 | 98.2 | 19247.3 | 338.4 | Harvested | 16.7 | 4.7 | 24.0 | 1.4 | 0.2 |
| Mainstem South Fork Junction (Lower Freshwater) | 2196.2 | 91.1 | 17848.0 | 347.4 | Harvested | 22.8 | 4.9 | 28.0 | 1.2 | 0.3 |
| Becks | 712.8 | 26.9 | 5263.4 | 93.6 | Harvested | 2.2 | 8.6 | 2.0 | 0.9 | 0.6 |
| South Fork | 1154.8 | 53.3 | 10433.7 | 221.3 | Harvested | 8.2 | 5.6 | 4.0 | 0.5 | 0.3 |
| Mainstem | 619.0 | 79.6 | 15355.0 | 512.7 | Harvested | 111.4 | 4.4 | 105.0 | 0.9 | 0.1 |
| Lower South Fork | 395.7 | 42.1 | 8119.8 | 261.4 | Harvested | 50.2 | 4.0 | 49.0 | 1.0 | 0.1 |
| Lower North Fork | 313.0 | 43.3 | 8352.2 | 231.4 | Harvested | 56.6 | 4.8 | 56.0 | 1.0 | 0.2 |
| Bridge | 744.9 | 64.7 | 12492.6 | 293.2 | Harvested | 5.7 | 4.9 | 0.0 | 0.0 | 0.1 |
| Upper North Fork | 1462.6 | 97.2 | 18752.8 | 413.2 | Harvested | 35.0 | 4.8 | 42.0 | 1.2 | 0.1 |
| Toms | 401.3 | 39.9 | 7691.4 | 175.9 | Harvested | 6.4 | 5.8 | 2.0 | 0.3 | 0.1 |
| McCloud | 386.4 | 33.7 | 6511.6 | 137.1 | Harvested | 6.1 | 3.7 | 2.0 | 0.3 | 0.0 |
| South Branch A | 2428.1 | 91.3 | 17611.0 | 340.3 | Harvested | 16.1 | 4.4 | 21.0 | 1.3 | 0.2 |

**Table H.1.** (cont.)

| | | | | | | | | | | |
|---|---|---|---|---|---|---|---|---|---|---|
| Corrigan | 1654.3 | 44.3 | 8556.9 | 192.2 | Harvested | 4.3 | 5.1 | 3.0 | 0.7 | 0.2 |
| Little South Fork (Headwaters Reserve) | 1232.8 | 26.2 | 5061.5 | 107.4 | Unharvested | 3.0 | 0.9 | 0.0 | 0.0 | 0.0 |
| Bear | 2597.9 | 93.0 | 24382.9 | 332.5 | Harvested | 20.9 | 1.7 | 13.0 | 0.6 | 0.1 |
| Munn | 175.4 | 7.8 | 1410.7 | 27.8 | Unharvested | 0.2 | 9.5 | 0.0 | 0.0 | 0.0 |
| Iverson | 137.6 | 7.7 | 1398.0 | 25.5 | Unharvested | 0.2 | 12.4 | 0.0 | 0.0 | 0.0 |
| Henningson | 121.1 | 6.8 | 1237.5 | 24.1 | Unharvested | 0.4 | 2.0 | 0.0 | 0.0 | 0.0 |
| Dollard | 413.3 | 25.3 | 4590.5 | 86.7 | Harvested | 0.8 | 4.7 | 0.0 | 0.0 | 0.0 |
| Xray | 177.4 | 7.6 | 1378.0 | 25.6 | Unharvested | 0.2 | 20.4 | 0.0 | 0.0 | 0.0 |
| Carlson | 122.9 | 7.4 | 1346.7 | 24.0 | Harvested | 0.3 | 12.3 | 0.0 | 0.0 | 0.0 |
| Eagle | 150.8 | 8.1 | 1464.4 | 26.8 | Harvested | 0.3 | 8.5 | 0.0 | 0.0 | 0.0 |
| XYZ | 504.5 | 25.8 | 4682.7 | 84.4 | Harvested | 0.9 | 11.6 | 0.0 | 0.0 | 0.0 |
| Arfstein | 942.9 | 60.5 | 10993.6 | 203.4 | Harvested | 3.9 | 6.7 | 0.0 | 0.0 | 0.0 |
| North Fork | 1370.5 | 81.8 | 14852.8 | 273.1 | Harvested | 4.8 | 7.7 | 1.0 | 0.2 | 0.0 |
| Ziemer | 201.5 | 7.7 | 1403.7 | 24.9 | Harvested | 0.2 | 29.4 | 4.0 | 20.0 | 0.0 |
| Yocom | 290.2 | 12.8 | 2319.4 | 40.2 | Harvested | 0.5 | 20.6 | 6.0 | 12.0 | 0.0 |
| Williams | 153.3 | 7.8 | 1423.3 | 23.5 | Harvested | 0.3 | 5.8 | 2.0 | 6.7 | 0.0 |
| South Fork | 694.1 | 60.9 | 11070.5 | 191.7 | Harvested | 4.1 | 11.7 | 49.0 | 12.0 | 0.0 |
| Uqlidisi | 124.7 | 8.5 | 1540.4 | 25.5 | Harvested | 0.1 | 40.0 | 2.0 | 20.0 | 0.0 |
| Quetelet | 614.0 | 56.2 | 10201.8 | 179.1 | Harvested | 3.9 | 11.5 | 48.0 | 12.3 | 0.0 |
| Ogilvie | 87.7 | 8.5 | 1542.6 | 25.2 | Harvested | 0.2 | 4.8 | 0.0 | 0.0 | 0.0 |
| Porter | 158.8 | 16.1 | 2932.7 | 51.6 | Harvested | 0.3 | 6.8 | 0.0 | 0.0 | 0.0 |
| Sequoyah | 84.5 | 7.5 | 1360.8 | 24.8 | Harvested | 0.2 | 9.8 | 0.0 | 0.0 | 0.0 |
| Treat | 94.1 | 8.4 | 1522.1 | 25.5 | Harvested | 0.1 | 8.2 | 0.0 | 0.0 | 0.0 |
| Richards | 71.2 | 7.0 | 1268.1 | 22.1 | Harvested | 0.4 | 9.6 | 4.0 | 10.0 | 0.0 |

**Table H.1.** (cont.)

| Watershed | Percent Harvested since 2005 | Percent Harvested since 1995 | Percent Harvested since 1985 |
|---|---|---|---|
| Prairie | 0.0 | 0.0 | 0.0 |
| Little Lost Man | 0.0 | 0.0 | 0.0 |
| Railroad | 0.1 | 0.3 | 0.3 |
| Lower South Fork | 0.2 | 0.5 | 0.5 |
| Upper South Fork | 0.2 | 0.5 | 0.5 |
| Carson | 0.1 | 0.3 | 0.4 |
| McCready | 0.1 | 0.5 | 0.5 |
| Cloney | 0.1 | 0.7 | 0.9 |
| Little Freshwater | 0.3 | 0.9 | 1.2 |
| Graham | 0.3 | 0.6 | 1.1 |
| Upper | 0.0 | 0.1 | 0.1 |
| Mainstem Incline C (Middle Freshwater) | 0.3 | 0.4 | 0.5 |
| Mainstem South Fork Junction (Lower Freshwater) | 0.4 | 0.6 | 0.7 |
| Becks | 0.7 | 0.9 | 0.9 |
| South Fork | 0.5 | 1.1 | 1.3 |
| Mainstem | 0.2 | 0.5 | 0.8 |
| Lower South Fork | 0.2 | 0.3 | 0.6 |
| Lower North Fork | 0.2 | 0.7 | 1.1 |
| Bridge | 0.2 | 0.9 | 1.1 |
| Upper North Fork | 0.2 | 0.5 | 1.0 |
| Toms | 0.3 | 0.3 | 0.4 |
| McCloud | 0.0 | 0.0 | 0.2 |
| South Branch A | 0.3 | 0.3 | 0.7 |

**Table H.1.** (cont.)

| | | | |
|---|---|---|---|
| Corrigan | 0.4 | 0.5 | 1.1 |
| Little South Fork (Headwaters Reserve) | 0.0 | 0.0 | 0.0 |
| Bear | 0.1 | 0.5 | 0.7 |
| Munn | 0.0 | 0.0 | 0.0 |
| Iverson | 0.0 | 0.0 | 0.0 |
| Henningson | 0.0 | 0.0 | 0.0 |
| Dollard | 0.0 | 0.0 | 0.4 |
| Xray | 0.0 | 0.0 | 0.0 |
| Carlson | 0.0 | 0.0 | 1.0 |
| Eagle | 0.0 | 0.0 | 1.0 |
| XYZ | 0.0 | 0.0 | 0.7 |
| Arfstein | 0.0 | 0.0 | 0.5 |
| North Fork | 0.0 | 0.0 | 0.5 |
| Ziemer | 0.0 | 0.0 | 0.5 |
| Yocom | 0.0 | 0.0 | 0.5 |
| Williams | 0.0 | 0.0 | 0.5 |
| South Fork | 0.0 | 0.0 | 0.5 |
| Uqlidisi | 0.0 | 0.0 | 0.5 |
| Quetelet | 0.0 | 0.0 | 0.5 |
| Ogilvie | 0.0 | 0.0 | 0.5 |
| Porter | 0.0 | 0.0 | 0.5 |
| Sequoyah | 0.0 | 0.0 | 0.5 |
| Treat | 0.0 | 0.0 | 0.5 |
| Richards | 0.0 | 0.0 | 0.5 |

# Appendix I. VSURF Model Outputs

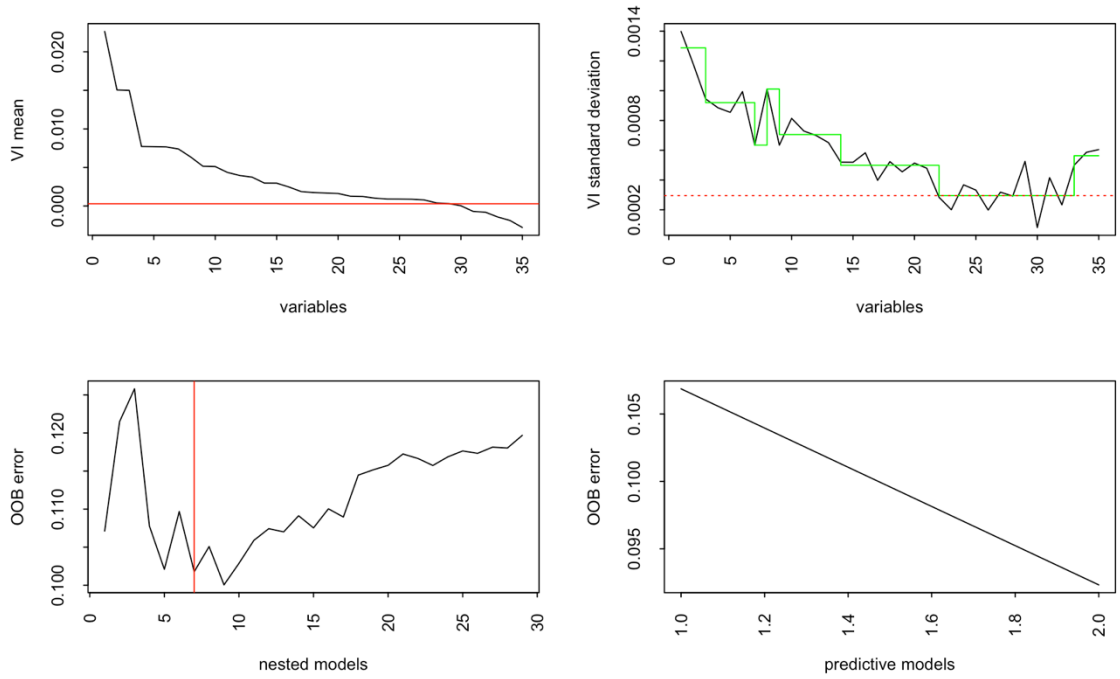


**Figure I.1.** VSURF results for the SRC offset model. The top left panel plots the mean variable importance (VI) computed for each predictor variable over 50 RF models, plotting variables below the red line that do not contribute to the model. The top right panel plots the standard deviation of each predictor variable. The bottom left panel plots the out-of-bag (OOB) error (averaged over 25 RF model runs) for each predictor variable using a nested RF modeling approach. Variables to the left of the red line can be used for interpretation but are highly autocorrelated. The bottom left panel plots the OOB error (averaged over 25 RF model runs) for each predictor variable using a sequential variable introduction RF modeling approach. These variables have the highest predictive power among all the predictor variables included in the model.

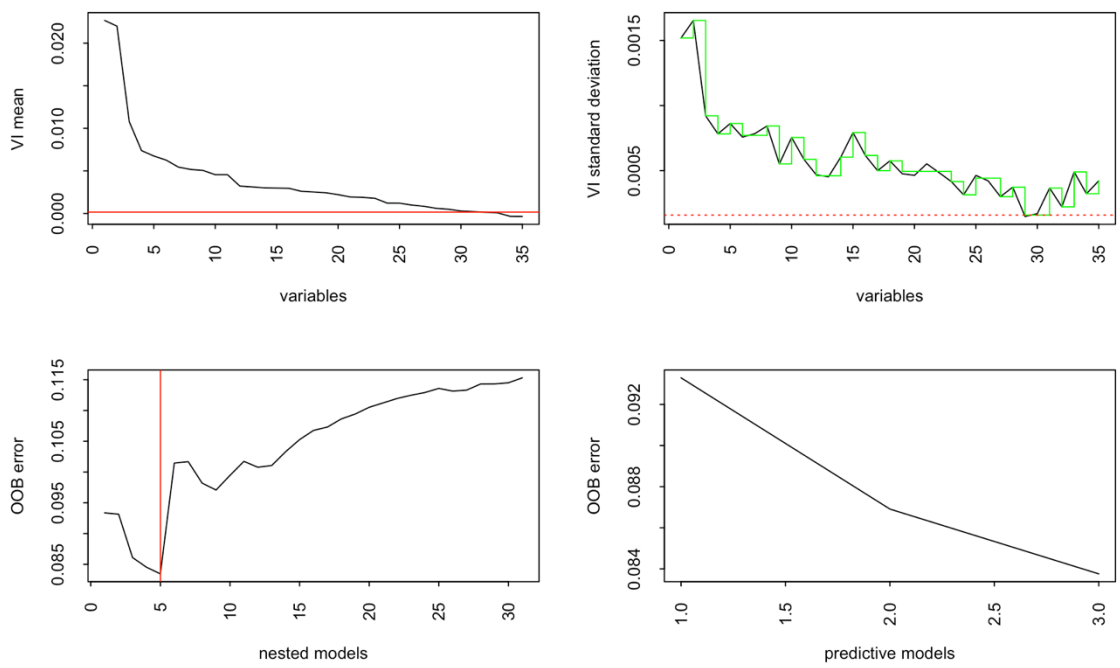


**Figure I.2.** VSURF results for the SRC slope model. The top left panel plots the mean variable importance (VI) computed for each predictor variable over 50 RF models, plotting variables below the red line that do not contribute to the model. The top right panel plots the standard deviation of each predictor variable. The bottom left panel plots the out-of-bag (OOB) error (averaged over 25 RF model runs) for each predictor variable using a nested RF modeling approach. Variables to the left of the red line can be used for interpretation but are highly autocorrelated. The bottom left panel plots the OOB error (averaged over 25 RF model runs) for each predictor variable using a sequential variable introduction RF modeling approach. These variables have the highest predictive power among all the predictor variables included in the model.

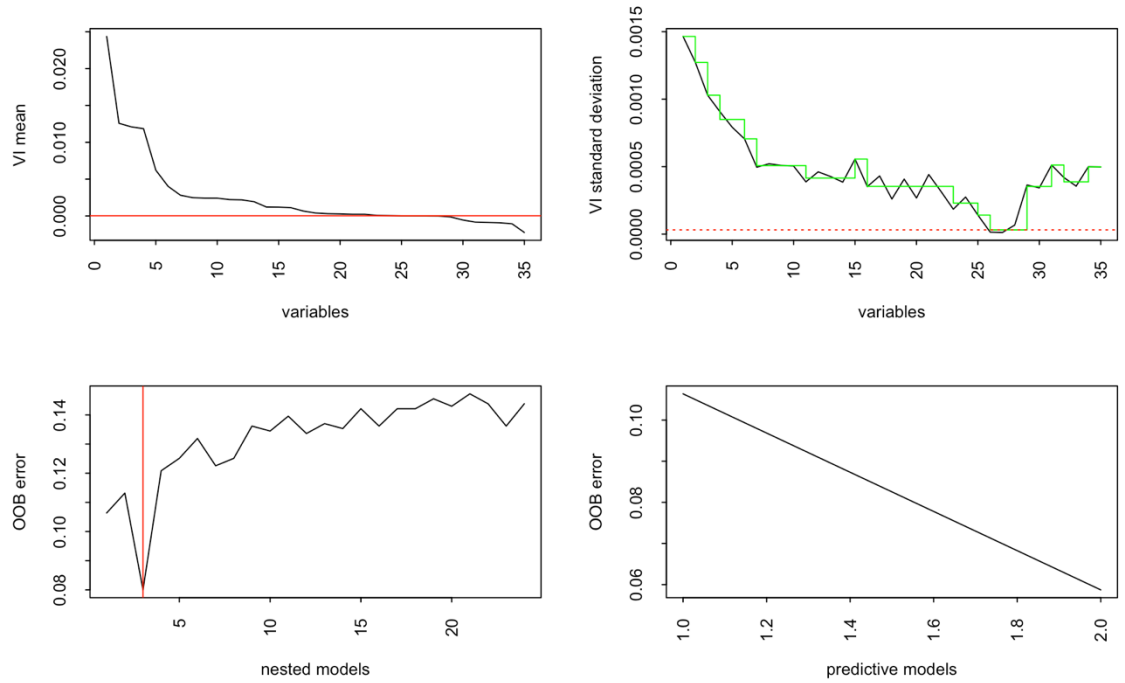


**Figure I.3.** VSURF results for SRC the shape model. The top left panel plots the mean variable importance (VI) computed for each predictor variable over 50 RF models, plotting variables below the red line that do not contribute to the model. The top right panel plots the standard deviation of each predictor variable. The bottom left panel plots the out-of-bag (OOB) error (averaged over 25 RF model runs) for each predictor variable using a nested RF modeling approach. Variables to the left of the red line can be used for interpretation but are highly autocorrelated. The bottom left panel plots the OOB error (averaged over 25 RF model runs) for each predictor variable using a sequential variable introduction RF modeling approach. These variables have the highest predictive power among all the predictor variables included in the model.

Appendix J. Sediment Rating Latitudinal Trends

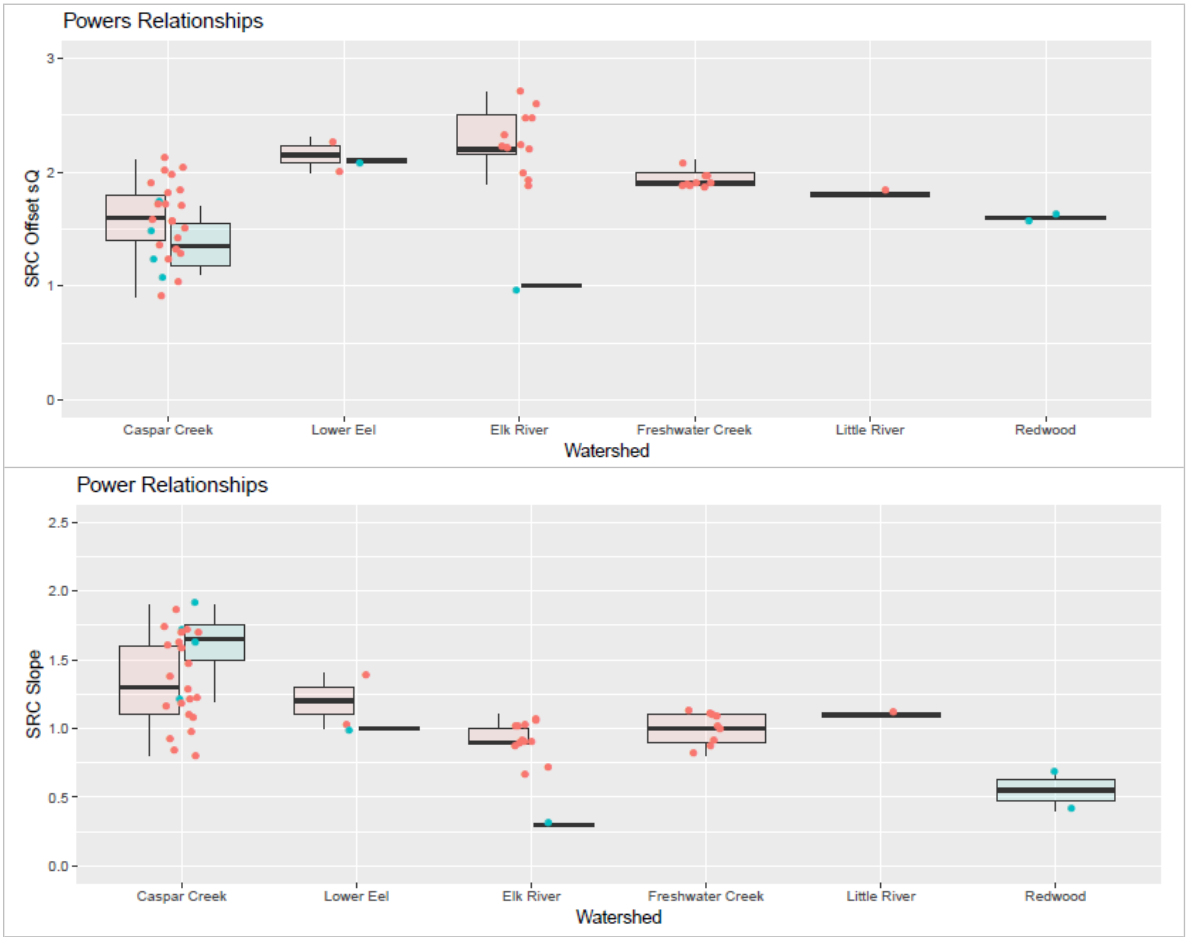


**Figure J.1.** The SRC offset and slope for power relationships are summarized by watershed and ordered by latitude. Harvested catchments are shown in orange (ordered left) and unharvest catchments are shown in green (ordered right). SRC offset values are plotted on a log axis.

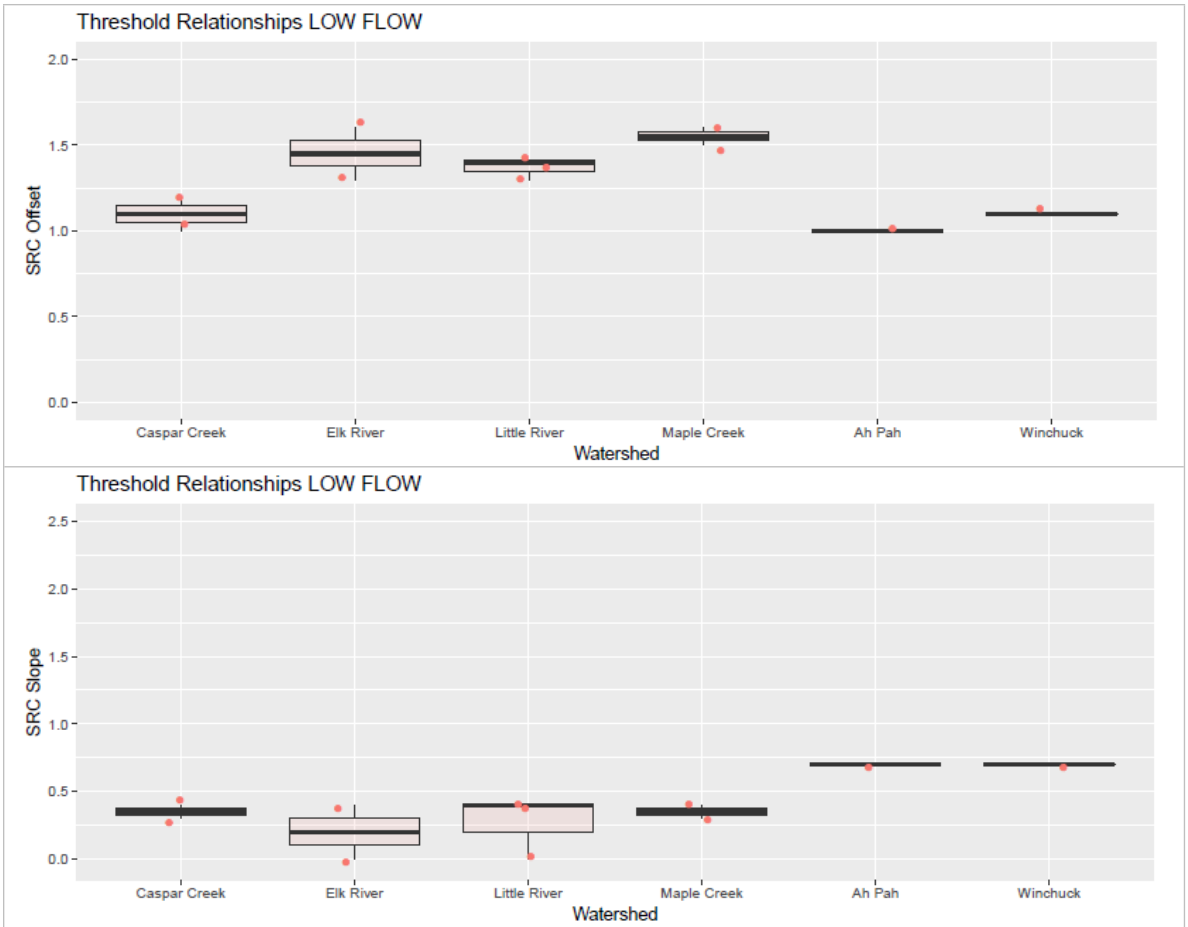


**Figure J.2.** SRC offset and slope for low flow threshold relationships. The high flow SRC offset (top panel) and slope (bottom panel) are summarized by watershed and ordered by latitude. All watersheds in this figure have been harvested. SRC offset values are plotted on a log axis.

# Appendix K. Multiple Linear Regression Models and Results

We created two multiple linear regression models in R using predictor variables informed by VSURF for SRC offset and slope. The model parameters, adjusted $R^2$ values, and significance levels are shown in the table below.

**Table K.1.**
*Table of Multiple Linear Regression Models*

| Model Parameters | Adj. $R^2$ | p-value |
|---|---|---|
| SRC Offset = 1.66 + (1.26 * Percent Harvested since 2010) – (4.073e-6 * Near-channel Local Relief) | 0.10 | 0.04 |
| SRC Slope = 1.57 – (0.31* Uplift Rate (Marine Terrace)) – (0 * Mean Annual Precip.) + (0 * 2yr-15min Precip. Intensity) | 0.18 | 0.01 |

91